Terrigenous climate signals in deep sea sediments: Insights from the inorganic and organic geochemistry

Dissertation

zur Erlangung des Doktorgrades der Naturwissenschaften

(Dr. rer. nat.)

Fachbereich für Geowissenschaften der

Universität Bremen

vorgelegt von

Wiebke Kallweit

Oktober 2011

Gutachter der Dissertation

PD Dr. Matthias Zabel
Prof. Dr. Thomas Wagner

Erklärung gemäß § 6 Abs. 5 der Promotionsordnung der Universität Bremen für die mathematischen, natur- und ingenieurwissenschaftlichen Fachbereiche

Hiermit versichere ich, dass ich die vorliegende Arbeit

1. ohne unerlaubte fremde Hilfe angefertigt habe,

2. keine anderen als die von mir im Text angegebenen Quellen und Hilfsmittel benutzt habe

und

3. die den benutzten Werken wörtlich oder inhaltlich entnommenen Stellen als solche

kenntlich gemacht habe.

Göttingen, 17.10.2011

_____

Wiebke Kallweit

Preface

This study was conducted in the framework of the European Graduate College “Proxies in Earth History” (EUROPROX). Funding was provided by the Deutsche Forschungsgemeinschaft (DFG). The research presented in this thesis has been carried out within the scope of the EUROPROX sub-project III.17 “Terrigenous climate signals in deep sea sediments: Assessment and quantification of alteration processes on primary signals”. This project has been proposed and supervised by PD Dr. Matthias Zabel (MARUM – Center for Marine Environmental Sciences, University of Bremen, Germany) and Prof. Dr. Thomas Wagner (School of Civil Engineering and Geosciences, Newcastle University, United Kingdom). The presented work has been submitted as dissertation. It has mainly been conducted using the laboratories of the marine geochemistry groups of the Department of Geosciences (Fachbereich 5 – Geowissenschaften) and MARUM, University of Bremen, Germany. Bacteriohopanepolyols have been measured in the hopanoid group of Dr. Helen M. Talbot at the School of Civil Engineering and Environmental Sciences, Newcastle University, United Kingdom.

The presented dissertation starts with an abstract summarizing the main research topics and results, followed by an introduction into the different research areas and investigated topics (Chapter 1). The main part of the thesis is comprised of three manuscripts submitted to or in preparation for submission to international peer reviewed journals for publication (chapters 2 – 4). Chapter 5 provides a summary of the main results and remaining open questions and includes an outlook on further research perspectives.

Table of contents

Abstract

Terrigenous material is transported to the marine environment in large quantities, mainly by fluvial and eolian transport. Its deposition within the marine sediments provides an archive of Earth's history, past climate conditions, source regions, transport processes, and their variations in time and space. The main objective of this thesis was the documentation of the transport of terrigenous material into the marine environment and the identification of terrigenous material (especially soil organic carbon; SOC) in sediments of continental margin systems. These investigations were mainly based on the analysis of the chemical composition, including lithogenic elements (e.g. Fe, Al) and element ratios, e.g. the Ti/Al-ratio as a proxy for transport energy and distance. A multi-proxy approach was chosen for studies on continental margin sediments, with a focus on the identification of SOC by biomarkers and reconstruction of paleoclimatic conditions over the last ~35 ka on the continent (Manuscript II) and within the marine water column (Manuscript III).

The first case study examines the chemical composition of eolian dust collected over the Atlantic Ocean off NW Africa between the equator and 35°N (Manuscript I). The results indicate a large variability in the chemical composition of the eolian dust which seems to be related to the latitudinal sampling position and the atmospheric dust amount during sampling. A higher variability is observed for samples taken under low dust conditions, which might be due to the increased influence of aerosols from other sources (biomass burning, sea spray or anthropogenic emissions) on these samples. This study shows that a source assignment or the identification of a 'primary signal' of eolian dust is not possible in this region. The large variability of the chemical composition should be considered if the eolian dust signal in marine sediments off NW Africa is used e.g. for reconstructions of paleoclimatic conditions. However, as largest dust amounts are probably deposited under high dust conditions, the variability exported to marine sediments might be substantially reduced.

The second case study (Manuscript II) investigates the abundance of SOC within two sediment cores from the Amazon shelf and deep sea fan. SOC within these marine sediments has been identified based on specific bacteriohopanepolyols (BHPs), produced by aerobic soil bacteria, and branched glycerol dialkyl glycerol tetraethers (GDGTs), also produced by soil-living (but presumably anaerobic) bacteria. Relative abundances of BHPs and branched GDGTs are strikingly constant, indicating a common source for these biomarkers. Unexpected high abundances of BHPs specific for aerobic methane oxidation led to the suggestion that the biomarkers have been

delivered from a floodplain lake environment. Comparison to a sample from a recent floodplain lake (Lago Socó, Brazil) reveals a high similarity in its BHP composition to the marine samples, therefore supporting the hypothesis of a floodplain lake source. It is consequently suggested that the material buried on the Amazon shelf and fan has already experienced a reworking history on the continent. This study shows that the supply of terrigenous organic carbon to the sediments from the Amazon shelf and fan is controlled by the reworking of organic carbon within the Amazon Basin. Similar processes might also occur in other large (tropical) river systems and should be taken into account when interpreting sedimentary records from continental margins and reconstructing the global carbon cycle.

The third case study (Manuscript III) investigates the deposition of terrigenous material in sediments from the Niger Fan over the last ~35 ka BP. The lithogenic element aluminum was measured as a proxy for bulk terrigenous material while soil organic carbon was identified from branched GDGTs and the BIT index. Carbonate and crenarchaeol (and their accumulation rates; AR) were used as proxies for marine productivity. Al AR are closely linked to the rate of mean sea level change and resulting shelf erosion after 15 ka BP, with an additional influence of the increased monsoonal precipitation during the African Humid Period. On the contrary, branched GDGT AR are determined by shelf erosion as well as the interplay of monsoonal precipitation and vegetation cover, resulting in changes of the intensity of soil erosion. The synchronicity of branched GDGT and crenarchaeol AR indicates that thaumarchaeotal productivity is enhanced by nutrients eroded from soils. During the last glacial period marine productivity was higher than during the Holocene, probably caused by a higher concentration of nutrients in surface waters during periods of high sediment discharge by the Niger River.

Reconstructions of sea surface temperatures (SST) are based on TEX_{86}^{H} and are cold-biased by 2 to 3°C in comparison with measured SSTs. It is suggested that this cold-bias is due to a high seasonality of thaumarchaeotal production, with a maximum during the cold summer months when riverine discharge is highest but primary productivity is at its lowest. Comparison to an SST-record based on Mg/Ca-ratios of planktonic foraminifera reveals that the temperature difference between the Holocene and the Last Glacial Maximum (LGM) is larger for TEX_{86}^{H}-SSTs compared to Mg/Ca-based SSTs (3°C and 2°C, respectively). This temperature difference between both SST reconstructions can be explained by a higher seasonality during the LGM.

This thesis contributes to the understanding of the chemical composition of Saharan/Sahelian dust which is deposited in the Atlantic Ocean off the NW African coast. It also provides insights into the deposition of terrigenous material on two large deep sea fans in the equatorial Atlantic Ocean

during the last ~35 ka. Specific biomarkers reflect the abundance of SOC within the marine sediments, which can considerably influence the radiocarbon ages of the total organic carbon (TOC). For estimating the terrigenous input in marine sediments it is important to differentiate between SOC and other terrigenous material as the SOC is only one fraction of the total terrigenous material. Estimates of the terrigenous input based e.g. on $\delta^{13}C$, C/N or the chemical composition can therefore deviate considerably from the BIT index if the SOC fraction is low. The presented thesis also contributes to the understanding of the delivery and fate of terrigenous organic material into continental margin systems which is important for the reconstruction of the global carbon cycle.

Kurzfassung

Terrigenes Material wird in großen Mengen in die Weltmeere eingetragen, hauptsächlich durch fluviatilen und äolischen Transport. Die Ablagerung terrigenen Materials in marinen Sedimenten stellt ein Archiv der Erdgeschichte dar und gibt Aufschluss über vergangene klimatische Bedingungen, Herkunftsgebiete und Transportprozesse, sowie ihre Variationen in Zeit und Raum. Die Hauptzielsetzung der vorliegenden Dissertation war die Dokumentation des Transports terrigenen Materials in das marine Milieu und die Identifikation von solchem (insbesondere von organischem Bodenkohlenstoff; SOC) in Sedimenten von Kontinentalrand-Systemen. Diese Untersuchungen basierten in erster Linie auf der Analyse der chemischen Zusammensetzung, einschließlich lithogener Elemente (z.B. Fe, Al) und Elementverhältnissen, z.B. dem Ti/Al-Verhältnis als einem Proxy für Transportenergie und -distanz. Für Untersuchungen an Kontinentalrandsedimenten wurde ein Multi-Proxy-Ansatz gewählt, dessen Fokus auf der Identifikation von organischem Bodenkohlenstoff anhand von Biomarkern und der Rekonstruktion paläoklimatischer Bedingungen der letzten ~35 ka auf dem Kontinent (Manuskript II) sowie in der marinen Wassersäule (Manuskript III) lag.

Die erste Fallstudie untersucht die chemische Zusammensetzung äolischen Staubs, der über dem Atlantischen Ozean vor NW Afrika zwischen dem Äquator und 35°N gesammelt wurde (Manuskript I). Die Ergebnisse indizieren eine große Variabilität in der chemischen Zusammensetzung von äolischem Staub, die mit der latitudinalen Beprobungsposition und dem atmosphärischen Staubgehalt während der Beprobung im Zusammenhang zu stehen scheint. Eine höhere Variabilität wird für Proben beobachtet, die während Zeiten mit geringem atmosphärischem Staubgehalt genommen wurden, was einem höheren Einfluss von Aerosolen anderer Herkunft (Verbrennung von Biomasse, Gischt oder anthropogene Emissionen) auf diese Proben zugeschrieben werden mag. Diese Studie zeigt dass eine Quellenzuordnung oder die Identifikation eines ‚primären Signals' äolischen Staubs in dieser Region nicht möglich ist. Die große Variabilität der chemischen Zusammensetzung sollte berücksichtigt werden wenn das Signal des äolischen Staubs in marinen Sedimenten vor NW Afrika verwendet wird, um z.B. paläoklimatische Bedingungen zu rekonstruieren. Da jedoch die größten Staubmengen vermutlich während Zeiten mit hohen atmosphärischen Staubgehalten abgelagert werden, könnte die Variabilität, die in die marinen Sedimente exportiert wird, erheblich reduziert sein.

Die zweite Fallstudie (Manuskript II) versucht organischen Bodenkohlenstoff in zwei Sedimentkernen vom Amazonasschelf und -Tiefseefächer zu quantifizieren. Organischer

Bodenkohlenstoff ist in diesen marinen Sedimenten auf der Basis von spezifischen Bakteriohopanpolyolen (BHPs), produziert von aeroben Bodenbakterien, und verzweigten Glycerol Dialkyl Glycerol Tetraethern (GDGTs), ebenfalls von bodenlebenden (aber mutmaßlich anaeroben) Bakterien produziert, identifiziert worden. Die relativen Anteile der BHPs und verzweigten GDGTs sind auffallend konstant, was eine gemeinsame Quelle für diese Biomarker indiziert. Unerwartet hohe Mengen von BHPs, welche spezifisch für aerobe Methanoxidation sind, deuten darauf hin, dass die Biomarker aus der Umgebung eines Sees der Überschwemmungsebenen angeliefert worden sind. Der Vergleich mit einer rezenten Probe aus einem solchen See (Lago Socó, Brasilien) zeigt eine hohe Ähnlichkeit in seiner BHP-Zusammensetzung mit den marinen Proben, was demzufolge die geäußerte Herkunftshypothese unterstützt. Folglich ist es wahrscheinlich dass das Material, welches auf dem Amazonasschelf und -Fächer abgelagert worden ist, bereits an Land eine Aufarbeitungs-Geschichte erlebt hat. Diese Untersuchung zeigt, dass das Signal terrigenen organischen Kohlenstoffs in den Sedimenten vom Amazonasschelf und -Fächer durch die Aufarbeitung organischen Kohlenstoffs im Amazonasbecken kontrolliert wird. Ähnliche Prozesse könnten ebenfalls in anderen großen (tropischen) Flusssystemen auftreten und sollten daher in Betracht gezogen werden, wenn Sedimentabfolgen von Kontinentalrändern diesbezüglich interpretiert werden und der globale Kohlenstoff-Kreislauf rekonstruiert wird.

Die dritte Fallstudie (Manuskript III) untersucht die Ablagerung terrigenen Materials in Sedimenten vom Nigerfächer während der letzten ~35 ka. Das lithogene Element Aluminium wird als ein Proxy für den Gesamteintrag terrigenen Materials verwendet, während organischer Bodenkohlenstoff durch die Identifikation von verzweigten GDGTs und den BIT Index nachgewiesen wurde. Karbonat und Crenarchaeol (und ihre Akkumulationsraten; AR) wurden als Proxies für die marine Produktivität benutzt. Nach 15 ka sind die Al AR eng mit der Rate der Meeresspiegel-Veränderung und der daraus resultierenden Schelferosion verbunden, mit einem zusätzlichen Einfluss des erhöhten Monsun-Niederschlags während der sogenannten ‚African Humid Period'. Im Gegensatz dazu sind die AR verzweigter GDGTs durch Schelferosion sowie durch das Zusammenspiel zwischen Monsun-Niederschlag und Vegetationsbedeckung bestimmt, welche in Veränderungen der Intensität der Bodenerosion resultieren. Die Synchronizität der verzweigten GDGTs und Crenarchaeol AR indiziert, dass die Produktivität der Thaumarchaeoten durch Nährstoffe, erodiert aus Böden, erhöht wird. Während des letzten Glazials war die marine Produktivität höher als während des Holozäns, was vermutlich durch höhere Konzentrationen von Nährstoffen im Oberflächenwasser während Zeitabschnitten hohen Sedimentaustrags durch den Niger verursacht wurde.

Rekonstruktionen der Meeresoberflächentemperaturen (SST) basieren auf TEX_{86}^{H} und zeigen um 2 bis 3°C kältere Werte als heutige SSTs. Dies steht mit einer hohen Saisonalität der Thaumarchaeoten-Produktivität in Zusammenhang, welche ein Maximum während der kalten Sommermonate hat, wenn die fluviatile Schüttung am höchsten, die Primärproduktion aber am niedrigsten ist. Der Vergleich mit einem SST-Datensatz basierend auf Mg/Ca-Verhältnissen planktonischer Foraminiferen zeigt, dass die Temperaturdifferenz zwischen dem Holozän und dem Letzten Glazialen Maximum (LGM) für die TEX_{86}^{H}-SSTs größer ist für die Mg/Ca-basierten SSTs (3°C bzw. 2°C). Diese Temperaturdifferenz zwischen den beiden SST-Rekonstruktionen kann durch eine höhere Saisonalität während des LGM erklärt werden.

Diese Dissertation trägt zum Verständnis der chemischen Zusammensetzung von Staub aus der Sahara/Sahel, welcher im Atlantischen Ozean vor NW Afrika abgelagert wird, bei. Es bietet außerdem Einblicke in die Ablagerung terrigenen Materials auf zwei großen Tiefseefächern im äquatorialen Atlantischen Ozean während der letzten ~35 ka. Spezifische Biomarker reflektieren die Menge an organischem Bodenkohlenstoff in den marinen Sedimenten, welcher die Radiokarbonalter des Gesamtkohlenstoffs (TOC) beträchtlich beeinflussen kann. Um den terrigenen Eintrag in marine Sedimente abzuschätzen ist es wichtig, zwischen organischem Bodenkohlenstoff und anderem terrigenen Material zu unterscheiden, da der organische Bodenkohlenstoff nur einen Teil des terrigenen Materials darstellt. Abschätzungen des terrigenen Eintrages, basierend z.B. auf $\delta^{13}C$, C/N oder der chemischen Zusammensetzung, können daher deutlich vom BIT Index abweichen wenn die Fraktion organischen Bodenkohlenstoffs gering ist. Die vorliegende Studie trägt weiterhin zum Verständnis des Eintrags und des Verbleibs terrigenen organischen Materials in Kontinentalrand-Systemen bei, welches für die Rekonstruktion des globalen Kohlenstoff-Kreislaufs von großer Bedeutung ist.

Important abbreviations

AR	Accumulation rate(s)
BHPs	Bacteriohopanepolyols
BIT	Branched and Isoprenoid Tetraether (Index)
CBT	Cyclization ratio of branched GDGTs
Da	Dalton
GDGTs	Glycerol dialkyl glycerol tetraethers
ITCZ	Intertropical Convergence Zone
ka BP	Thousand years before present
Ma	Million years before present
MAT	Mean annual air temperature
MBT	Methylation index of branched GDGTs
NBCC	North Brazil Coastal Current
OC	Organic carbon
SAL	Saharan Air Layer
SSDC	Sahara Sahel Dust Corridor
SOC	Soil organic carbon
SST	Sea surface temperature
TEX_{86}	TetraEther indeX of tetraethers consisting of 86 carbon atoms
TOC	Total organic carbon
TOMS	Total Ozone Mapping Spectrometer
VPDB	Vienna Pee Dee Belemnite standard
wt%	Weight percent
YD	Younger Dryas
$\delta^{13}C$	Stable carbon isotopic composition in per mill (‰) relative to VPDB

List of figures

List of tables

1. Introduction

1.1 Motivation and main objectives

The main aim of this thesis was to gain deeper insights into the sources, the transport and deposition of terrigenous material in the Atlantic Ocean. The transport of terrigenous material into marine environments occurs via eolian pathways, by rivers or ephemeral streams, ice or icebergs but also by coastal erosion and volcanic activity. However, the majority of terrigenous material is affected by fluvial transport (84 %), while eolian transport makes up for more than 7 % and the activity of icebergs affects less than 7 % of the terrigenous material (Lisitzin, 1996). Besides storing information about its sources and transport processes, terrigenous material deposited in marine sediments can store information about climatic conditions and therefore acts as an archive of Earth's history. Consequently, investigation of various proxies observed in these sediments can elucidate our knowledge about paleo-environmental conditions. Examples include the reconstruction of paleoclimatic conditions (e.g. precipitation) and vegetation based on pollen records (e.g. Dupont and Weinelt, 1996; Haberle and Maslin, 1999; Lézine and Cazet, 2005; Hessler et al., 2010), bulk organic proxies (e.g. δ^{13}C, C/N) (e.g. Holtvoeth et al., 2005; Collins et al., 2010) or specific elements and element ratios (e.g. K/Al for the chemical maturity) (e.g. Matthewson et al., 1995; Schneider et al., 1997; Zabel et al., 1999; Zabel et al., 2001). Specific organic compounds (lipid biomarkers) can identify terrigenous input especially from higher plants (e.g. certain steroids, lignin or long-chain odd-carbon-numbered *n*-alkanes) (e.g. Hinrichs and Rullkötter, 1997; Holtvoeth et al., 2003; Schefuß et al., 2004; Boot et al., 2006), but also of soil organic carbon (e.g. Hopmans et al., 2004; Cooke et al., 2008b; Cooke et al., 2009; Kim, 2010; Rethemeyer et al., 2010). New biomarker proxies allow for the reconstruction of paleo-soil pH and continental mean air temperatures (Weijers et al., 2007a; Weijers et al., 2007b; Peterse et al., 2009b; Bendle et al., 2010). The grain-size distribution of siliciclastic marine sediments has been used to distinguish between fluvial and eolian transport (Stuut et al., 2002; Holz et al., 2004; Tjallingii et al., 2008; Meyer, 2011). However, the interpretation of sedimentary signals can sometimes be complicated by alteration processes affecting the primary signal during transport of the particles through the water column (e.g. Fowler and Knauer, 1986). Considering that element ratios in marine sediments are used to reconstruct paleoclimatic conditions (e.g. Zabel et al., 2001; Mulitza et al., 2008) it appears important to know how the primary signal responds to environmental changes and how this signal is altered in the marine water column. In a first

attempt the chemical composition of eolian dust collected at sea level off the NW African coast has been investigated for identification of the 'primary signal(s)'. This is important background information for the identification of alterations of this primary signal in the water column or during deposition.

Continental margin systems constitute the transitional zone between continental and open marine environments. Large amounts of terrigenous material are deposited in this environment, but resuspension of sediments and remineralization of organic compounds are common (Hedges and Keil, 1995; Aller, 1998; Burdige, 2007). Understanding the processes controlling the sedimentary conditions is important for the reconstruction of paleo-environmental conditions which are based on the interpretation of proxy records from marine sediments. Knowledge about the fate of (terrigenous) organic carbon (OC) is important for the assessment of the global carbon cycle and the preservation potential of organic carbon (Berner, 1989; McKee et al., 2004; Burdige, 2005). Accordingly, the main focus of this thesis was on the deposition of fluvially transported terrigenous material in continental margin sediments of the equatorial Atlantic Ocean. Major attention was turned on the comparison between different (inorganic and organic) proxies in marine sediments deposited during the last ~35 ka BP. Two distinct river-continental margin systems have been chosen for this approach. Material delivered by the Amazon River is deposited in a subaqueous delta on the broad shelf while sediment accumulation on the shelf proximal to the river mouth is typical for suspended matter from the Niger River (Walsh and Nittrouer, 2009). Both environments are influenced by sea level fluctuations during glacial-interglacial transitions with the lowered sea level during glacials allowing for a more direct delivery and deposition of terrigenous material on the deep sea fans. The case study from the Amazon continental margin concentrates on the deposition of (old) terrigenous material and the importance of reworking processes. Additionally, continental conditions (soil pH and mean air temperature) were reconstructed based on specific biomarker proxies. Besides evaluating the delivery of terrigenous material by the Niger River paleo-sea surface temperatures (SSTs) in the Gulf of Guinea were reconstructed in the Niger Fan case study. Reconstructed SSTs were compared to published Mg/Ca-based SST estimates as an attempt to assess the comparability and reliability of different proxies for SST reconstructions.

The main objectives of this thesis are to:

- Improve our understanding of the sources, transport and deposition of terrigenous material into marine environments

- Characterize the 'primary signature' of eolian dust collected over the Atlantic Ocean off the NW-African continent
- Test the applicability of soil-marker BHPs as proxy for the delivery of soil organic carbon into marine sediments
- Track the transport of terrigenous material (especially soil organic carbon) into marine sediments
- Reconstruct changes in terrigenous input during the Holocene and latest Pleistocene based on the analysis of different organic and inorganic proxies
- Compare the different proxy records to assess how terrigenous input is reflected by different proxies
- Reconstruct paleo-sea surface temperatures and compare the results of different methods (Niger)
- Relate the proxy records to environmental changes between the last glacial period and the recent interglacial

1.2 Eolian dust

Atmospheric transport is an important pathway for the delivery of terrigenous material into the marine environment. Large amounts of mineral dust are delivered from semi-arid and arid regions, with a clearly higher "dustiness" of the northern hemisphere (Rea, 1994). The three major dust source areas are the desert regions of eastern and central Asia, Arabia and northern Africa (Pye, 1987; Rea, 1994). In the southern hemisphere only minor dust source regions are found, emitting dust from the arid regions of southern Africa (Namibian and Kalahari Deserts), South America (Atacama Desert and parts of Patagonia) and Australia. Estimates of yearly eolian dust emission are mainly between 1000 and 3000×10^6 tons per year (Goudie and Middleton, 2001 and references therein).

1.2.1 Saharan dust – sources and transport

The northern African dust source region has been referred to as the Sahara Sahel Dust Corridor (SSDC) which extends between 12 and 28°N and constitutes the world's largest recent dust source area. Major dust sources within the SSDC are the Bodélé Depression (Chad Basin), the Hoggar Massif and the West African carbonate-rich Atlantic coastal basin (Moreno et al., 2006) (Fig. 1.1). The Bodélé Depression – largely covered by desiccated diatomaceous deposits of paleolake

Megachad (Moreno et al., 2006; Bristow et al., 2009) – has received special attention as it has been denoted to be the largest single dust source on earth (e.g. Goudie and Middleton, 2001; Prospero et al., 2002; Washington and Todd, 2005; Bristow et al., 2009). The high activity of this dust source is due to the combination of highly erodible sediments and an erosive wind, namely the Low Level Jet (LLJ) which is part of the Harmattan wind system (Washington and Todd, 2005).

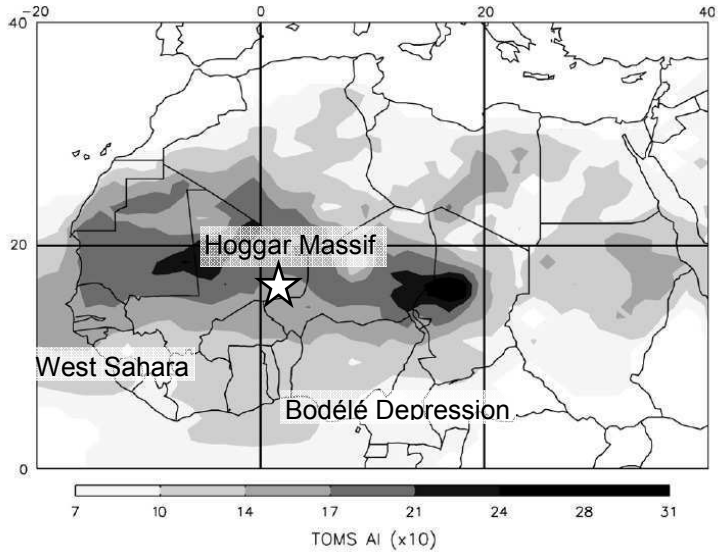

Figure 1.1. Long-term mean TOMS AI (×10) (1980–1992) (modified after Engelstaedter et al., 2006). The three major dust source regions of the Sahara Sahel Dust Corridor are clearly visible.

The Harmattan is a specific part of the northeast trade winds which has its largest activity in boreal winter and carries huge amounts of dust from the Bodélé Depression to coastal West Africa. The shallow northeast trade wind layer transports dust at a height of only 500 to 1500 m from the Atlas Mountains and coastal plains in a direction nearly parallel to the coast (Pye, 1987). The majority of this dust is deposited in the proximal Atlantic Ocean between the Canary Islands and the Cape Verde Islands (Sarnthein et al., 1981). Long-distance dust transport occurs at mid-tropospheric level (about 3000 m) by the Saharan Air Layer (SAL) which is especially active in boreal summer (Pye, 1987). The SAL is divided into two branches at the West African coast, eolian dust in the northern branch being deposited in the vicinity of the Canary Islands while dust transported in the western branch may reach the Caribbean or South America (Prospero and Carlson, 1972). A series of large easterly waves which propagate westward at a velocity of 8 m/s characterizes dust transport in the SAL (Reed et al., 1977). Saharan dust is also transported towards the Middle East and eastern Asia (e.g. China) (Ganor, 1994; Tanaka et al., 2005), the Mediterranean and to Europe (e.g. Loye-Pilot et al., 1986; Avila et al., 1997; Moulin et al., 1998;

Borbély-Kiss et al., 2004), sometimes even reaching Scandinavia (Franzén, 1989; Franzén et al., 1994; Stuut et al., 2009 and references therein).

The NW African climate is mainly controlled by the seasonal shift of the Intertropical Convergence Zone (ITCZ) which is also the boundary between northeast (north of the ITCZ) and southeast (south of the ITCZ) trade winds. The ITCZ is located at its northernmost position at 20°N in boreal summer (Nicholson, 2000), leading to an extended influence of the humid southeastern monsoonal flow (Knippertz et al., 2003). During boreal winter, the ITCZ is at its southernmost position at 5°N (Nicholson, 2000) allowing the dry northeast trade winds to penetrate far into NW Africa. The resulting dust plume over the Atlantic Ocean shifts from a position at 5 to 20°N during boreal winter to its summer position between 10 and 25°N (deMenocal and Rind, 1993; Stuut et al., 2005). Eolian dust may make up for a large fraction of the terrigenous material in the marine sediments under this dust plume as in other oceanic regions downwind of deserts (Stuut et al., 2002). End-member modeling of the grain-size distribution of siliciclastic marine sediments has been used to differentiate between terrigenous material that has been delivered by riverine or eolian transport (Stuut et al., 2002; Holz et al., 2004; Tjallingii et al., 2008; Meyer, 2011). The deposition of eolian dust – containing iron as oxides or oxyhydroxides or within clay minerals – in ocean waters may furthermore influence biogeochemical cycles, especially in oceanic regions where macronutrients like nitrate are abundant, but iron and other micronutrients (e.g. silica) limit phytoplankton growth (Duce et al., 1991; Martin et al., 1991; Chen and Siefert, 2004; Jickells et al., 2005; Maher et al., 2010). However, only a small fraction of the iron present in mineral dust is soluble in ocean waters or bioavailable to marine phytoplankton (Hand et al., 2004; Mahowald et al., 2005; Schroth et al., 2009).

1.2.2 Study area

Eolian dust samples were taken off the NW African coast mainly in the vicinity of the Saharan-Sahelian dust plume but also in adjacent regions covering an oceanic area between the equator and 35°N. 93 eolian dust samples analyzed in this study were taken on cellulose acetate filters during several cruises (e.g. with the German research vessels Meteor and Poseidon) between 2003 and 2008. The oceanic area covered by dust sampling is shown in Figure 1.2, together with the summer and winter positions of the ITCZ.

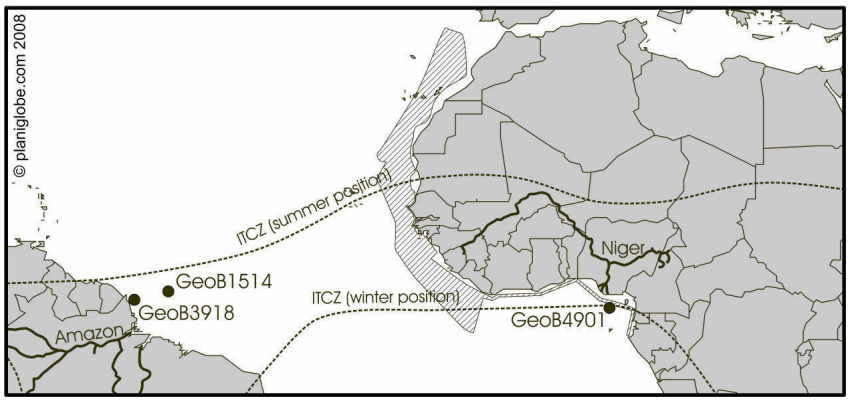

Figure 1.2. Map of the Atlantic Ocean showing ITCZ positions, the rivers Amazon and Niger, as well as sampling locations. Core locations GeoB3918, GeoB1514 and GeoB4901 are marked by black dots. Dust samples were taken within the hatched area.

1.3 Riverine transport

1.3.1 Organic carbon in continental margin systems

Continental margin systems reflect the transitional zone between the continents and the oceans. These environments are important archives for land-ocean interactions and their variability in time and space and in relation with climatic oscillations. High nutrient concentrations are common in coastal waters due to nutrient delivery from the continents and upwelling of nutrient-rich deep waters, leading to a high productivity in surface waters (Wollast, 1991). Additionally, large amounts of terrigenous material are transported to the continental margin systems, mainly by rivers. The organic material transported by rivers can have a large variety of sources, including vascular plant remains, OC produced within the river, soil organic carbon or petrogenic OC derived from weathering of rocks. OC from the latter two pools can be significantly pre-aged and is therefore often refractory and depleted of radiocarbon, but has a high potential for preservation in marine sediments (Dickens et al., 2004; Hwang et al., 2005). However, only a small portion (33 to 50 % or even less) of the terrigenous material delivered into the ocean is actually deposited in the marine sediments (Hedges and Keil, 1995; Burdige, 2007). This is caused by an intense remineralization of OC which is a common process in continental margin systems. Sediment reworking processes are especially important on wide and highly energetic continental margins (e.g. the Amazon continental margin) and may lead to an increased degradation of refractory organic material (Aller, 1998). Accordingly, the fate of terrigenous OC after its delivery into the marine environment plays an important role in the global carbon cycle (Berner, 1989; McKee et al., 2004; Burdige, 2005).

Nevertheless, terrigenous material deposited in continental margin sediments contains information on paleo-continental conditions, e.g. temperature, precipitation or vegetation (Galy et al., 2011). OC in marine sediments has consequently been widely used to study the deposition of terrigenous OC in these sediments and to reconstruct paleo-environmental conditions on the adjacent continent (e.g. Bird et al., 1995; Schefuß et al., 2003; Cooke et al., 2008b; Eglinton and Eglinton, 2008 and references therein). However, for an accurate interpretation of terrigenous OC in marine sediments the provenances of the organic signatures need to be assessed as OC might originate from specific source regions and might therefore not reflect a basin-integrated signal (Galy et al., 2011).

1.3.2 The equatorial Atlantic Ocean – Surface currents

The major surface current systems of the (equatorial) North Atlantic Ocean are shown in Figure 1.3. The shallow eastern boundary current which flows southward along the North African continent and transports cool water from higher latitudes originates from the North Atlantic Drift and is called the Canary Current (CC) in the vicinity of the Canary Islands. This current deflects from the continental margin at about 25 to 15°N to form the westward-flowing North Equatorial Current (NEC; Sarnthein et al., 1982; Mittelstaedt, 1991). Only a minor part of the CC continues to flow southward along the West African continental margin and feeds the Guinea Current (GC; Mittelstaedt, 1991). The GC is the southern extension of the North Equatorial Counter Current (NECC; Sarnthein et al., 1982; Richardson and Walsh, 1986) which flows eastwards between 3 and 6°N (Pokras, 1987) and is strongest in boreal summer and early fall (Mittelstaedt, 1991).

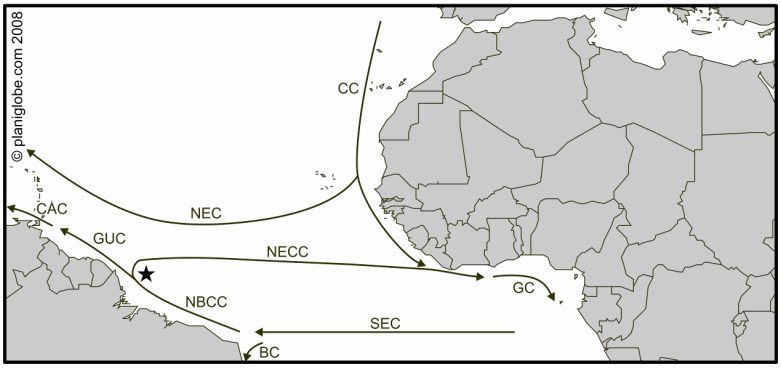

Figure 1.3. Surface currents in the Atlantic Ocean. North Equatorial Current (NEC), Canary Current (CC), Guyana Current (GUC), Caribbean Current (CAC), North Equatorial Countercurrent (NECC), Guinea Current (GC), North Brazil Coastal Current (NBCC), South Equatorial Current (SEC), Brazil Current (BC), North Brazil Coastal Current retroflection (★). Map adapted from Sarnthein et al. (1982); Richardson & Walsh (1986); Peterson & Stramma (1991); Stramma & Schott (1999); Henrich et al. (2003).

The South Equatorial Current (SEC) is part of the Equatorial Under Current (EUC) and flows westwards across the Atlantic Ocean (Pokras, 1987). The SEC splits up into two branches near the northeastern coast of Brazil, the southward flowing Brazil Current (BC) and the northwestward flowing North Brazil Coastal Current (NBCC; Richardson and Walsh, 1986; da Silveira et al., 1994; Stramma et al., 1995). The NBCC is the only cross-equatorial surface current transporting heat and salt into the North Atlantic Ocean (Metcalf and Stalcup, 1967; Peterson and Stramma, 1991). During boreal winter and spring the NBCC may extend into the Guyana Current (GUC) and further north into the Caribbean Current (CAC; Philander and Pacanowski, 1986; Richardson and Walsh, 1986). Between July and November, however, the NBCC is weakened and a part of the water masses is retroflected at about 8°N to turn into the NECC flowing eastwards towards the West African coast (Richardson and Walsh, 1986; Schott et al., 1995).

1.3.3 Study areas

The Amazon

The Amazon River discharges large amounts of sediments and water into the Atlantic Ocean (Meybeck, 1996). The dispersal and distribution of the suspended matter discharged by the Amazon River is influenced by the NBCC on seasonal and longer timescales (Philander and Pacanowski, 1986; Maslin, 1998; Wilson et al., 2011). Many studies have shown that large amounts of terrigenous material have been deposited in sediments from the Amazon shelf and deep sea fan (Showers and Angle, 1986; Debrabant et al., 1997; Goñi, 1997; Haberle, 1997; Hinrichs and Rullkötter, 1997; Schlünz et al., 1999; Boot et al., 2006). This location seemed therefore suitable for testing the applicability of specific biomarkers (bacteriohopanepolyols) as tracers for SOC into marine sediments (Cooke et al., 2008b; Cooke et al., 2009; Rethemeyer et al., 2010).

Two cores have been chosen to evaluate the deposition of terrigenous material in continental margin sediments off this largest tropical river. Holocene sedimentation occurs mainly on the Amazon shelf. Gravity core GeoB3918-2 (3.7050°N; 50.4050°W; Fig. 1.2) was taken during Meteor cruise M34/4 from a water depth of 50 m and consists of olive gray to very dark gray terrigenous clays (Wefer et al., 1997). During the last glacial period sediment was mainly deposited on the Amazon deep sea fan. To examine the terrigenous input in glacial deposits core GeoB1514-6 (5.1383°N; 46.5750°W; Fig. 1.2) – located on the Eastern Levee complex of the Amazon Fan – was analyzed. This gravity core has been taken during Meteor cruise M16/2 from a water depth of

3509 m and consists of about 35 cm Holocene clay-bearing nannofossil ooze at the core top. A red iron crust separates the Holocene sediments from the Pleistocene olive gray, bioturbated muds which extend to the core basis and are partly pyrite-bearing (Schulz et al., 1991).

The Gulf of Guinea and the Niger

Another major tropical river is the Niger River which passes several vegetation zones in western Africa (Martins and Probst, 1991) and drains into the Gulf of Guinea. Similar to the situation in the western equatorial Atlantic lowered sea level during the last glacial period led to a more direct deposition of sediments on the Niger Fan (Burke, 1972). In addition to the riverine delivery of terrigenous material, eolian dust from the Sahara is deposited in the Gulf of Guinea especially during boreal winter (Pokras and Mix, 1985). Gravity core GeoB4901-8 (2.6783°N; 6.7200°E; Fig. 1.2) has been sampled during Meteor cruise 41/1 from a water depth of 2184 m. This core from the Niger Fan consists of greenish gray clay-bearing diatomaceous nanno-ooze and is highly bioturbated.

1.4 Methodological approach

The methodological approach used in this study will be briefly introduced in the following sections. While the case study on the 'primary signal' of eolian dust was based on an inorganic approach, namely on the chemical composition of the dust particles in combination with satellite images and the calculation of back trajectories, multi-proxy approaches were chosen for the interpretation of terrigenous material delivered to continental margin sediments. The focus of these case studies was on biomarker research, but element concentrations and bulk parameters such as stable carbon isotopes and total organic carbon were analyzed in addition. Analytical methods will not be discussed here as the applied methods – Inductively Coupled Plasma-Atomic Emission Spectroscopy (ICP-AES) and X-ray fluorescence spectroscopy (XRF) for element concentrations and high performance liquid chromatography coupled to a mass spectrometer with an atmospheric pressure chemical ionization source (HPLC-APCI-MS) for biomarker analysis – are standard procedures in inorganic and organic geochemistry.

1.4.1 Elements and element ratios

Continental rocks are subject to chemical and physical weathering and to erosional processes. The mineralogy of the source rocks determines the element composition of the terrigenous detritus.

The chemical composition of dust particles, for example, has therefore been used as a proxy for the identification of the source areas (Chester et al., 1971; Chiapello et al., 1997; Moreno et al., 2006). However, element compositions in sediments can also be used to gain information about source regions, but likewise about transport processes or weathering intensity (see below). Elements such as Al, Ti, K, Rb and Zr have been interpreted to reflect a terrigenous (lithogenic) signal (e.g. Schneider et al., 1997; Zabel et al., 2001). Several chemical elements are preferentially associated with a distinct grain size fraction or specific minerals. Titanium, for example, occurs mainly in heavy minerals such as titanomagnetite, ilmenite, augite and rutile and is therefore mostly present in the coarse grain size fraction (Spears and Kanaris-Sotiriou, 1976; Boyle, 1983). Aluminum, on the contrary, is predominantly associated with the fine-grained aluminosilicate fraction (Calvert, 1976). The Ti/Al-ratio can therefore be used as an indicator of grain size and transport energy (Boyle, 1983; Zabel et al., 1999). Potassium occurs in potassium feldspar (e.g. Schneider et al. (1997); Martinez et al. (1999)) and in clay minerals, especially illite (e.g. Yarincik et al. (2000)). Potassium feldspar and illite, however, both reflect low chemical weathering rates under arid conditions. Accordingly, the K/Al-ratio can be used as a proxy for the intensity of chemical weathering (Zabel et al., 2001). Recently deposited carbonate in marine sediments is mainly of biogenous origin, indicating that calcium in marine sediments reflects primarily a marine signal (Adegbie et al., 2003).

The analysis of element concentrations constitutes one part of all case studies included in this thesis. However, the focus of these analyses has been chosen individually based on the research question for each case study. The chemical composition of eolian dust – with a focus on lithogenic elements and potassium – has been used to assess the 'primary signal' of dust input to the Atlantic Ocean off NW Africa. In sediments from the Amazon shelf and fan the Ti/Al-ratio has been used as an inorganic proxy for the delivery of terrigenous material. Aluminum abundances were measured for sediments from the Niger Fan. Additionally, a good age model for this setting allowed for the calculation of (Al) accumulation rates.

1.4.2 Lipid biomarkers

Biomarkers are molecular fossils stable under geological conditions, dating back up to several billion years before present. These organic compounds are resistant against degradation and taxonomically specific, implying that they can be assigned to their producers (Brocks and Pearson, 2005). Studying biomarkers can reveal information about environmental conditions such as redox conditions, temperature changes and sediment and water chemistry, microbial communities,

biogeochemical processes and (paleo-)climatic conditions (e.g. Brocks and Summons, 2004; Brocks and Pearson, 2005 and references therein). Lipids are extensively used as biomarkers due to their high structural complexity. Additionally, despite the loss of functional groups during diagenesis the remaining hydrocarbon skeletons still bear biological and ecological information (Brocks and Summons, 2004; Peters et al., 2004; Brocks and Pearson, 2005). The development of new analytical methods over the last decade now allows for the measurement of highly polar and high molecular weight molecules with a mass larger than 1000 Da (e.g. Hopmans et al., 2000; Talbot et al., 2001). The measurement of glycerol dialkyl glycerol tetraethers has already become a routine operation and proxies based on these compounds are widely used in earth sciences (e.g. Schouten et al., 2008; Peterse et al., 2009a; Weijers et al., 2009b; Huguet et al., 2010; Tyler et al., 2010; Rommerskirchen et al., 2011).

1.4.2.1 Bacteriohopanepolyols

Bacteriohopanepolyols (BHPs) are the biological precursors of the geohopanoids (including hopanoic acids, hopanols, hopenes and hopanes) that have been described to be among the most abundant natural products on earth (Ourisson and Albrecht, 1992). BHPs are biosynthesized by many prokaryotes and are believed to be lipid membrane components (Rohmer et al., 1984; Ourisson et al., 1987; Sáenz, 2010). However, hopanoid biosynthesis is not ubiquitous among bacteria with only ~50 % of strains studied producing them in liquid culture (Rohmer et al., 1984; Farrimond et al., 1998). Furthermore, sequencing of the genomes of > 600 bacteria revealed that only < 10 % contain the squalene-hopene-cyclase gene necessary for hopanoid production (Pearson et al., 2007).

The side chains of BHPs have a high structural variability which includes the addition of hydroxyl- and amine-groups or polar moieties, e.g. carbohydrates (Rohmer, 1993). Some BHPs have only been detected in a restricted number of taxa and can therefore be used for identifying their producers in environmental samples (e.g. Talbot and Farrimond, 2007). The hexafunctionalized compound aminobacteriohopanepentol, for example, has only been found to be produced by type I methanotrophic bacteria (Neunlist and Rohmer, 1985; Cvejic et al., 2000), making it a useful indicator for aerobic methane oxidation (Coolen et al., 2008; Zhu et al., 2010). Adenosylhopane and related compounds, however, are predominantly found in soils (Cooke et al., 2008a; Xu et al., 2009; Cooke, 2010; Rethemeyer et al., 2010; Kim et al., 2011) and have therefore been used to track the transport of soil organic carbon into aquatic environments (Cooke et al., 2008b; Cooke et al., 2009). BHPs have been investigated in sediments from the Amazon shelf and deep sea fan.

Additionally, BHPs were measured in six samples from the Niger Fan to test the diversity of BHPs in this region (section 5.1.2.3).

1.4.2.2 Glycerol dialkyl glycerol tetraethers

Glycerol dialkyl glycerol tetraethers (GDGTs) are the membrane lipids of many eubacteria and Archaea (Schouten et al., 2000). Bacterial GDGTs are comprised of branched carbon chains and are presumably produced by anaerobic bacteria (Sinninghe Damsté et al., 2000; Weijers et al., 2006b; Weijers et al., 2009a) in soils and peats (e.g. Schouten et al., 2000; Weijers et al., 2006b). On the contrary, archaeal GDGTs have the typical isoprenoid carbon skeleton and are produced by Crenarchaeota, Euryarchaeota and Thaumarchaeota, occurring ubiquitously in open oceans (Karner et al., 2001), lakes (Auguet and Casamayor, 2008) and soils (Leininger et al., 2006). In the marine and lacustrine water column pelagic type 1 Crenarchaeota have been proposed to be the main producers of isoprenoid GDGTs (Karner et al., 2001; Keough et al., 2003). Accordingly, a very typical and highly abundant isoprenoid GDGT with four cyclopentane rings and one cyclohexane ring has been named crenarchaeol (Sinninghe Damsté et al., 2000). However, recent molecular biological studies have shown that the producers of crenarchaeol are ammonia-oxidizing Archaea (Könneke et al., 2005; Wuchter et al., 2006a; Herfort et al., 2007) which constitute an own archaeal phylum, the Thaumarchaeota (Brochier-Armanet et al., 2008; Spang et al., 2010; Pitcher et al., 2011). Thaumarchaeota adjust their membranes to environmental conditions by the introduction of one to three cyclopentane rings into the GDGTs (Schouten et al., 2000). The average number of cyclopentane moieties is correlated with annual mean sea surface temperature. This relationship is reflected by the TEX_{86}-index (TetraEther indeX of tetraethers consisting of 86 carbon atoms) which has been introduced by Schouten et al. (2002) and has been widely applied in oceans (e.g. Sluijs et al., 2006; Wuchter et al., 2006b; Rueda et al., 2009) and lakes (e.g.Powers et al., 2004; Blaga et al., 2009), and new calibrations have been introduced for marine (Kim et al., 2008; Kim et al., 2010) and lacustrine (Powers et al., 2010; Pearson et al., 2011) sediments. SST-reconstructions based on the TEX_{86}-proxy have been carried out for marine sediments dating back to the Lower Cretaceous (Aptian; ~120 Ma) (Schouten et al., 2003), indicating a wide temporal applicability but also the suitability of the TEX_{86}-proxy for reconstructing SSTs of oceans under Greenhouse conditions (Schouten et al., 2007). However, several factors have been shown to bias TEX_{86}-based SST reconstructions, including subsurface production of GDGTs (Huguet et al., 2007; Lee et al., 2008; Rommerskirchen et al., 2011) and a high seasonality of thaumarchaeotal productivity (Herfort et al., 2006; Huguet et al., 2006; Leider

et al., 2010). Under oxic conditions selective degradation can cause a bias of TEX_{86}-SST estimates towards warmer temperatures (Huguet et al., 2009; Kim et al., 2009). An additional bias might be caused by the in situ production of Archaea within the marine sediments (Lipp et al., 2008; Shah et al., 2008) and by the delivery of isoprenoid GDGTs by rivers to continental margin sediments (Herfort et al., 2006; Weijers et al., 2006a).

The possible bias of TEX_{86} by isoprenoid GDGTs delivered from land, however, can be assessed by applying the Branched and Isoprenoid Tetraether-Index (BIT). This proxy has been introduced by Hopmans et al. (2004) as a proxy for the relative amount of terrigenous vs. marine organic matter in sediments. BIT values range from 0 in open marine settings to 0.9 – 1 in soils (Weijers et al., 2006a). Branched GDGTs include four to six methyl groups attached to and up to two cyclopentyl moieties included in their alkyl chains (Weijers et al., 2007a). The BIT index is the ratio between the three branched GDGTs without cyclopentyl moieties and crenarchaeol. Recently it has been shown that the BIT index might underestimate terrigenous input if the organic matter is not soil- or peat-derived (Walsh et al., 2008). Accordingly, the BIT index can be used for identifying soil organic carbon in aquatic sediments (Weijers et al., 2009b).

The distribution of branched GDGTs in soils and peats is mainly controlled by temperature and soil pH. The latter is correlated with the cyclization ratio of branched GDGTs (CBT), a measure for the relative amount of cyclopentyl moieties within the branched GDGTs. The degree of methylation, expressed in the methylation index of branched GDGTs (MBT), depends on soil pH and mean annual air temperature (MAT) (Weijers et al., 2007a). Accordingly, branched GDGTs and MBT/CBT proxies have been used for the reconstruction of paleoclimatic conditions from marine (Weijers et al., 2007b; Rueda et al., 2009; Bendle et al., 2010) and lacustrine sediments (Blaga et al., 2009; Tyler et al., 2010; Loomis et al., 2011) and soils (Sinninghe Damsté et al., 2008; Peterse et al., 2009a; Weijers et al., 2011). However, increasing evidence exists indicating that branched GDGTs are not only produced in soils and peats as previously suggested (Weijers et al., 2006b) but also in situ within lakes and possibly even river channels (Tierney and Russell, 2009; Bechtel et al., 2010; Tierney et al., 2010; Zink et al., 2010; Loomis et al., 2011; Zhu et al., 2011).

GDGTs have been analyzed in all continental margin sediments examined in this thesis. However, while the BIT index was calculated for all settings sea surface temperatures based on TEX_{86} were only reconstructed for the Gulf of Guinea where the BIT was relatively low. On the contrary, GDGTs for the calculation of CBT/MBT values and therefore reconstruction of soil pH and MAT were only measured in Amazon shelf and fan sediments with a high BIT.

1.4.3 Stable carbon isotopes

Stable carbon isotopes have widely been used to determine the origin of organic carbon in sediments. The relative inputs of marine and terrigenous organic matter can be assessed by stable carbon isotope analysis of total organic carbon in marine sediments (e.g. Showers and Angle, 1986; Westerhausen et al., 1993; Schlünz et al., 1999). This application is based on deviating carbon isotopic values caused by the different photosynthetic pathways of carbon fixation in plants. Higher plants can be separated in C_3 plants which fix CO_2 following the Calvin-Benson cycle (nearly all trees and shrubs as well as grasses and sedges in of from temperate and cold climate zones) and C_4 plants using the Hatch-Slack-cycle (mostly (sub-)tropical grasses and sedges) (Farquhar et al., 1989; Cerling et al., 1997). Carbon isotopic values of C_3 plants range from -22 to -36 ‰ (average: -27 ‰) while the carbon isotopic values of C_4 plants vary between -10 and -15 ‰ (average: -13 ‰) (Deines, 1980; O'Leary, 1988; Mariotti, 1991). Organic matter produced by marine phytoplankton, on the contrary, has carbon isotopic values of -19 to -22 ‰ (Meyers, 1994). Stable carbon isotopes have been used to identify terrigenous contributions in Amazon (shelf and) fan sediments.

1.5 Thesis Outline

Different regions of the Atlantic Ocean have been chosen to assess the terrigenous input to these locations based on various inorganic and organic parameters. The results of these studies are reported in three manuscripts in the following chapters.

Chapter 2: Chemical composition of eolian dust over the Atlantic Ocean off NW-Africa
Wiebke Kallweit and Matthias Zabel (in preparation for submission to Journal of Geophysical Research)

The Sahara-Sahel Dust Corridor of North Africa has been reported to be the world's largest dust source area. Many studies have tried to identify the different source regions and the chemical and physical properties of the eolian dust from these regions. The main objective of this study was to better assess the primary signal of the eolian dust as a 'background value' for the interpretation of element ratios in marine sediments. However, the results clearly indicate a large variability in the chemical composition of the eolian dust. The extent and the possible reasons for this variability are discussed in this manuscript.

Chapter 3: Biomarker evidence for old carbon transport to the Late Quaternary Amazon shelf and deep sea fan

Wiebke Kallweit, Helen M. Talbot, Gesine Mollenhauer, Arnoud Boom, Thomas Wagner and Matthias Zabel (submitted to Geochimica et Cosmochimica Acta; under review)

The fate of terrigenous organic carbon after its delivery into the marine environment is of great importance for the global carbon cycle. Continental margin systems with large rivers are of special importance as large amounts of terrigenous material are deposited in these regions. However, reworking plays an important role in these environments. Additionally, terrigenous organic carbon may have been substantially pre-aged during storage in soils and floodplains.

The terrigenous input into sediments from the Amazon shelf and deep sea fan has been investigated based on the Al/Ti-ratios, soil-marker BHPs, branched GDGTs and the BIT index. Further BHPs were measured to identify additional carbon sources. Unexpectedly invariant BHP and branched GDGT compositions indicate that the material was delivered from one single source region, possibly a floodplain lake based on the high abundances of BHPs specific for aerobic methane oxidation. The results indicate that the deposition of reworked OC is more important than commonly considered. An additional topic of the manuscript is the reconstruction of paleo-continental mean air temperatures and soil pH-values.

Chapter 4: Multi-proxy reconstruction of terrigenous input and sea-surface temperatures in the eastern Gulf of Guinea over the last ~35 ka

Wiebke Kallweit, Gesine Mollenhauer and Matthias Zabel (submitted to Marine Geology)

A well-dated core from the Gulf of Guinea off the Niger River mouth has been chosen to evaluate the input of terrigenous organic carbon into the eastern equatorial Atlantic during the last ~35 ka BP. Besides the BIT index accumulation rates of terrigenous (aluminum and branched GDGTs) and marine compounds (carbonate and crenarchaeol) were calculated to assess the importance of terrigenous input and marine productivity. Al AR and branched GDGT AR were compared to records of paleo-discharge and the rate of mean sea level change to reveal which factors control the deposition of terrigenous material on the Niger Fan.

Additionally, paleo-sea surface temperatures (SSTs) were reconstructed using the TEX_{86}^{H}-index (Kim et al., 2010). TEX_{86}^{H}-SST estimates were compared to published SST-reconstructions based on

the Mg/Ca-ratio of planktonic foraminifera (Weldeab et al., 2007b). TEX_{86}^{H} -based SSTs show a cold-bias and a larger temperature difference between the Holocene and the last glacial period of this record compared to Mg/Ca-SST estimates. Possible reasons for the cold-bias and the paleoclimatic implications of the record are discussed.

2. Manuscript I

Chemical composition of eolian dust over the Atlantic Ocean off NW-Africa

Wiebke Kallweit[a], Matthias Zabel[b]

[a] University of Bremen, Department of Geosciences, P.O. Box 330440, 28334 Bremen, Germany

[b] University of Bremen, MARUM – Center for Marine Environmental Sciences, P.O. Box 330440, 28334 Bremen, Germany

Manuscript in preparation for submission to *Journal of Geophysical Research – Atmospheres*.

Abstract

The chemical composition of eolian dust sampled at sea level off the West-African coast has been investigated by ICP-AES. Additional information about the source regions and transport paths of the eolian dust were gained from daily satellite images generated by the total ozone mapping spectrometer and calculation of four-day back trajectories. The chemical composition of the eolian dust samples is highly variable and seems to be related to the latitudinal sampling position and the relative dust amount in the atmosphere. Highest variability is generally observed in samples taken under dust-free conditions while element ratios of samples from high-dust conditions are relatively close to crustal values. The samples have been influenced by the admixture of sea spray aerosols. Strongly elevated K/Al-ratios especially in the region between the equator and 10°N indicate the admixture of biomass burning aerosols. The admixture of different aerosols and the modification by environmental factors such as wind strength and transport path have presumably led to the large variability in the chemical composition. Hence a clear source assignment was not possible for the dust samples. The large variation in the chemical composition of eolian dust needs to be considered if the element ratios of the dust fraction of marine sediments are interpreted. However, as sediments integrate over a long time period and include many dust events, the variability in the chemical composition of marine sediments might be reduced in comparison to the individual eolian dust signals.

2.1 Introduction

Eolian dust has been recognized as having large effects on the Earth's climate and ecosystems (e.g. Tegen et al., 1996; Goudie and Middleton, 2001; Prospero et al., 2002). This includes an impact on the Earth's radiation balance (Li et al., 1996; Tegen et al., 1996; Moulin et al., 1997), precipitation (Prospero and Lamb, 2003), cloud nucleation properties (Wurzler et al., 2000) and air chemistry (Middleton and Goudie, 2001). Deposition of eolian dust may enhance biological productivity in oceans (e.g. Baker et al., 2003 and references therein; Jickells et al., 2005) or fertilize terrestrial ecosystems like the Amazon rainforest after long-distance transport (Swap et al., 1992; Bristow et al., 2010).

The world's largest dust source area is located on the African continent and has been designated as the Sahara Sahel Dust Corridor. This region includes major dust source regions such as the Bodélé Depression, the Hoggar Massif and the West African carbonate-rich Atlantic coastal basin (Moreno et al., 2006). Dust transport from the African continent to the Atlantic Ocean occurs in three distinct wind systems (Pye, 1987). Dust from the Atlas Mountains and coastal plain is transported in the shallow trade wind layer nearly parallel to the coast. This low layer dust transport occurs throughout the year at an altitude of only 500 – 1500 m and deposits its dust load in the proximal parts of the Atlantic Ocean. High-level dust transport occurs at a mid tropospheric level of about 3000 m in the Saharan Air Layer (SAL) which is especially active in boreal summer (Pye, 1987). Transport in the SAL is characterized by a series of large easterly waves propagating westward at a velocity of 8 m/s (Reed et al., 1977). The SAL is divided into two branches, the northern branch transporting dust towards the Canary Islands and the western branch transporting eolian dust across the Atlantic until the Caribbean and South America (Prospero and Carlson, 1972). As specific part of the northeast trade winds the Harmattan transports dust from the central Sahara and especially the Bodélé Depression to the west. The Harmattan is a year-round feature but reveals its highest activity during boreal winter (Pye, 1987).

The Saharan dust plume shows a clear latitudinal shift between summer and winter conditions (Fig. 2.1; Ginoux et al., 2001). This shift is caused by the movement of the Intertropical Convergence Zone (ITCZ) from its summer position at 20°N to ~5°N in boreal winter (Sunnu et al., 2008). The origin of eolian dust and the pathways of dust transports are largely affected by the shift of the ITCZ (Husar et al., 1997; Middleton and Goudie, 2001).

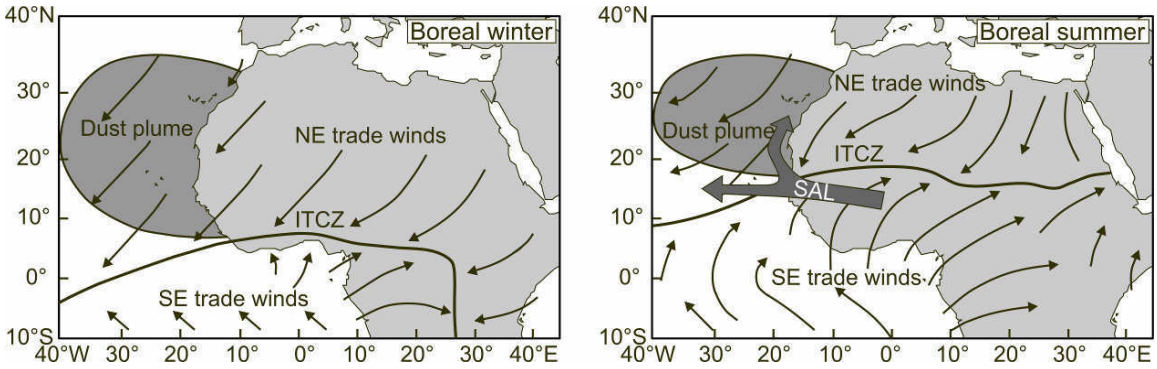

Figure 2.1: Seasonal shift in the latitudinal position of the ITCZ, resulting dust plumes and atmospheric conditions (modified after Ruddiman, 2001; Stuut et al., 2005). Left: Boreal winter conditions; right: boreal summer conditions. Arrows indicate the main wind directions. ITCZ = Intertropical Convergence Zone. SAL = Saharan Air Layer.

Many studies have focused on the characterization of eolian dust and the dust source regions (e.g. Chester et al., 1971; Schütz and Rahn, 1982; Chiapello et al., 1997; Caquineau et al., 1998; Middleton and Goudie, 2001; Caquineau et al., 2002; Stuut et al., 2005). Several of these studies have also characterized the elemental composition of eolian dust from different source regions (Moreno et al., 2006; Castillo et al., 2008; Bristow et al., 2010) or from dust samples taken during its transport over the Atlantic Ocean (Bergametti et al., 1989; Jiménez-Vélez et al., 2009). Comparison between different studies reveals similarities in the chemical composition. However, other studies report a high variability in element concentrations between the dust samples (Gaudichet et al., 1995; Johansen et al., 2000).

In this context we aimed at identifying the chemical composition of eolian dust and its spatial and temporal variation. This is especially important for the characterization and interpretation of element ratios and concentrations measured in the eolian dust fraction of marine sediments. 93 samples of eolian dust have been collected at sea level off the West-African coast between the equator and 35°N (Fig. 2.2). Here we present the results of the analysis of the chemical composition of these samples by ICP-AES. Element data were compared to the daily satellite images of the Total Ozone Mapping Spectrometer (TOMS) (http://jwocky.gsfc.nasa.gov/aerosols/aerosols_v8.html) and the aerosol optical depth revealed from these images. Additional information on dust sources and wind directions were gained by calculation of four-day back trajectories using the Lagrangian Integrated Trajectory (HYSPLIT) model of the National Oceanic and Atmospheric Administration (NOAA) (http://ready.arl.noaa.gov/HYSPLIT.php). Back trajectories were calculated for four different altitudes (10, 500, 1000 and 3000 m). These data provide insight into the variability of the element

composition of eolian dust and the complexity of different factors influencing the elemental signature.

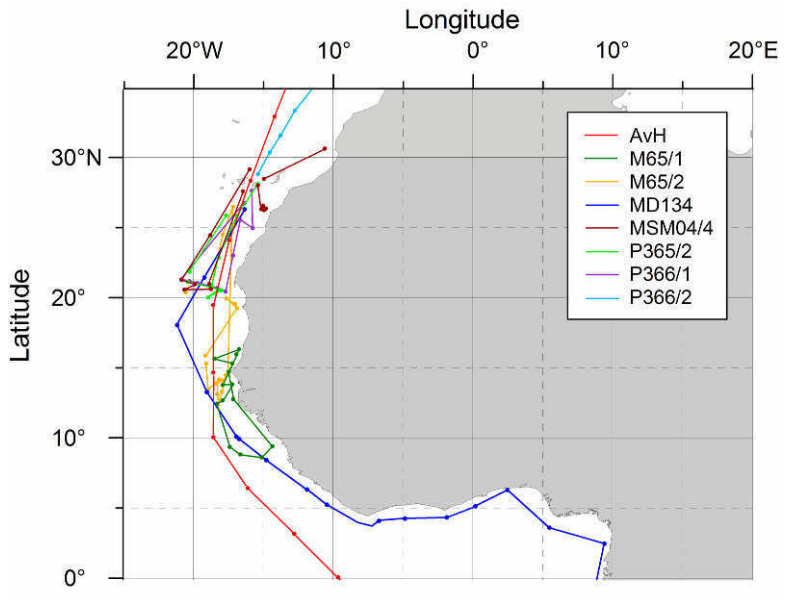

Figure 2.2. Cruise tracks (sampling locations) of eolian dust samples off the West-African coast. Meteor cruises are denoted with M (e.g. M41/1: Meteor cruise 41 leg 1), Poseidon cruises with P (e.g. P365/2: Poseidon cruise 365 leg 2). MSM04/4 = Maria S. Merian cruise 04 leg 4, AvH = Alexander von Humboldt cruise 44-04-01, MD134 = Marion Dufresne cruise 134. A list of all samples can be found in Supplementary Table 2.S1.

2.2 Experimental

2.2.1 Sampling

The eolian dust load at sea level was sampled between 2003 and 2008 during different seasons on eight cruises off the NW-African coast e.g. with the German research vessels Meteor and Poseidon. For this purpose a high-volume dust sampler was installed in the mast of the ship. The surrounding air was sucked in by an engine inside the dust sampler and the aerosols were collected on cellulose acetate filters (Whatman, Type 41). To prevent contamination by the ship's exhaust the dust sampler was equipped with a wind direction sensor system. Sampling was stopped at low wind speed or when the relative wind deviated more than 90° from the ship's heading. Filters were stored in plastic bags until analysis.

2.2.2 Total digestion

Total digestion was carried out with two microwave systems (MLS Mega II; MLS Ethos 1600). For this purpose, filter pieces of about 5 × 5 cm in size were placed in Teflon liners and 3 ml concentrated HNO_3 (65 %), 2 ml of HF (47 %) and 2 ml of HCl (30 %) were added. All acids were of suprapure quality. After heating at a temperature of 215°C under a pressure of at maximum 30 bar, the acids were evaporated to near dryness and the residues were re-dissolved in 0.5 ml concentrated HNO_3 and 4.5 ml deionized water (MilliQ). Homogenization was achieved by heating the solutions again to 200°C in the microwave systems. Solutions were filled up to 50 ml by adding 45 ml of deionized water.

Measurement of elements was carried out with inductively coupled plasma atomic emission spectrometry (ICP-AES; Perkin Elmer, Optima 3300 R). Several pieces of unused filters have been digested and measured following the same procedure to gain background values of element concentrations. Measured element concentrations were corrected for these background values.

2.3 Results

Scanning electron micrographs mainly show silicates and SiO_2 but also carbonates and apatite as well as diatom fragments and organic matter (Fig. 2.3) within the eolian dust samples. Additionally, gypsum has been detected which is partly present in delicate needles that must have grown on the filters during the sampling period (Fig. 2.3b). Gypsum formation on filters has already been described three decades ago and seems to be the result of the reaction between calcite in dust with atmospheric sulfur species (Glaccum and Prospero, 1980).

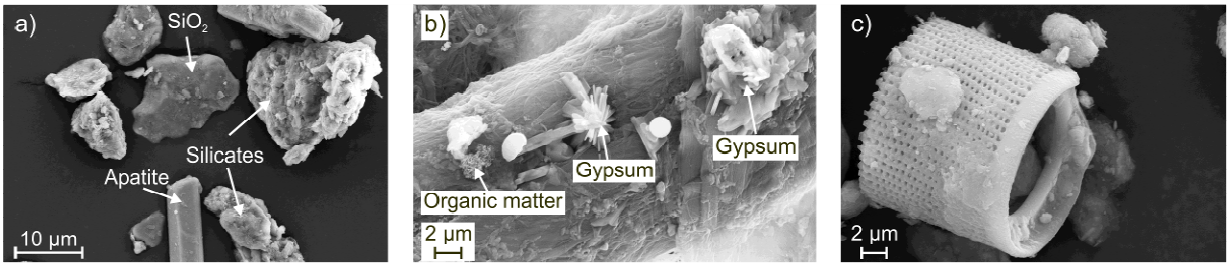

Figure 2.3. Scanning electron micrographs of eolian dust. a) Silicates, SiO_2 and apatite in dust from Meteor cruise M65/2. b) Organic matter and gypsum crystals on a cellulose acetate filter from Maria S. Merian cruise MSM04/4. c) Diatom fragment found in dust sample from Meteor cruise M65/2.

Element concentrations within the eolian dust samples investigated in this study are highly variable, which can also be observed when different elements are plotted together in a ternary diagram. A ternary diagram including iron, potassium and aluminum is shown in Figure 2.4.

Samples included in this plot were differentiated according to their mean latitudinal sampling position. A clear latitudinal trend in element abundances, however, is not visible. The samples plot in a line leading from the K apex to a value of about 40 % Fe. Lowest K abundances (mainly less than 20 %) and the least scatter are noted for samples taken between 10 and 20°N. Element abundances from other publications (see caption of Figure 2.4 for references) show a deviating trend with comparably low K concentrations and a trend towards increased relative Fe contents. This is especially apparent for samples taken at Fuerteventura while the relative Fe abundances in aerosol samples are more similar to our data.

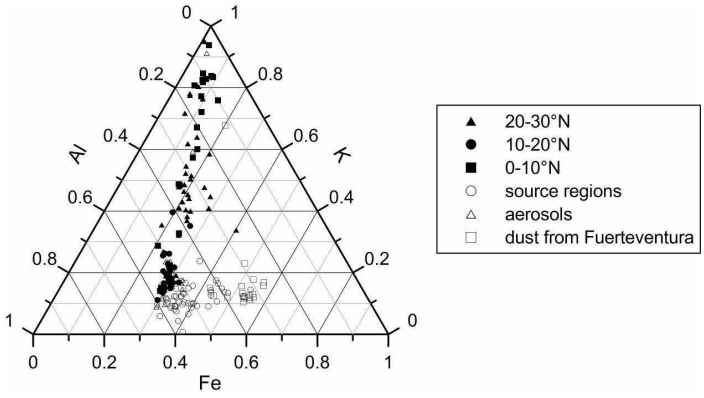

Figure 2.4. Ternary diagram including Fe, K and Al. Samples are from this study (filled symbols) and from the literature (open symbols). Published values have been taken from Chester et al. (1979), Bergametti et al. (1989), Arimoto et al. (1995), Gaudichet et al. (1995), Hermann et al. (1996), Johansen et al. (2000), Goudie & Middleton (2001), Moreno et al. (2006), Castillo et al. (2008), Formenti et al. (2008), Jiménez-Vélez et al. (2009) and Bristow et al. (2010).

Calculated element ratios are mainly in the range of reported values (Supplementary Table 2.S1). Element ratios have been plotted against the mean latitudinal sampling position of the respective samples. It is obvious that the sampling location influences not only the absolute element ratios but in particular the scatter of the values. Figure 2.5a shows the Fe/Al-ratio plotted against latitude from the equator to 35°N. It is apparent that the Fe/Al-ratio ranges between 0.5 and 0.6 in the majority of our samples. However, several differences can be noted when considering the mean latitudinal distribution of Fe/Al-ratios. Largest scatter is observed in the region between the equator and 10°N (values between 0.35 and 1.40) and north of 20°N (Fe/Al between 0.16 and 0.99; one outlier at 1.55; Supplementary Table 2.S1). Contrastingly, samples taken between 10 and 20°N show a very constant Fe/Al-ratio plotting in a narrow band between 0.47 and 0.70.

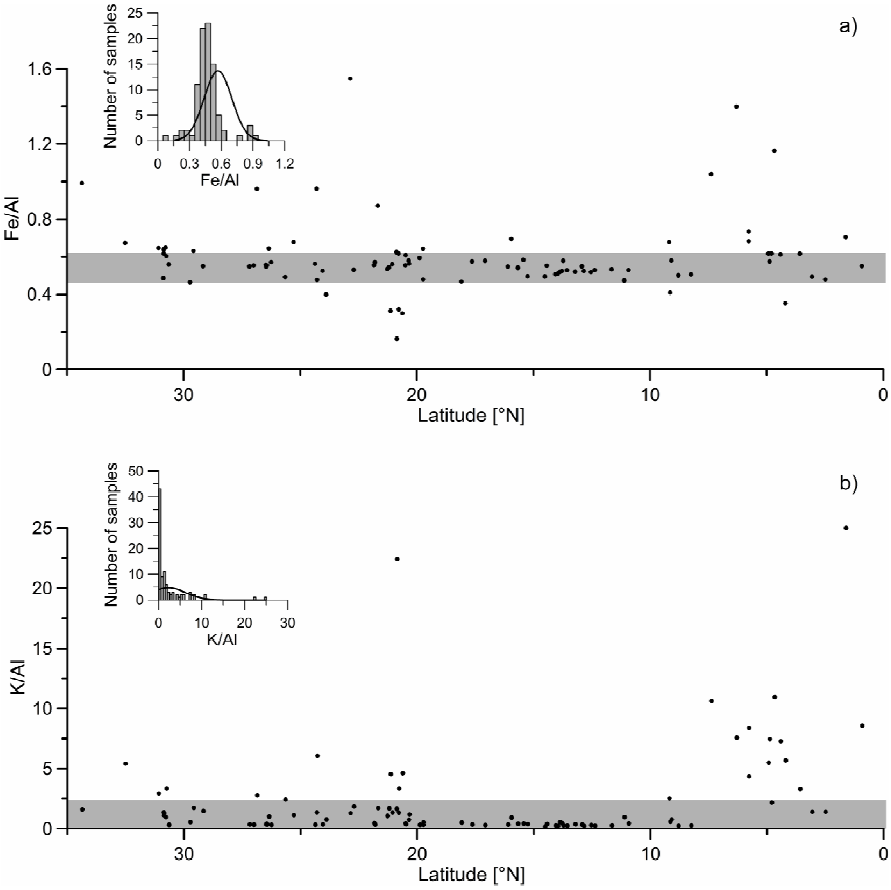

Figure 2.5. Element ratios plotted against the mean latitudinal sampling location. a) Fe/Al-ratio. b) K/Al-ratio. Inserted figures show histograms of the respective element ratios. Gray bars indicate the range where the majority of samples plot.

Similar observations can be made when the K/Al-ratio is plotted against mean sampling latitude (Fig. 2.5b). The majority of samples plots between K/Al-ratios of 0 and 2, reflecting elevated potassium concentrations. Large deviations from the median value of 0.5 are observed between 0 and 10°N, with outliers reaching values up to 12 or even higher (one value above 20). A narrow range of K/Al-ratios is noted between 10 and 20°N where values scatter only between 0.19 and 0.97. North of 20°N the values plot within a broader range 0.32 to 6.07; one outlier at 22.42), but deviations as large as in the equatorial samples are generally not observed.

Latitudinal distributions of other element to Al ratios – specifically the Ti/Al- and Ca/Al-ratios (Supplementary Table 2.S1) – show features similar to those of the Fe/Al- and K/Al-ratios. Additionally, element ratios including only elements with a mainly lithogenic source (Ba, Fe, Ti, Al) show a normal distribution while element to aluminum-ratio distributions including elements with an additional source deviate from the Gaussian distribution (Fig. 2.5). This applies for example for Ca and K which both have a lithogenic source but may also be derived from sea spray aerosols.

2.4. Discussion

2.4.1 Ternary diagrams

Median element concentrations and element to aluminum ratios of high dust samples have been reported to be close to those of the Upper Continental Crust (Arimoto et al., 1995; Washington et al., 2009; Bristow et al., 2010; Trapp et al., 2010). This can be supported by the results obtained in this study even though e.g. the majority of Fe/Al-ratios from our study (around 0.55) is slightly higher than the reported values (0.4 to 0.48; Washington et al., 2009). However, it has also been shown that the dust concentrations as well as the element ratios within the dust are highly variable from one day to another (Arimoto et al., 1995; Arimoto, 2001; Sunnu et al., 2008). A very high variability in elemental composition has also been observed during this study where very different values were measured even of samples taken at one position on several days in sequence. Even though element ratios have been used as tracers for dust origin before (e.g. Bergametti et al., 1989; Chiapello et al., 1997) it has proven very difficult to use specific elements for the identification of dust cloud origins (Arimoto, 2001; Trapp et al., 2010; this study). Mineral aerosols from different sources are already mixed during uplifting of the particles, leading to a fast homogenization of the aerosols and hindering a clear source assignment (Schütz and Sebert, 1987; Trapp et al., 2010).

The large scatter in element distributions is clearly recognized in ternary diagrams, especially if at least one element with a not-only lithogenic source is included. It is also apparent that literature values plot only partly in the range of our data but show a deviating trend for many samples. If one sea spray element (e.g. potassium; Fig. 2.4a) is plotted together with the two lithogenic elements Fe and Al data scatter along a line originating at the K apex. This implies that the K content of the samples is highly variable while the Fe/Al-ratio stays rather constant (~0.5). A similar trend can be observed if other sea spray elements (Mg or Ca) are plotted instead of K, suggesting that the lithogenic element composition is rather constant while the large variability in element distributions is caused by the admixture of sea spray elements. This can also be inferred from a significant correlation between the different sea spray elements for samples taken north of 10°N, even though it should be considered that these elements have additional lithogenic sources. Carbonates (and therefore calcium) have been reported to be abundant in Western Saharan and northern Saharan samples (e.g. Schütz and Sebert, 1987; Chiapello et al., 1997; Moreno et al., 2006) while magnesium (from dolomites) was reported to be typical for the NE-trade winds (Chester et al., 1972). However, as this trend was not observed in our samples and based on the

correlation of the sea spray elements, we suggest that carbonates – even though they have been identified in SEM micrographs – play a minor role in our samples. It is therefore likely that the dust present in our samples did not originate from the carbonate-rich Western Sahara but from more siliciclastic source regions.

Contrastingly, for literature values no correlation between sea spray elements was found, arguing against the admixture of considerable amounts of sea spray aerosols to these samples. In comparison with our data highest similarity is observed for aerosol samples taken over the Atlantic Ocean (Jiménez-Vélez et al., 2009) – probably due to the influence of sea spray – or the equatorial African continent (Gaudichet et al., 1995; Goudie & Middleton, 2001). Aerosol samples from the main source regions (Moreno et al., 2006; Bristow et al., 2010) or from Fuerteventura (Bergametti et al., 1989) on the contrary show considerably higher Fe concentrations than our samples.

2.4.2 Latitudinal trends

Nevertheless, certain distinctions can be made based on the latitudinal distribution of element to aluminum-ratios. The most prominent feature is a very narrow range of element ratios between 10 and 20°N (Fig. 2.5). The majority of the samples from these latitudes were collected during summer, many of them within a dust cloud as revealed from TOMS satellite images. This is consistent with reports of highest dust transport activity within the SAL in boreal summer (Pye, 1987; Prospero et al., 2002). The detection of diatom fragments (Fig. 2.3c) in some of our samples leads to the conclusion that the dust collected in this region originated at least partly from the Bodélé Depression as the diatom fragments show a high similarity to those described from the Chad Basin by Moreno et al. (2006). Back trajectories calculated with the Hysplit model also confirm this source assignment. Even though winds at lower levels mainly show a coast-parallel direction, representing the NE-trade winds, or come from the open ocean, the 3000 m-trajectory – corresponding to the height of the SAL – clearly points to the African continent. For many samples this trajectory can even be tracked back to the Bodélé Depression. The relatively constant chemical composition of aerosol samples from this region indicates that dust was transported from the Chad Basin even if TOMS satellite images do not show a high atmospheric dust concentration.

A much greater variability in element to aluminum-ratios can be observed between the equator and a position of 10°N. Most samples at these latitudinal positions were taken during summer and therefore south of the ITCZ and within the range of the southeast trade winds as is confirmed by the low-level back trajectories. The back trajectory at an altitude of 3000 m, however, originates

from the African continent for most of these samples. Nevertheless, TOMS satellite images reveal that dust-free conditions prevailed during many sampling periods and that only low dust amounts were transported in other time periods. The large scatter in element ratios might have been caused by these low dust amounts in the atmosphere (section 2.4.3).

A large scatter in element to aluminum-ratios is also observed in samples taken north of 20°N. Even though the aerosols were mainly transported to the sampling locations by the NE-trade winds the air parcels transporting them actually originated from the northern or northwestern Atlantic. The oceanic origin of the air masses implies that only little dust transport from the African continent occurred. This can be confirmed by the TOMS satellite images showing little or no dust in the atmosphere during the sampling periods.

The Fe/Al-ratio has been reported to be considerably higher if the dust has been emitted from a Sahelian source than if the dust is derived from the northern Sahara (1.51 – 1.76 vs. 0.99 – 1.24; Bergametti et al., 1989). However, other studies have established clearly lower Fe/Al-ratios (0.10 – 0.78) for eolian dust irrespective of the different source regions (e.g. Goudie and Middleton, 2001; Moreno et al., 2006; Jiménez-Vélez et al., 2009; Bristow et al., 2010). Data of this study are within the range of reported values with a maximum between 0.5 and 0.6 and only four samples representing a Fe/Al-ratio larger than 1. A source assignment according to Bergametti et al. (1989) is not possible for our samples.

A clear discrepancy is noted by the comparison of K/Al-ratios from our study and published values. While published K/Al-ratios are mainly below 0.5 (median at 0.29), about 60 % of our samples show elevated K/Al-ratios (> 0.5). Most literature values describe dust from the source regions (Moreno et al., 2006; Castillo et al., 2008; Bristow et al., 2010) which reflects the primary signal and has not yet been mixed with sea spray or biomass burning aerosols. Strongly elevated K/Al-ratios have been reported in plumes of biomass burning aerosols (Andreae, 1983; Gaudichet et al., 1995). According to the maps of the fire information for resource management system (FIRMS; http://maps.geog.umd.edu/firms) biomass burning is very common in a band between 10°N and the equator. Highest K/Al-ratios in our samples have been recorded exactly in this region and especially in the samples taken during the summer months. According to Torres et al. (2002) the biomass burning season in Central Africa starts in July. This is consistent with our observations of only slightly elevated K/Al-ratios for samples taken in the end of June in contrast to very high K/Al-ratios in samples from August. Samples taken during winter do usually not show elevated K/Al-ratios.

Elevated K/Al-ratios have also been reported for some dust samples from Fuerteventura (Bergametti et al., 1989) but these were – with one exception – below 1 and therefore lower than the values from this study. However, elevated K/Al-ratios suggest that biomass burning has also influenced several of our samples taken north of 20°N. Back trajectories and FIRMS fire maps reveal that for many samples with an elevated K/Al-ratio at least one trajectory (often at 3000 m altitude) originated in or passed through a region where biomass burning occurred. Even though biomass burning can not explain all elevated K/Al values it seems to have a large impact on the potassium content of eolian dust. However, evidence exists that elevated K concentrations may also be caused by the admixture of sea spray aerosols (section 2.4.1). This might be especially valid for those samples showing elevated K concentrations but no clear connection to biomass burning areas, but also for samples taken north of 20°N.

2.4.3 Atmospheric dust amounts and the chemical composition

A certain relationship can be observed between the dust amount in the atmosphere (based on TOMS satellite images) and the element to aluminum-ratios calculated for our samples (Supplementary Table 2.S1). Figure 2.6 shows the Fe/Al- and K/Al-ratios sorted by the relative dust amount that was present in the atmosphere during sampling as revealed by TOMS. It is obvious – especially in the Fe/Al-ratios – that the lower the dust amount in the atmosphere the larger the variability in element ratios. This could explain the large scatter in element to aluminum-ratios north of 20°N where only small dust amounts – if any – were present in the atmosphere. In contrast to this, many samples taken between 10 and 20°N were collected under high-dust conditions and therefore show a much smaller scatter in their chemical composition. It is suggested that under high-dust conditions aerosols mainly reflect the signature of the source region whereat the admixture of different aerosols (e.g. from sea spray) only has a negligible influence on the chemical composition of these samples. Contrastingly, the signature of the dust source regions is overprinted by the admixture of different aerosols under low-dust conditions.

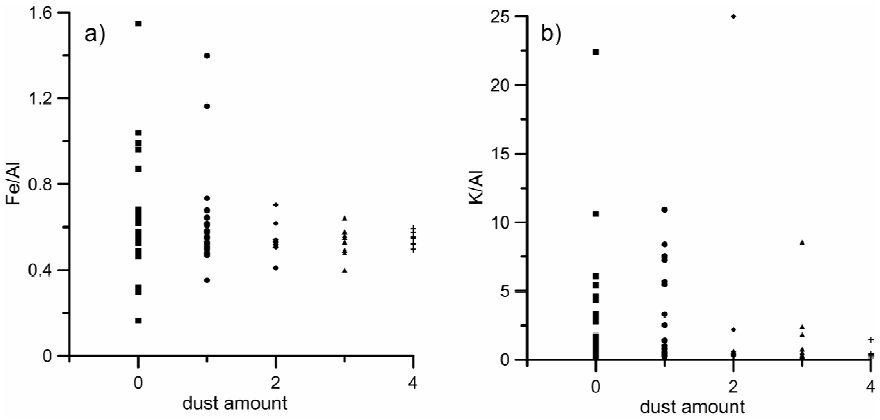

Figure 2.6. Dust amount in the atmosphere as derived from TOMS satellite images plotted against a) the Fe/Al-ratio and b) the K/Al-ratio. Dust amounts are subdivided into five groups from 0 (no dust) to 4 (very much dust).

However, the relationship between the dust amount in the atmosphere and the aerosol chemical composition seems to be influenced by additional factors that lead to a more complicated picture. Wind direction and transport path of the dust can vary considerably between different atmospheric heights. TOMS satellite images mainly reflect the dust concentration in the middle and upper troposphere and in the stratosphere, and therefore in the heights of long distance transport. In contrast to this, aerosols transported below 1000 m altitude are usually not detected by TOMS (Torres et al., 1998; Prospero et al., 2002; Torres et al., 2002). While TOMS satellite images might therefore imply that a sample has been taken under dust-free conditions, back trajectories might reveal that dust was transported from the continent on a lower altitude which was then collected by the dust sampler. Additionally, air parcels might have circulated over the Atlantic Ocean during the days before sampling or the aerosol might even have an overall non-African source. A high variability in the chemical composition of eolian dust is caused by the mixture of dust from different source regions during transport as well as the admixture of sea spray-, biomass burning- and anthropogenic aerosols.

All these factors mentioned above do not only have an impact on the chemical composition but also on the grain-size distribution of eolian dust (Stuut et al., 2005). Moreover, the chemical composition of the eolian dust is also influenced by the grain-size distribution. This is already apparent if samples from the source regions are separated in different grain-size fractions as it has been done by Castillo et al. (2008). With phyllosilicates being especially abundant in the finer fractions of the dust the concentrations of Al, Fe and Mg are high in the fine fraction whereas Ti and K abundances – and therefore Ti/Al- and K/Al-ratios – increase with coarsening of the material. However, a large spread in the grain sizes of aerosols has been reported from the region off the West-African coast, mainly assigned to differing wind strength and dust availability.

Additionally, very similar grain-size distributions can be caused by dust transport from very different source regions and along totally different transport paths (Stuut et al., 2005). The same has been observed in this study for the chemical composition of eolian dust which explains its large variability and clearly complicates the source assignment of the particles.

It has become very clear that many different factors can influence the chemical composition of eolian dust. The combination of these factors leads to a higher diversity of element signatures in dust as it would be expected from the signals of the main dust source regions only. This variability has to be taken into account when interpreting the chemical composition of the dust fraction in marine sediments. However, it should be kept in mind that sediments reflect a much longer time period than eolian dust samples. The sedimentary signal therefore always integrates a large quantity of dust events which might reduce the variability of element concentrations and ratios measured in sediments. Further research is needed concerning the coupling between the chemical composition of eolian dust and that of marine sediments, including an assessment of the alteration processes affecting the primary signal.

2.5 Conclusions

The chemical composition of eolian dust sampled off the NW-African coast is highly variable. This variability in element ratios and concentrations is apparently linked to the latitudinal sampling position and the relative dust amount in the atmosphere. If dust samples are plotted according to their latitudinal sampling position it is noted that a large scatter in element ratios occurs between the equator and 10°N and north of 20°N while samples taken between 10 and 20°N show relatively constant, near-crustal values. Back trajectories and diatom fragments in some samples reveal that at least a part of these aerosols was transported by the Saharan Air Layer (SAL) and originated in the Chad Basin. The relatively constant element ratios in samples taken between 10 and 20°N are probably due to the fact that many of the samples were taken under high-dust conditions. Decreasing atmospheric dust amounts generally lead to a higher variability in the chemical composition of the aerosols. This might have caused the larger scatter in element ratios of samples taken between the equator and 10°N as well as north of 20°N. A possible explanation for the larger variability in the chemical composition of samples taken under low-dust conditions might be an increasing importance of aerosol admixtures e.g. from sea spray or biomass burning. The latter mainly influences the K/Al-ratio which can be extremely increased in fire plumes. Biomass burning is especially abundant in a band between the equator and 10°N which is clearly observed in the highly elevated K/Al-ratios of our samples taken in this region.

The chemical composition of eolian dust is initially defined by the rocks and sediments of the source regions. During transport several additional factors influence the chemical composition of the dust, including wind direction and strength as well as the transport path. The grain-size distribution is also modified by these factors but grain size also influences the chemical composition as Al, Fe and Mg are present especially in the finer material whereas highest K and Ti concentrations can be found in the coarse fraction. The large variability in the chemical composition of eolian dust is certainly caused by the interplay of all these factors. A clear source assignment is thereby significantly hindered. For the interpretation of sedimentary records it should be considered that the aerosols deposited in the Atlantic Ocean can have very different chemical compositions which might also be expressed in the sediments. However, as sediments reflect a much longer time period and integrate over a large quantity of dust events the variability in the chemical composition of marine sediments might be reduced in comparison to the eolian dust signal.

Acknowledgments

We thank Karsten Enneking and Silvana Pape for laboratory assistance. Petra Witte is thanked for help with the preparation of SEM images. This research was funded by the DFG-graduate college EUROPROX.

2.6 Supplementary Table

Supplementary Table 2.S1. Sampling location, element ratios and relative dust amounts for eolian dust samples.

	Start		Stop						
Sample no.[a]	Longitude [°W]	Latitude [°N]	Longitude [°W]	Latitude [°N]	Fe/Al	K/Al	Ti/Al	Ca/Al	dust amount[b]
AvH-5	-14.1717	32.9283	-15.9050	28.3533	0.56	0.32	0.07	1.48	0
AvH-6	-15.9050	28.3533	-17.3767	24.1167	0.57	0.32	0.07	0.99	0
AvH-7	-17.3767	24.1167	-18.5583	19.4917	0.57	0.35	0.07	0.90	0
AvH-8	-18.5583	19.4917	-18.5567	14.6700	0.58	0.29	0.07	0.89	0
AvH-9	-18.5567	14.6700	-18.5550	10.0750	0.53	0.25	0.07	0.67	2
AvH-10	-18.5550	10.0750	-16.0983	6.4217	0.51	0.27	0.06	0.47	2
AvH-11	-16.0983	6.4217	-12.7983	3.1717	0.62	2.17	0.04	2.83	2
AvH-12	-12.7983	3.1717	-9.6467	0.0600	0.70	25.96	0.04	42.73	2
M65/1-1	-17.3600	14.6500	-16.8840	15.8615	0.50	0.39	0.06	0.63	4
M65/1-2	-16.9063	15.8873	-16.6910	16.3005	0.55	0.35	0.06	1.14	4
M65/1-3	-16.6692	16.2807	-18.4077	15.6248	0.70	0.92	0.06	1.44	4
M65/1-4	-18.3525	15.6085	-17.0702	15.2640	0.58	0.44	0.08	0.98	1
M65/1-5	-17.1187	15.2447	-17.7895	13.7923	0.49	0.19	0.09	0.22	4
M65/1-6	-17.7895	13.7923	-17.1775	13.7708	0.52	0.45	0.07	0.59	4
M65/1-7	-17.1558	13.7643	-17.8418	12.6697	0.52	0.37	0.07	0.57	2
M65/1-8	-17.8672	12.6488	-18.2178	12.4323	0.52	0.30	0.07	0.47	2
M65/1-9	-18.2178	12.4323	-17.2950	9.4233	0.53	0.44	0.08	0.78	2
M65/1-10	-17.2950	9.4233	-16.5933	8.8733	0.41	0.57	0.08	0.77	2
M65/1-11	-16.5933	8.8733	-15.1255	8.7093	0.50	0.25	0.07	0.36	1
M65/1-12	-15.1255	8.7093	-14.3572	9.4593	0.58	0.77	0.08	0.93	1
M65/1-13	-14.3735	9.4745	-17.0733	12.7467	0.47	0.97	0.09	0.98	1
M65/1-14	-17.0767	12.7813	-17.4272	14.6775	0.58	0.28	0.07	0.98	3
M65/2-1	-17.6075	14.5922	-17.8529	13.3279	0.51	0.24	0.07	0.33	0
M65/2-2	-17.8532	13.3069	-18.1536	12.5382	0.55	0.34	0.07	0.51	0
M65/2-3	-18.1747	12.5296	-18.2093	13.1574	0.52	0.24	0.06	0.46	1
M65/2-4	-18.2160	13.1787	-18.2640	13.9488	0.53	0.25	0.07	0.41	1
M65/2-5	-18.2457	13.9380	-17.9016	14.1832	0.51	0.27	0.07	0.32	1
M65/2-7	-18.1379	14.1988	-18.8652	13.5475	0.52	0.54	0.06	0.72	1
M65/2-8	-18.8776	13.5386	-19.0497	15.3199	0.55	0.40	0.07	0.95	1
M65/2-9	-19.0493	15.9320	-16.8449	19.3399	0.58	0.35	0.07	1.39	4
M65/2-10	-16.8414	19.3830	-17.5648	20.0914	0.64	0.33	0.06	1.55	3
M65/2-11	-17.5587	20.1052	-16.9540	19.6607	0.59	0.32	0.06	0.94	4
M65/2-12	-20.5071	20.4764	-20.6592	20.5108	0.55	0.45	0.07	0.99	4
M65/2-16	-18.6974	20.7690	-17.8338	24.6526	0.53	1.84	0.06	2.62	3
M65/2-17	-17.8081	24.6684	-17.0719	26.6329	0.49	2.42	0.05	1.00	3
MD134-1	-16.3040	26.3002	-19.1808	21.4722	0.40	0.77	0.12	3.03	3
MD134-2	-19.2500	21.3610	-21.1537	18.0968	0.48	0.53	0.16	0.81	3
MD134-3	-21.1535	18.0963	-21.1513	18.0895	0.47	0.50	0.22	1.50	1
MD134-4	-21.1513	18.0333	-19.0297	13.3032	0.54	0.42	0.07	1.15	2
MD134-5	-18.9954	13.2200	-16.9102	10.0833	0.53	0.27	0.06	0.67	2
MD134-6	-16.7113	9.9227	-14.8200	8.4562	0.68	2.53	0.09	1.51	1
MD134-7	-14.7449	8.3972	-11.9081	6.3473	1.04	10.61	0.12	3.18	0
MD134-8	-11.8071	6.2886	-10.4532	5.2498	0.68	4.36	0.03	1.27	0
MD134-9	-10.3954	5.2212	-6.7687	4.1199	1.16	10.93	0.00	1.96	1
MD134-10	-6.6837	4.1247	-4.8778	4.2739	0.35	5.68	0.09	2.60	1
MD134-11	-4.7939	4.2809	-1.9360	4.5275	0.61	7.27	0.06	3.71	1
MD134-12	-1.8664	4.5508	0.1294	5.2097	0.57	7.46	0.14	1.34	1
MD134-13	0.2029	5.2345	2.4641	6.3025	0.73	8.39	0.08	1.25	1
MD134-14	2.4640	6.3024	2.4434	6.3011	1.40	7.58	0.12	1.30	1
MD134-15	2.4949	6.2366	5.4572	3.6198	0.62	5.49	0.07	1.62	1
MD134-16	5.6198	3.5575	5.4983	3.6198	0.62	3.31	0.08	1.89	1
MD134-17	5.5312	3.6127	9.3944	2.5024	0.49	1.40	0.06	2.11	1
MD134-18	9.3946	2.5014	9.3908	2.4727	0.48	1.40	0.02	6.39	1
MD134-19	9.3780	2.4140	8.7591	-0.5659	0.55	8.56	0.06	1.97	3
MSM04/4-1	-14.9000	28.4667	-10.2667	30.7000	0.63	1.73	0.06	3.68	0
MSM04/4-2	-10.2667	30.7000	-10.1000	30.8500	0.65	0.97	0.06	3.08	0
MSM04/4-3	-10.1000	30.8500	-10.1000	30.8500	0.62	1.10	0.06	5.06	0
MSM04/4-4	-10.1000	30.8500	-10.2667	30.8500	0.64	1.29	0.05	3.14	0
MSM04/4-5	-10.2667	30.8500	-10.4833	30.8833	0.49	1.37	0.06	2.48	0
MSM04/4-6	-10.4833	30.8833	-10.5500	30.6000	0.60	3.34	0.08	5.79	0
MSM04/4-7	-14.8833	26.2500	-14.9333	26.3667	0.55	0.35	0.06	0.91	0
MSM04/4-8	-14.9333	26.3667	-14.9667	26.5833	0.56	0.36	0.06	1.06	1
MSM04/4-9	-14.9667	26.5833	-14.7500	26.3333	0.55	0.39	0.06	1.03	1
MSM04/4-10	-14.9833	26.5667	-15.0667	26.3333	0.55	0.42	0.07	1.30	4
MSM04/4-11	-15.0667	26.3333	-15.3333	28.0167	0.55	0.36	0.06	0.80	4
MSM04/4-12	-15.9500	29.1500	-15.9167	29.1833	0.55	1.47	0.07	1.62	4
MSM04/4-13	-15.8667	29.2167	-18.7000	24.5000	0.96	2.77	0.16	2.22	0
MSM04/4-14	-18.7500	24.4333	-20.8000	21.2833	1.55	1.30	0.08	1.52	0
MSM04/4-15	-20.8000	21.2833	-19.8333	20.9833	0.31	4.54	0.04	3.83	0
MSM04/4-16	-19.8333	20.9833	-18.0167	20.5833	0.32	3.35	0.04	3.16	0
MSM04/4-17	-17.9833	20.5833	-18.7167	20.6500	0.30	4.63	0.03	4.16	0
MSM04/4-18	-18.7000	20.7167	-18.8333	21.0000	0.16	1.29	0.02	18.58	0
MSM04/4-19	-18.8333	21.0000	-16.4000	27.5667	0.48	6.07	0.05	6.14	0

Supplementary Table 2.S1. *continued*.

	Start		Stop						
Sample no.[a]	Longitude [°W]	Latitude [°N]	Longitude [°W]	Latitude [°N]	Fe/Al	K/Al	Ti/Al	Ca/Al	dust amount[b]
P365/2-2	-20.4333	21.1833	-18.0167	20.5833	0.63	1.65	0.09	2.52	0
P365/2-3	-18.0167	20.5833	-18.9788	20.0782	0.56	1.18	0.06	2.58	0
P365/2-4	-18.9788	20.0782	-18.1834	20.6292	0.58	0.75	0.06	1.77	0
P365/2-5	-18.7167	20.8333	-18.2359	22.8496	0.55	0.45	0.06	1.04	1
P365/2-6	-18.2359	22.8496	-16.9264	25.8815	0.56	0.33	0.06	1.21	3
P365/2-7	-16.9264	25.8815	-15.4300	28.1248	0.55	0.33	0.06	1.06	1
P366/1-1	-16.2118	26.8043	-20.8058	21.2748	0.52	0.36	0.06	0.64	0
P366/1-2	-20.8058	21.2748	-20.8058	21.2748	0.53	1.07	0.09	0.80	0
P366/1-3	-20.8055	21.2748	-20.2190	21.1274	0.54	1.69	0.06	1.49	0
P366/1-4	-20.2190	21.2174	-19.6600	20.9847	0.56	1.35	0.06	1.44	0
P366/1-5	-19.6600	20.9847	-18.1682	20.6048	0.62	1.34	0.07	2.40	0
P366/1-6	-18.1682	20.6048	-17.6048	20.3585	0.61	0.38	0.06	2.16	1
P366/1-7	-17.6048	20.3585	-17.0337	22.9992	0.87	1.71	0.10	3.84	0
P366/1-8	-17.0337	22.9992	-16.4927	25.6002	0.96	1.36	0.08	1.61	0
P366/1-9	-16.4927	25.6002	-15.6137	24.9843	0.68	1.12	0.08	1.22	0
P366/1-10	-15.6137	24.9843	-15.6678	27.7210	0.64	1.02	0.06	0.97	1
P366/2-1	-15.2960	28.9811	-14.4836	30.4832	0.46	0.54	0.04	0.00	0
P366/2-2	-14.4823	30.4848	-13.6958	31.6666	0.65	2.92	0.08	2.52	0
P366/2-3	-13.6954	31.6664	-12.7307	33.3474	0.67	5.41	0.06	2.58	0
P366/2-4	-12.6692	33.4232	-11.1400	35.2904	0.99	1.61	0.06	1.77	0

[a] Sample number. Abbreviations as follows: Research vessels: AvH = Alexander von Humboldt cruise 44-04-01; M = Meteor; MD = Marion Dufresne; MSM = Maria S. Merian; P = Poseidon. Numbers indicate cruise and leg followed by the sample number. Example: M65/1-1 = Meteor cruise 65 leg 1, sample 1.

[b] Relative dust amount in the atmosphere as derived from TOMS satellite images. Numbers range from 0 (no dust) to 4 (very much dust).

3. Manuscript II

Biomarker evidence for old carbon transport to the Late Quaternary Amazon shelf and deep sea fan

Wiebke Kallweit[a], Helen M. Talbot[b], Gesine Mollenhauer[c], Arnoud Boom[d], Thomas Wagner[b], Matthias Zabel[a]

[a] University of Bremen, MARUM – Center for Marine Environmental Sciences, P.O. Box 330440, 28334 Bremen, Germany

[b] School of Civil Engineering and Geosciences, Newcastle University, Drummond Building, Newcastle upon Tyne, NE1 7RU, United Kingdom

[c] Alfred-Wegener Institute for Polar and Marine Research, Am Handelshafen 12, 27570 Bremerhaven, Germany

[d] Department of Geography, University of Leicester, Bennett Building, Leicester, LE1 7RH, United Kingdom

Manuscript under review for publication in *Geochimica et Cosmochimica Acta*.

Abstract

Knowledge about the sedimentation pathways of terrigenous organic carbon from continental source areas to marine sediments is important for estimating the global carbon budget and for paleoclimatic reconstructions. Continental margins in front of large rivers, such as the Amazon, are globally important sites for carbon production and burial, but also known to be areas of intense sediment reworking. New biomarker data from Holocene shelf and Late Quaternary deep sea fan sediments from the Amazon reveal that the redistribution of old carbon from the river catchment was far more persistent and widespread than previously thought, which has broader implications on the interpretation of the sedimentary carbon record of tropical and possibly other continental margin systems and ocean carbon budgets.

The delivery of soil organic carbon (SOC) to sediments from the Amazon shelf and fan was investigated based on soil-marker bacteriohopanepolyols (BHPs) and branched glycerol dialkyl glycerol tetraethers (GDGTs). Radiocarbon dating revealed that within the same beds total organic carbon (TOC) in the Amazon shelf sediments is substantially older than bivalve shells reflecting the

depositional age. On the Amazon Fan, however, ^{14}C ages of TOC indicate a considerably lower influence of old organic carbon. We observe unexpectedly invariant BHP and branched GDGT compositions in both cores indicating that biomarkers were primarily delivered from one single type of source. Unexpected high abundances of BHPs specific for aerobic methane oxidation show strong similarities with one sample from the current Amazon catchment. This observation led to the suggestion that biomarkers were primarily eroded from floodplain lakes that developed within the variable boundaries of the Late Quaternary Amazon watershed. This study emphasized the important role of the reworking of organic carbon on carbon supply and burial on large parts of the Amazon continental margin and possibly on other, similar depositional settings.

3.1 Introduction

Large amounts of terrigenous organic carbon (OC) are delivered to the oceans by rivers, but only 33 to 50 % (or even less) of this terrigenous material is ultimately deposited in the marine sediments (e.g. Hedges and Keil, 1995; Burdige, 2007). The fate of terrigenous OC after its delivery into the marine environment, however, can have a significant influence on the global carbon cycle (McKee et al., 2004; Burdige, 2005). Continental margin systems are of special importance as the majority of riverine suspended organic matter is deposited along these margins. If the riverine suspended matter is channeled directly into the deep sea, submarine fans develop which contain large amounts of terrigenous material (e.g. Ittekkot et al., 1986; Flood et al., 1995). The massive supply of organic matter from land coupled with the marine productivity stimulated by riverine nutrient supply is partly compensated by very high OC remineralization rates (Hedges and Keil, 1995; Aller, 1998). Further modification comes from reworking and subsequent lateral displacements of fine-grained sediments, controlled by strong and variable bottom currents (Mollenhauer et al., 2002; Inthorn et al., 2006). These processes might lead to age offsets between different compounds within marine sediments (e.g. Ohkouchi et al., 2002; Mollenhauer et al., 2003; Mollenhauer et al., 2005). The Amazon shelf and fan region is one area where intense reworking of the sediments coupled with an enhanced degradation of refractory organic material occurs (Aller, 1998; Burdige, 2007).

Many studies have reported the presence of elevated amounts of ancient (^{14}C-depleted or dead) organic carbon in river and continental shelf sediments (Sommerfield et al., 1995; Masiello and Druffel, 2001; Blair et al., 2003; Gordon and Goñi, 2003; Guo et al., 2004; Goñi et al., 2005; Galy et al., 2008). The old organic carbon is derived from soils, kerogen in the bedrocks, or black carbon, or a combination of these sources, depending on the regional setting. On the Amazon shelf and

fan, sedimentary organic matter is dominated by terrigenous material (Hinrichs and Rullkötter, 1997; Boot et al., 2006), mainly derived from soils (Aller et al., 1986; Hedges et al., 1986a). Sub-surface soil layers in the Amazon Basin have been shown to have relatively old radiocarbon ages, on the order of several thousand years at less than 1 m depth (Martinelli et al., 1996; Pessenda et al., 1998; Pessenda et al., 2001; Pessenda et al., 2010 and references therein). Radiocarbon ages might be biased by the presence of charcoal (Dickens et al., 2004) – one species of black carbon (Schmidt and Noack, 2000) – which provided evidence of fires occurring during the late Pleistocene and Holocene (Pessenda et al., 2010). Additionally, significant pre-aging of the organic matter may occur during temporary storage on floodplains which is a common process in the Amazon Basin (Raymond and Bauer, 2001; Blair et al., 2004). This may also lead to the delivery of old organic carbon into the marine environment. Characterizing and quantifying the contribution of soil organic matter to marine sediments is thus important for an accurate understanding of the timing and transfer modes of organic matter during transport from land to sea.

Tracing SOM in marine sediments

A commonly used tool to investigate the supply of soil organic carbon (SOC) (Walsh et al., 2008; Weijers et al., 2009b) into the marine environment is the Branched and Isoprenoid Tetraether-Index (BIT) that has been introduced by Hopmans et al. (2004). This proxy is based on the distribution of glycerol dialkyl glycerol tetraethers (GDGTs), the membrane lipids of many bacteria and Archaea (Schouten et al., 2000). It quantifies the relative abundances of branched GDGTs, which have particularly been found in soils and peats (e.g. Schouten et al., 2000; Weijers et al., 2006b) and are presumably produced by anaerobic bacteria (Weijers et al., 2006b; Weijers et al., 2009a), and crenarchaeol, a typical isoprenoid GDGT produced predominantly by pelagic Thaumarchaeota in the marine and lacustrine water columns (Sinninghe Damsté et al., 2002; Powers et al., 2004; Pitcher et al., 2011). BIT values in soils vary between 0.9 and 1 due to low amounts of crenarchaeol in soils (Weijers et al., 2006a). Branched GDGTs, however, can also be used for the reconstruction of mean air temperatures (MAT) and soil pH (Weijers et al., 2007a). These reconstructions are based on the cyclization ratio of branched tetraethers (CBT), correlated with soil pH, and the methylation index of branched tetraethers (MBT) which depends on soil pH and MAT.

Another group of lipid biomarkers with the potential of tracing SOC delivery are specific bacteriohopanepolyols (BHPs), the membrane lipids of a diverse range of bacterial taxa (Rohmer et al., 1984; Ourisson et al., 1987; Sáenz, 2010). Cooke et al. (2008b; 2009) have shown that

adenosylhopane and related compounds – common and abundant in soils, but rare in open marine settings – can be used to track SOC transport into aquatic environments.

Here we present results from two sediment cores which have been recovered from the Amazon shelf (GeoB3918) and deep sea fan (GeoB1514). We investigated the relative importance of SOC within these marine sediments using the BIT index and soil-marker BHPs. The results are compared to the Al/Ti-ratio as a bulk inorganic tracer of terrigenous (lithogenic) material in marine sediments. To identify other processes of microbial carbon cycling in the sediments, we also investigated other BHPs. This includes BHPs diagnostic for aerobic methane oxidation, i.e. aminobacteriohopanepentol (aminopentol; structure **1e** in Appendix 3.1) and related compounds (see Talbot and Farrimond, 2007 for review of BHP specificity and source organisms). We show evidence to support the conclusion that the terrigenous material deposited on the Amazon shelf and fan has been mainly delivered from one source, presumably a floodplain lake setting, which indicates that burial of reworked OC is much more important in Amazon shelf and fan sediments than commonly considered. Additionally, MAT reconstructions on the Amazon shelf reflect recent temperatures which argues against an increased input from the Andes during the Holocene as proposed by Bendle et al. (2010).

3.2 Experimental

3.2.1 Study area and sampling

With an annual sediment discharge of 1.2 billion tons today the Amazon River is the most important pathway for the transport of suspended terrigenous matter to the ocean (Meybeck, 1996). During interglacials with high sea level the material is deposited near the river mouth or on the Amazon shelf, being transported northwestward along the innermost shelf by the North Brazil Coastal Current. Contrastingly, during glacials when large parts of the current shelf area were exposed, the suspended material from the river was channeled through canyons and deposited more directly on the deep Amazon Fan (Milliman et al., 1975). Increased organic carbon (OC) contents in glacial sediments of the deep Amazon Fan confirm the more direct supply of OC to the deep ocean which has implications for the regional and global carbon budget during past glacial periods (Keil et al., 1997; Schlünz et al., 1999; Burdige, 2005).

In this study we analyzed two gravity cores from a very shallow and a deep water setting. The sampling site of gravity core GeoB3918-2 is located on the Amazon shelf at a water depth of 50 m (3.7050°N; 50.4050°W). Gravity core GeoB1514-6 was taken on the Amazon Fan from a water

depth of 3509 m (5.1383°N; 46.5750°W) (Fig. 3.1). Since their recovery, both cores were stored at -20°C in the ODP core repository in Bremen. Samples were taken at intervals of approximately 20 cm (GeoB3918-2; 27 samples) and 25 cm (GeoB1514-6; 30 samples, freeze-dried and homogenized by grinding.

One additional sediment sample has been taken from Lago Socó (3.7531°N; 70.5126°W) located near the Colombian town of Puerto Nariño. Lago Socó is part of a complex várzea wetland within the Amazon floodplain and has a permanent connection with the Loretoyacu River which is a tributary to the Amazon River. The material was collected at the water interface during the dry season.

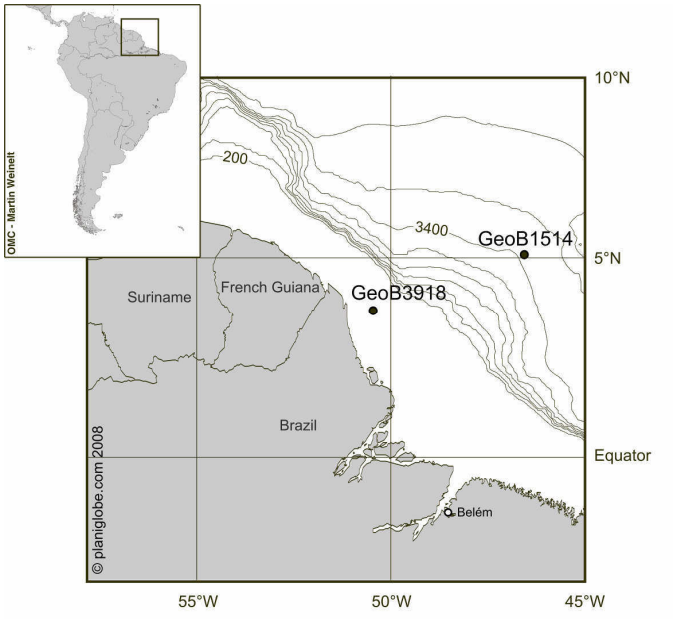

Figure 3.1. Map of the sampling locations of gravity cores GeoB3918-2 and GeoB1514-6.

3.2.2 Bulk parameters

Total organic carbon (TOC) contents of GeoB3918 were measured with a LECO CS 200. TOC contents and $\delta^{13}C$ values of parallel core GeoB1514-7 were taken from Schlünz et al. (1999). AMS radiocarbon dating was conducted at the National Ocean Sciences Accelerator Mass Spectrometry (NOSAMS) Facility at Woods Hole Oceanographic Institution (USA) on 3 and 4 samples of TOC from cores GeoB3918 and GeoB1514, respectively (Table 3.1). Radiocarbon ages of two bivalve shells obtained from the Leibniz laboratory AMS facility in Kiel (provided by H. Arz) were converted into calendar years using the CALIB 6.0 algorithm (Stuiver et al., 2010) and the Marine09 data set (Reimer et al., 2009). However, the ^{14}C-ages of TOC were not calibrated as the Marine09 data set (Reimer et al., 2009) was not suitable given the high amount of terrigenous material in these

samples. A mixed calibration seemed also inappropriate as the relative abundance of terrigenous organic carbon in the samples could not be determined. Element concentrations were measured by a Spectro Xepos Energy Dispersive Polarization X-ray Fluorescence Analyzer (EDP-XRF).

Table 3.1. ^{14}C ages and $\delta^{13}C$ values for bulk TOC samples from GeoB3918 and GeoB1514. Please note that ^{14}C ages have not been calibrated.

core	depth [m]	$\delta^{13}C$ [‰]	^{14}C age [yrs BP]	age error [yrs]
GeoB3918	0.30 - 0.36	-25.67	3740	35
GeoB3918	2.30 - 2.36	-25.64	4050	35
GeoB3918	4.50 - 4.56	-25.31	3910	35
GeoB1514	0.40 - 0.50	-23.86	13650	75
GeoB1514	2.22 - 2.32	-24.60	19500	100
GeoB1514	4.22 - 4.32	-24.85	23100	160
GeoB1514	6.80 - 6.90	-26.89	30200	180

3.2.3 Extraction and derivatization

3.2.3.1 GDGTs

About 5 g of freeze-dried, homogenized sediment were extracted with 25 ml of methanol (MeOH), dichloromethane:methanol (DCM:MeOH 1:1, v/v) and DCM, respectively. Each addition of solvents was followed by 5 minutes of sonication and 5 minutes of centrifugation. A known amount of a C_{46}-GDGT was added as internal standard before the extraction. Total lipid extracts were combined, washed with bi-distilled water (Seralpure) to remove salts, dried over anhydrous Na_2SO_4 and concentrated under nitrogen. Extracts were then re-dissolved in DCM and desulfurized using a Pasteur pipette filled with activated copper filaments. The total lipid extract was placed on the column, eluted with 4 ml of DCM and dried under nitrogen. The total lipid extracts were separated into three fractions applying column chromatography on silica gel columns. Hydrocarbons were eluted with 2 ml of *n*-hexane, ketones with 2 ml DCM:*n*-hexane (2:1, v/v) and alcohols with 2 ml MeOH.

For GDGT-measurement 50 % of the MeOH-fraction were dried, weighed, re-dissolved in DCM and filtered through 0.45 µm syringe filters (Whatman) as described by Hopmans et al. (2000) and Hopmans et al. (2004). The solvents were evaporated under nitrogen and lipids were re-dissolved in *n*-hexane:isopropanol (99:1, v/v) with a concentration of 2 mg/ml (Schouten et al., 2009) for HPLC-measurement.

3.2.3.2 BHPs

The extraction method for the measurement of BHPs is based on the Kates modification of the original Bligh and Dyer extraction (Bligh and Dyer, 1959; Kates, 1975). The extraction procedure has been described in detail by Cooke et al. (2008a), except for the use of DCM instead of chloroform. After addition of the internal standards 5α-pregnane-3β,20β-diol and 5α-androstan-3β-ol samples were acetylated by heating with 2 ml pyridine and 2 ml acetic anhydride for 1 hour at 50°C. The extracts were left at room temperature over night to complete the reaction. They were then evaporated to dryness under N_2, re-dissolved in MeOH/propan-2-ol (60:40, v/v) and filtered through 0.45 µm PTFE syringe filters. For LC-MS^n analysis extracts were dried again under nitrogen and re-dissolved in a defined volume (500 µl) of MeOH/propan-2-ol (60:40, v/v).

3.2.4 Chromatography

3.2.4.1 Analytical HPLC-APCI-MS for GDGT measurement

GDGTs were measured by normal-phase high performance liquid chromatography (HPLC) using an Agilent 1200 series HPLC system and detected by mass spectrometry (MS) using an Agilent 6120 single-quadrupole instrument and atmospheric pressure chemical ionization (APCI). A detailed description of the instrumental settings for GDGT measurement is given by Leider et al. (2010). GDGT concentrations were calculated from the characteristic base peak ion peak areas of individual GDGTs relative to the base peak area of the internal standard at m/z 744. The BIT index (Hopmans et al., 2004) was calculated based on the peak areas of branched GDGTs and crenarchaeol for the estimation of soil organic carbon input to the core locations. Soil pH and MAT were reconstructed from peak areas using the MBT-/CBT-proxies and the global calibration by Weijers et al. (2007a). Analytical precision was determined by repeated extraction and measurement of a lab-internal sediment standard and duplicate analysis of selected samples. The analytical error for GDGT quantification was ± 10 %, deviation of BIT values was < 0.01 units. The deviation for MBT was 0.01, for CBT 0.02. Reconstructed MAT show a deviation of 0.5°C while reconstructed pH values deviate by 0.05 units.

3.2.4.2 Analytical HPLC-APCI-MS for BHP measurement

BHPs were measured by reversed-phase HPLC-APCI-MS as described previously (e.g. Cooke et al., 2008a). BHP structures were assigned based on the comparison with published mass spectra

(Talbot et al., 2003b; Talbot et al., 2003a; Talbot et al., 2007b; Talbot et al., 2007a; Talbot et al., 2008; Rethemeyer et al., 2010).

A semi-quantitative estimate of abundance (± 20 %) was calculated from the characteristic base peak ion peak areas of individual BHPs in mass chromatograms (from SCAN 1) relative to the m/z 345 ($[M+H–CH_3COOH]^+$) base peak area response of the acetylated 5α-pregnane-3β,20β-diol internal standard. Relative response factors for BHT representing non-nitrogen containing BHPs and the average of four N-containing BHP including aminotriol, adenosylhopane, BHT-cyclitol ether and BHT-glucosamine were used to adjust the peak areas relative to that of the internal standard, where BHPs containing one or more N atoms give an averaged response ca. 12 times that of the standard and those with no N give a response 8 times that of the standard.

3.3 Results

3.3.1 Radiocarbon dating

The sediments from shelf core GeoB3918 were deposited during the youngest part of the Holocene. Radiocarbon dating of bivalve shells from 3.84 and 4.49 meters core depth reveals a depositional age of 450 ± 40 and 580 ± 40 years BP, respectively. However, ^{14}C-dating of three TOC samples yielded significantly older ages ranging around 4000 ^{14}C years BP for GeoB3918 (Table 3.1), emphasizing the presence of old carbon in these sediments.

The uppermost ~30 cm of core GeoB1514 from the Amazon Fan consist of Holocene calcareous clay which is separated from the Pleistocene terrigenous clays by an iron-rich crust as often described from the Amazon Fan (e.g. Damuth and Flood, 1984). Radiocarbon dating on TOC has been conducted on four samples from between 0.4 and 6.9 m. The resulting radiocarbon ages of the organic carbon range from 13650 to 30200 ^{14}C-years BP (Table 3.1). In this core no complementary radiocarbon dating has been conducted on carbonate materials. However, comparison of TOC ^{14}C ages and the potential depositional ages of the corresponding sediment samples (based on comparison with the Bendle et al. (2010) MAT record; section 3.4.1) indicates that old OC might be less important in Amazon Fan sediments.

3.3.2 Bulk parameters

TOC contents range from 0.59 to 0.72 weight (wt) % (GeoB3918) and 0.29 to 1.00 wt% (GeoB1514). While values in GeoB3918 scatter around 0.64 wt% within a relatively narrow range

(Fig. 3.2a) the TOC record in core GeoB1514 decreases from ~1 wt% to about 0.6 wt% at 5 m (Fig. 3.2c). A second sharp decrease in TOC content is observed near the top of the profile at about 0.3 m. Surface and near surface sediments have a very low TOC content of ~0.3 wt%. Values for $\delta^{13}C$ in GeoB3918 are depleted and range from -25.3 to -25.7 ‰ (Table 3.1). $\delta^{13}C$ values in parallel core GeoB1514-7 (Schlünz et al., 1999) range from -19.7 to -27.7 ‰ and become more depleted with depth. Values change from about -20 ‰ in surface sediments to values around -24.5 ‰ below 0.6 m. At ~5 m a shift towards even more depleted values around -26.4 ‰ is noted (Fig. 3.2e). The Al/Ti-ratio in GeoB3918 (Fig. 3.2b) fluctuates around a mean value of 19.05. In GeoB1514 Al/Ti-ratios fluctuate around a mean value of 20.17 above 5 m. At this depth a clear shift to lower Al/Ti-ratios (mean value of 18.14 below 5 m (Fig. 3.2d)) is noted.

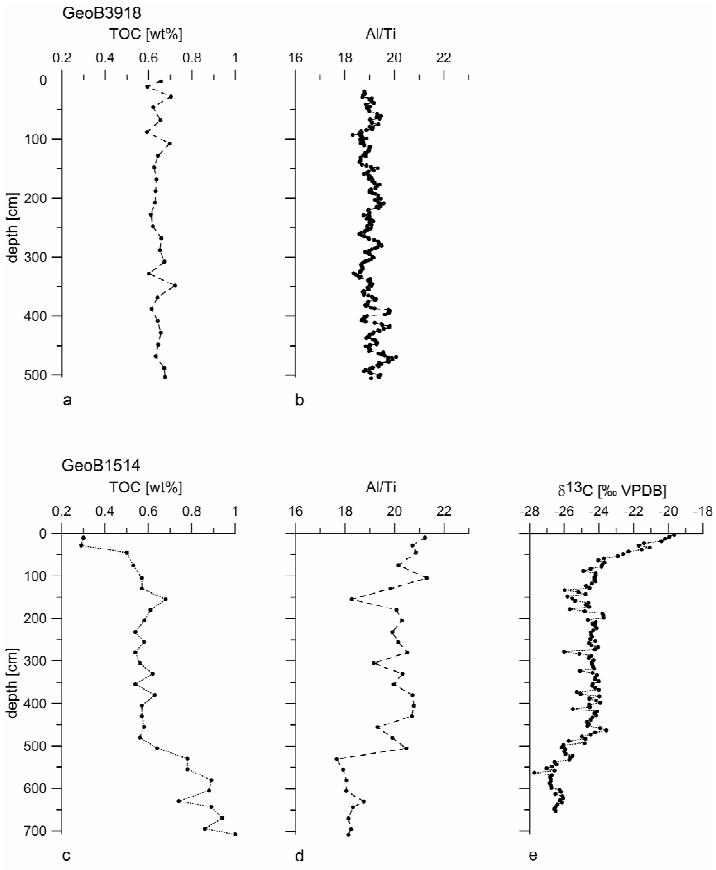

Figure 3.2. Downcore profiles of a) TOC of GeoB3918-2, b) Al/Ti-ratio of GeoB3918-2 (5-point average), c) TOC of GeoB1514-6, d) Al/Ti-ratio of GeoB1514-6, e) $\delta^{13}C$ values of GeoB1514-7 (from Schlünz et al., 1999).

3.3.3 Glycerol dialkyl glycerol tetraethers

Concentrations of soil-derived (branched) GDGTs (see e.g. Hopmans et al., 2004; Weijers et al., 2007a for GDGT structures) vary between 43.2 and 68.6 μg/g TOC on the shelf (GeoB3918; Table

3.2; Fig. 3.3a) and between 9.6 and 327.9 μg/g TOC in the deep water core (GeoB1514; Table 3.3; Fig. 3.3f). Crenarchaeol concentrations range from 24.3 to 52.6 μg/g TOC (GeoB3918; Fig. 3.3b) and from 6.5 to 77.6 μg/g TOC (GeoB1514; Fig. 3.3g), with high fluctuations especially observed in the deeper core. The BIT index is high in both cores fluctuating around 0.62 in GeoB3918 (Fig. 3.3c) and approaching values around 0.9 to 0.8 below ~0.7 m in GeoB1514 (Fig. 3.3h).

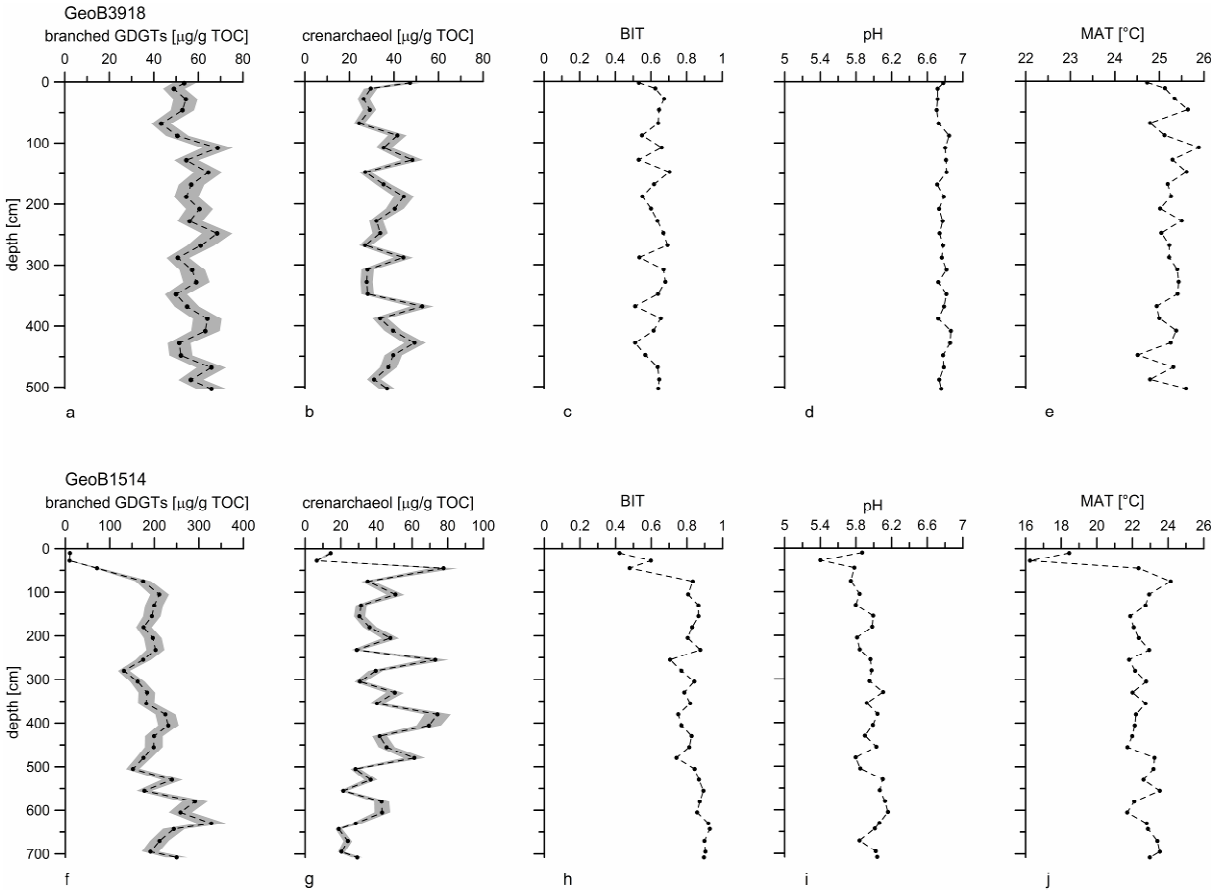

Figure 3.3. Downcore profiles of GDGTs. GeoB3918-2: a) branched GDGTs, b) crenarchaeol, c) BIT index, d) MBT-based soil pH-values, e) MBT/CBT-based mean air temperatures (MAT). GeoB1514-6: f) branched GDGTs, g) crenarchaeol, h) BIT index, i) MBT-based soil pH-values, j) MBT/CBT-based MAT. Shaded areas reflect the analytical error (± 10 %) of GDGT concentrations.

Table 3.2. Concentrations [μg/g TOC] of GDGTs, BIT, MBT, CBT and reconstructed MAT and pH in core GeoB3918.

Depth [m]	TOC [wt%]	1022	1036	1050	1292	BIT	MBT	CBT	MAT [°C]	pH
0.02	0.66	39.7	11.8	2.1	47.2	0.53	0.76	0.75	24.7	6.8
0.11	0.59	37.2	10.2	1.6	29.5	0.62	0.77	0.78	25.1	6.7
0.28	0.70	41.6	10.7	2.1	26.3	0.67	0.77	0.78	25.3	6.7
0.46	0.62	40.9	10.2	1.8	29.1	0.64	0.78	0.78	25.6	6.7
0.68	0.65	32.4	9.2	1.7	24.3	0.64	0.76	0.77	24.8	6.7
0.88	0.59	37.8	11.0	1.8	41.5	0.55	0.76	0.73	25.1	6.8
1.08	0.70	52.7	13.5	2.4	35.3	0.66	0.78	0.75	25.9	6.8
1.28	0.64	41.1	12.0	1.5	48.2	0.53	0.77	0.74	25.3	6.8
1.48	0.62	48.7	13.3	2.4	27.1	0.70	0.77	0.74	25.6	6.8
1.68	0.64	43.3	11.5	2.0	35.3	0.62	0.77	0.78	25.2	6.7
1.88	0.63	41.2	11.5	1.8	44.3	0.55	0.77	0.75	25.3	6.8
2.08	0.63	45.4	12.5	2.5	40.3	0.60	0.77	0.77	25.0	6.7
2.28	0.61	42.7	11.2	2.1	32.1	0.64	0.77	0.76	25.5	6.8
2.48	0.62	52.6	13.7	2.1	33.8	0.67	0.77	0.77	25.0	6.7
2.68	0.66	46.0	12.7	2.2	27.0	0.69	0.77	0.76	25.2	6.8
2.88	0.65	38.5	10.4	1.9	44.2	0.53	0.77	0.76	25.2	6.8
3.08	0.67	43.3	11.7	2.2	28.1	0.67	0.77	0.74	25.4	6.8
3.28	0.60	45.3	11.8	2.0	27.7	0.68	0.78	0.78	25.4	6.7
3.48	0.72	37.9	10.0	2.1	28.2	0.64	0.77	0.74	25.4	6.8
3.68	0.64	41.2	11.4	2.3	52.6	0.51	0.76	0.75	24.9	6.8
3.88	0.61	48.5	13.1	2.4	33.8	0.65	0.77	0.78	25.0	6.7
4.08	0.64	47.7	12.9	2.4	39.6	0.61	0.76	0.72	25.4	6.9
4.28	0.66	38.5	10.9	1.9	49.2	0.51	0.76	0.72	25.3	6.9
4.48	0.64	38.5	11.6	2.0	39.7	0.57	0.75	0.75	24.5	6.8
4.68	0.63	49.9	13.3	2.6	37.4	0.64	0.77	0.75	25.3	6.8
4.88	0.67	42.7	11.8	2.0	31.0	0.65	0.76	0.77	24.8	6.7
5.03	0.68	50.5	13.0	2.3	36.9	0.64	0.78	0.76	25.6	6.8

Table 3.3. Concentrations [μg/g TOC] of GDGTs, BIT, MBT, CBT and reconstructed MAT and pH in core GeoB1514.

Depth [m]	TOC [wt%]	1022	1036	1050	1292	BIT	MBT	CBT	MAT [°C]	pH
0.10	0.30	7.4	1.6	1.5	14.3	0.53	0.70	1.10	18.4	5.9
0.28	0.29	6.5	1.5	1.7	6.5	0.67	0.69	1.28	16.2	5.4
0.45	0.50	55.6	11.0	4.6	77.6	0.50	0.78	1.13	22.3	5.8
0.75	0.53	143.5	25.9	5.5	35.0	0.83	0.82	1.15	24.1	5.7
1.05	0.57	167.3	36.6	7.0	50.6	0.80	0.79	1.11	22.9	5.8
1.30	0.57	159.2	33.1	7.1	31.4	0.86	0.79	1.13	22.7	5.8
1.55	0.68	148.9	38.3	7.1	30.4	0.86	0.76	1.05	21.9	6.0
1.80	0.61	135.7	34.4	5.7	36.2	0.82	0.76	1.06	22.1	6.0
2.05	0.58	154.6	35.2	6.7	47.8	0.80	0.78	1.12	22.4	5.8
2.32	0.54	160.9	35.2	6.5	28.9	0.87	0.79	1.11	22.9	5.8
2.55	0.58	134.3	33.9	6.7	73.0	0.70	0.76	1.06	21.8	6.0
2.80	0.54	101.7	25.0	5.0	39.6	0.77	0.76	1.06	22.1	6.0
3.05	0.56	127.1	30.1	5.2	30.7	0.83	0.78	1.07	22.8	6.0
3.30	0.62	139.3	36.5	7.8	50.3	0.78	0.75	1.01	22.0	6.1
3.55	0.54	142.5	33.2	6.1	40.2	0.81	0.78	1.08	22.7	5.9
3.80	0.63	173.1	42.7	8.8	74.3	0.75	0.76	1.03	22.2	6.0
4.05	0.57	178.0	44.2	9.0	69.5	0.76	0.76	1.05	22.1	6.0
4.30	0.57	154.6	37.2	7.3	41.8	0.82	0.77	1.09	22.0	5.9
4.55	0.58	150.6	40.4	7.4	45.7	0.81	0.75	1.04	21.7	6.0
4.80	0.56	142.2	26.5	6.9	61.2	0.74	0.80	1.13	23.2	5.8
5.05	0.64	122.0	24.7	5.1	28.2	0.84	0.79	1.11	23.2	5.8
5.30	0.78	185.0	44.8	9.6	36.7	0.86	0.76	1.01	22.6	6.1
5.55	0.78	141.2	30.4	5.9	21.4	0.88	0.78	1.02	23.5	6.1
5.80	0.89	220.1	60.3	10.5	42.9	0.87	0.75	1.00	22.1	6.1
6.05	0.88	193.3	55.8	9.5	43.2	0.85	0.74	0.99	21.7	6.2
6.30	0.74	254.6	63.4	9.9	28.3	0.91	0.77	1.03	22.8	6.1
6.43	0.89	190.9	46.2	6.6	18.8	0.92	0.77	1.05	22.9	6.0
6.70	0.94	170.6	34.8	6.2	23.9	0.89	0.80	1.11	23.4	5.8
6.95	0.86	152.4	32.3	6.4	20.3	0.90	0.79	1.04	23.5	6.0
7.08	1.00	195.7	47.3	7.0	29.2	0.89	0.78	1.04	23.0	6.0

Reconstructed soil pH-values in GeoB3918 vary around 6.77 while reconstructed MAT range from 24.5 to 25.9°C (Fig. 3.3d and e). CBT-based soil pH-values in GeoB1514 are lower and vary around 5.9 (Fig. 3.3i). For Pleistocene samples of GeoB1514 MAT between 21.7 and 24.1°C (Fig. 3.3j) were

reconstructed. For comparison, MAT estimates for Holocene samples from the Amazon Fan are very low (18.5 and 16.3°C).

3.3.4 Bacteriohopanepolyols

A maximum of 21 different BHPs (see Appendix 3.1 for BHP structures) were identified in the samples from the Amazon shelf and fan. Total concentrations range from 730 to 2860 μg/g TOC (GeoB3918; Table 3.4) and from 110 to 2510 μg/g TOC (GeoB1514; Table 3.5). Even more pronounced than in the GDGT records, large and apparently regular fluctuations are observed in the total BHP concentrations (Fig. 3.4a and e) varying by a factor of 2 to 3 in both cores.

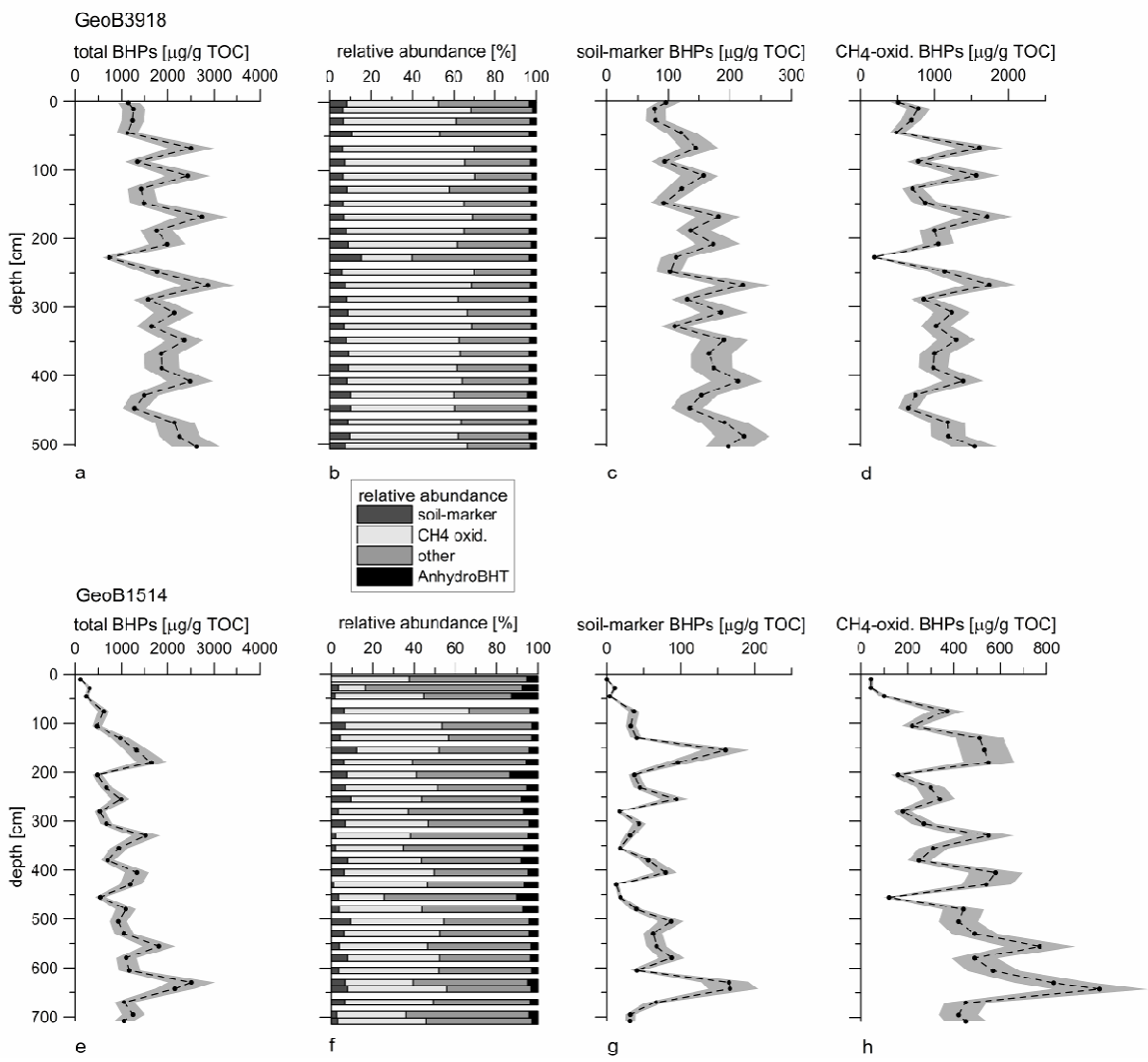

Figure 3.4. BHP concentrations and distributions. BHPs are divided into soil-marker BHPs (1f, 2f, 2g', 1g, 2g, 1g'; see Appendix 3.1 for structures), BHPs specific for aerobic methane oxidation (1c, 1d, 1e, 4/5c, 4/5e plus a compound with an unknown structure (m/z 788)), other (1a, 2a/3a, 1b, 1h - 1k, 2k) and AnhydroBHT (1l). GeoB3918-2: a) Total BHP concentrations, b) BHP composition, c) soil-marker BHPs, d) BHPs specific for aerobic methane oxidation. GeoB1514-6: e) Total BHP concentrations, f) BHP composition, g) soil-marker BHPs, h) BHPs specific for aerobic methane oxidation. Shaded areas reflect the analytical error (± 20 %) of BHP concentrations.

Table 3.4

Concentrations [µg/g TOC] of BHPs in core GeoB3918. The top line indicates the BHP sub-groupings into soil-marker BHPs, BHPs specific for aerobic methane oxidation, other and AnhydroBHT as in Fig. 3.4.

	soil	soil	soil	soil	soil	soil	CH_4-oxid.	CH_4-oxid.	CH_4-oxid.	CH_4-oxid.	CH_4-oxid.	CH_4-oxid.	other	other	other	other	other	other	other	other	AnhydroBHT	
Depth [m]	m/z 746[a]	m/z 760[a]	m/z 761[a]	m/ 775[a]	m/z 802[a]	m/z 816[a]	m/z 712[a]	m/z 714[a]	m/z 772[a]	m/z 788[a]	m/z 828[a]	m/z 830[a]	m/z 655[b]	m/z 669[b]	m/z 771[b]	m/z 943[b]	m/z 957[b]	m/z 1002[a]	m/z 1060[a]	m/z 1118[a]	m/z 613[a]	Total BHPs
	1f	**2f**	**1g**	**2g**	**1g'**	**2g'**	**4 or 5c**	**1c**	**1d**		**4 or 5e?**	**1e**	**1a**	**2a/3a**	**1b**	**1k**	**2k**	**1h**	**1i**	**1j**	**1l**	
0.02	56	6.3	9.1	–	19	5.8	13	150	57	45	12	230	370	17	29	–	–	71	7.3	7.8	42	1150
0.11	47	5.9	6.7	–	15	2.4	13	230	89	69	20	360	260	5.1	23	–	–	71	9.5	8.9	21	1260
0.28	53	4.2	6.4	–	13	2.9	11	210	70	24	13	350	320	9.1	28	–	–	68	10	9.2	36	1240
0.46	76	10	12.7	–	17	4.0	10	140	42	38	11	240	360	9.8	29	–	–	66	5.9	10	42	1120
0.68	98	9.3	13.8	–	24	0.0	22	590	190	4.3	41	750	470	14	39	–	–	140	23	18	53	2500
0.88	58	5.9	8.7	–	18	3.4	18	240	79	22	19	400	290	6.9	32	–	–	78	11	13	37	1340
1.08	100	14	13.4	–	20	6.2	22	520	180	38	39	760	410	17	51	–	–	150	24	19	48	2430
1.28	79	10	12.1	–	16	4.6	18	200	82	88	16	300	390	13	38	–	–	84	12	8.6	47	1420
1.48	61	5.1	4.0	–	21	1.9	14	310	110	56	22	360	330	8.5	27	–	–	92	13	10	36	1480
1.68	110	9.2	21.7	–	34	8.6	26	600	210	44	40	790	540	15	52	–	–	140	21	20	62	2740
1.88	85	9.2	13.3	–	23	4.9	16	310	130	14	22	510	410	9.8	30	–	–	86	11	12	56	1750
2.08	110	11	19.8	–	31	4.7	23	310	110	49	22	540	490	12	47	–	–	130	18	16	46	1990
2.28	69	6.0	9.2	–	22	5.7	9.1	53	20	8.5	4.7	81	280	10	33	–	–	74	7.2	9.7	27	730
2.48	68	4.1	9.2	–	17	3.8	22	380	120	34	28	550	310	13	29	–	–	100	13	16	41	1760
2.68	150	14	5.4	–	40	10	38	660	220	0.0	48	770	530	15	49	–	–	190	22	23	79	2860
2.88	83	13	11.6	–	23	0.0	23	300	96	17	18	400	380	12	36	–	–	92	10	10	52	1580
3.08	110	12	20.0	–	41	4.9	30	440	150	20	36	550	470	12	36	–	–	120	15	14	53	2130
3.28	67	8.8	7.6	–	25	2.4	21	290	110	29	31	540	300	9	39	–	–	99	16	16	37	1650
3.48	120	15	16.7	–	34	8.4	36	520	200	83	21	430	560	19	35	–	–	160	17	13.0	74	1360
3.68	94	12	17.5	–	33	8.2	24	290	110	22	28	530	430	1.5	37	–	–	120	15	15	64	1850
3.88	98	14	24.2	–	34	4.2	23	380	120	16	23	420	470	16	31	–	–	110	10	11	60	1870
4.08	140	8.4	19.0	–	39	7.7	22	520	180	15	29	610	550	16	41	–	–	160	21	11	89	2480
4.28	99	12	14.6	–	26	2.8	17	210	83	69	17	340	380	11	33	–	–	84	14	7.4	67	1490
4.48	84	5.1	11.1	–	30	4.5	12	180	75	15	15	340	300	14	34	–	–	83	14	12	51	1280
4.68	110	12	15.7	–	43	8.2	18	450	150	0.0	26	530	480	16	33	–	–	150	11	14	70	2140
4.88	140	11	12.7	–	48	9.7	27	460	160	8.8	27	500	560	12	28	–	–	130	20	11	83	2250
5.03	120	12	10.4	–	46	6.3	23	530	180	8.0	41	760	560	14	52	–	–	150	19	14	70	2620

– not detected

[a] $[M + H]^+$

[b] $[M + H - CH_3COOH]^+$

Table 3.5

Concentrations [µg/g TOC] of BHPs in core GeoB1514. The top line indicates the BHP sub-groupings into soil-marker BHPs, BHPs specific for aerobic methane oxidation, other and AnhydroBHT as in Fig. 3.4.

	soil	soil	soil	soil	soil	soil	CH_4-oxid.	CH_4-oxid.	CH_4-oxid.	CH_4-oxid.	CH_4-oxid.	CH_4-oxid.	other	other	other	other	other	other	other	other	AnhydroBHT	
Depth [m]	m/z 746[a]	m/z 760[a]	m/z 761[a]	m/ 775[a]	m/z 802[a]	m/z 816[a]	m/z 712[a]	m/z 714[a]	m/z 772[a]	m/z 788[a]	m/z 828[a]	m/z 830[a]	m/z 655[b]	m/z 669[b]	m/z 771[b]	m/z 943[b]	m/z 957[b]	m/z 1002[a]	m/z 1060[a]	m/z 1118[a]	m/z 613[a]	Total BHPs
	1f	**2f**	**1g**	**2g**	**1g'**	**2g'**	**4 or 5c**	**1c**	**1d**		**1e**	**4 or 5e?**	**1a**	**2a/3a**	**1b**	**1k**	**2k**	**1h**	**1i**	**1j**	**1l**	
0.10	–	–	–	–	–	–	–	16	6.3	–	19	–	61	–	–	–	–	–	–	1.0	6.1	110
0.28	5.9	–	2.5	–	1.8	–	2.5	18	5.9	–	15	–	200	24	5.1	–	–	4.5	2.4	1.6	24	310
0.45	–	–	3.8	–	–	–	3.2	35	13	8.1	38	2.0	65	2.7	7.4	–	–	19	2.4	5.5	29	230
0.75	18	3.6	10	–	3.1	1.8	7.7	140	41	10	160	13	190	5.6	22	–	–	99	18	15	22	610
1.05	27	–	5.1	–	–	–	4.6	92	17	7.8	88	6.8	98	2.3	16	–	–	72	11	13	13	470
1.30	23	2.3	9.6	–	2.1	2.6	7.9	320	47	6.5	120	13	220	9.6	23	11	–	93	15	16	28	970
1.55	120	6.5	28	4.6	2.8	–	30	320	33	15	120	11	250	9.9	20	–	–	250	27	14	56	1320
1.80	57	7.4	28	3.5	–	–	14	340	31	14	140	6.9	550	23	25	26	–	230	31	24	97	1650
2.05	14	2.9	11	4.2	2.2	2.2	4.6	84	11	4.3	49	4.4	140	5.2	12	–	–	43	11	8.6	66	480
2.32	24	4.1	14	–	2.2	–	7.2	160	31	11	81	6.5	150	5.2	13	11	–	96	11	6.6	37	670
2.55	64	12	18	–	–	–	9.6	170	24	24	104	8.2	250	11	14	–	–	160	25	12	80	990
2.80	13	–	3.8	–	–	–	5.5	100	14	4.5	54	2.7	170	5.7	18	14	4.6	64	7.1	9.3	37	530
3.05	28	–	14	–	–	1.5	13	120	25	8.7	101	7.1	170	5.9	10	–	–	97	14	21	31	670
3.30	21	–	10	–	–	–	10	290	48	9.8	190	–	320	12	24	–	–	410	52	42	76	1520
3.55	18	–	–	–	–	–	12	160	24	15	93	3.4	330	11	16	18	5.3	140	19	15	66	940
3.80	34	6.3	15	–	–	–	9.3	140	19	11	65	3.3	220	5.9	10	–	–	85	13	6.5	58	700
4.05	56	7.6	12	–	2.2	1.8	14	300	53	5.5	200	11	270	21	13	–	–	230	44	24	66	1330
4.30	5.5	–	6.6	–	–	–	16	330	43	11	130	8.0	330	8.5	20	16	–	150	20	13	81	1190
4.55	4.5	–	–	2.9	9.9	1.1	4.8	73	9.5	3.5	29	2.0	250	8.7	28	16	–	30	4.9	2.3	55	540
4.80	33	–	6.4	–	–	–	16	230	31	11	140	8.8	330	7.4	23	–	–	150	14	12	80	1090
5.05	58	6.0	20	–	0.8	1.6	17	160	35	14	180	12	190	8.0	12	8.8	–	140	18	8.0	40	930
5.30	44	–	14	1.5	–	3.0	18	240	40	30	150	12	210	17	19	8.1	–	160	22	12	46	1050
5.55	51	6.2	8.4	–	1.7	–	43	450	63	38	160	18	440	17	19	30	–	340	33	23	59	1800
5.80	55	9.7	19	3.3	–	–	20	260	24	14	160	14	220	7.6	15	23	–	170	23	26	39	1100
6.05	23	–	13	4.4	–	–	22	350	45	23	120	11	240	14	15	19	–	200	24	12	35	1170
6.30	120	30	14	–	–	–	24	510	58	26	190	20	710	49	46	41	–	470	41	34	130	2510
6.43	110	12	28	–	13	3.2	33	620	81	31	250	19	420	31	45	30	–	300	36	18	68	2150
6.70	46	2.0	11	–	5.4	1.8	7.1	210	36	42	150	5.9	250	13	36	–	–	160	21	18	38	1050
6.95	31	–	–	–	–	–	12	250	36	19	100	6.0	370	23	19	24	–	250	38	17	58	1250
7.08	20	4.4	5.2	–	1.0	–	15	240	38	16	130	8.1	300	12	18	–	–	190	14	11	29	1050

– not detected

[a] $[M + H]^+$

[b] $[M + H - CH_3COOH]^+$

Notably, the relative abundances of the different groups of BHPs in both cores – soil-marker BHPs, 35-aminoBHPs, 32,35-Anhydrobacteriohopanetetrol (AnhydroBHT; degradation product) and "others" (see caption of Fig. 3.4 for differentiation of compound groups) – remain roughly constant with depth, despite variations in the concentration of the compounds (Figures 3.4b and f). Figure 3.5 shows that the standard deviation (1σ) of the mean relative abundance of individual BHPs is approximately identical to a deviation of ± 20 % within each core, which is the recent analytical limitation for BHP quantification. This implies that relative BHP abundances are identical within analytical error for GeoB3918 suggesting that there is no variation in the composition throughout the record. A slightly higher variability is observed in the BHP composition of GeoB1514 (Fig. 3.4f), with largest variations in the unspecific compounds BHT (**1a**), aminobacteriohopanetriol (aminotriol; **1c**) and BHT cyclitol ether (**1h**). Compositional variations, however, are not linked to changes of absolute concentrations.

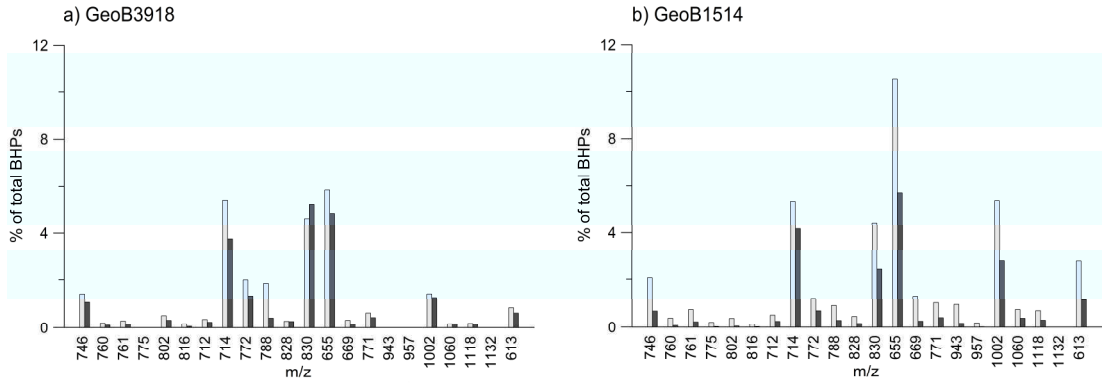

Figure 3.5. Comparison between the standard deviation (1σ; light gray bars) and the analytical error in quantification (20 %; dark gray bars) for mean relative abundances of individual BHPs of a) GeoB3918-2 and b) GeoB1514-6. Individual compounds are ordered according to their sub-grouping in Fig. 4.

3.3.4.1 Soil-marker BHPs

Soil-marker BHPs (including adenosylhopane (**1f**), its C-2 methylated homologue (**2f**) as well as the non-methylated (**1g** and **1g'**, respectively) and methylated (**2g** and **2g'**) forms of the group-2- and group-3-adenosylhopane-type compounds; Fig. 3.4c and g) were identified in sediments from the Amazon shelf and deep sea fan. Relative abundances of soil-marker BHPs are comparatively low and range from 5.7 to 15 % (GeoB3918; Table 3.4) and 0 to 12 % (GeoB1514; Table 3.5) of total BHPs. Low concentrations of soil-marker BHPs and branched GDGTs, as well as BIT, are observed in the uppermost samples of GeoB1514 with a clear increase at ~0.7 m.

3.3.4.2 BHPs indicative of aerobic methane oxidation

Concentrations of BHPs specific for aerobic methane oxidation show large but relatively regular fluctuations similar to those of the total BHPs in both cores (Fig. 3.4d (GeoB3918) and Fig. 3.4h (GeoB1514)). On the Amazon shelf, BHPs specific for aerobic methane oxidation comprise about 50 % of the total BHPs (Fig. 3.4b), which is remarkably high. Further down the fan, at station GeoB1514, aerobic methane oxidation markers are slightly less important but still high (about 40 % of total BHPs; Fig. 3.4f).

3.4 Discussion

3.4.1 Source of river-transported pre-aged organic material

Soil OC is an important constituent of sediments from the Amazon shelf and deep sea fan as evidenced by the presence of branched GDGTs and soil-marker BHPs. The high ^{14}C ages of bulk organic matter measured for GeoB3918 (Table 3.1) are consistent with earlier observations of old OC on the Amazon shelf (Kuehl et al., 1986; Sommerfield et al., 1995). Given the reports of high ^{14}C-ages of soils from the Amazon Basin (e.g. Martinelli et al., 1996; Pessenda et al., 2010) it is likely that the soil-derived OC in the shelf samples contributes to the observed high ^{14}C-ages even though SOC likely consists of a mixture of older and younger material (Trumbore, 1993; Trumbore et al., 1995; Martinelli et al., 1996).

An important compound group in our samples are BHPs specific for aerobic methane oxidation, especially on the Amazon shelf. The source for these diagnostic BHPs cannot be unambiguously proven but several potential sources can be excluded. First of all, as the source organisms of these specific BHPs are aerobes, recent in-situ production within the Amazon shelf and fan sediments does not seem plausible as sediments become anoxic at 20 to 30 cm below the sediment surface (GeoB1514; Schulz et al. (1994)). Additionally, high concentrations of hexafunctionalized compounds such as aminopentol (**1e**) are quite uncommon in marine sediments due to the dominance of sulfate reduction over methanogenesis which limits the release of methane into the water column (Farrimond et al., 2000; Talbot et al., 2003c; Cooke et al., 2008b). Despite the presence of methane in Amazon shelf (Figueiredo et al., 1996) and fan (Flood et al., 1995; Shipboard Scientific Party, 1995) sediments it seems unlikely that free methane can escape into the oxic parts of the sediments or the overlying water column as upwardly diffusing methane is consumed already at the base of the sulfate reduction zone (GeoB3918: 1 m depth; GeoB1514: 5

m depth) (Barnes and Goldberg, 1976; Blair and Aller, 1995). Furthermore, soils are not known to contain larger amounts of aminopentol and related compounds (Farrimond et al., 2000; Xu et al., 2009; Cooke, 2010; Rethemeyer et al., 2010) and can therefore also be excluded as major source. Instead the BHP composition of both cores rather resembles that of lacustrine sediments (Farrimond et al., 2000; Talbot et al., 2003c), also including floodplains as one important and widespread sub-setting of tropical watersheds. In fact, large floodplain lakes are well known from the Amazon Basin (e.g. Räsänen et al., 1991; Dunne et al., 1998) and analysis of one sample from such a floodplain lake (Lago Socó) reveals a high similarity in BHP inventory to the samples from the Amazon shelf and fan, including high amounts of BHPs specific for aerobic methane oxidation (Fig. 3.6). Higher relative abundances of BHT (**1a**) and aminotriol (**1c**) in the deep sea fan samples probably indicate a stronger 'marine' influence while additional amounts of BHT cyclitol ether (**1h**) are difficult to allocate to a single source, as they might be derived from the marine environment but also from the river, lake or even from land.

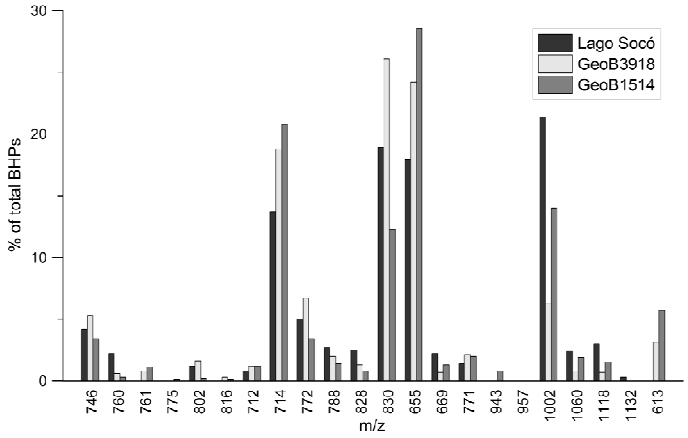

Figure 3.6. Relative abundances of BHPs measured in a sample from the floodplain lake Lago Socó in comparison to mean BHP abundances in GeoB3918-2 and GeoB1514-6.

The high constancy in BHP composition (Fig. 3.4b and f) argues for a persistent mechanism that delivers BHPs from one single source environment. We consequently suggest that compounds were produced (BHPs specific for aerobic methane oxidation) or temporarily stored (soil-marker BHPs) in a floodplain lake environment prior to erosion and redeposition on the shelf and fan and thus contribute to the old carbon. It seems likely that branched GDGTs were also delivered from the same source as the relative abundances of branched GDGTs are nearly identical within analytical error (± 10 %) in shelf sediments and Pleistocene sediments from the deep sea fan. While branched GDGTs were at least partially produced in soils, possibly close to floodplain lakes,

it might also be possible for in-situ production of branched GDGTs to occur in the floodplain lake itself. At this point we cannot distinguish between both potential sources. Lacustrine in-situ production of branched GDGTs has been suggested for tropical lakes before (Tierney and Russell, 2009; Tierney et al., 2010), leading to offsets between reconstructed and actual mean air temperature (MAT) and soil pH. Tierney and Russell (2009) reported a CBT-derived pH value of sediments from Lake Towuti (Sulawesi, Indonesia) of 7.5 while soil pH in the lake catchment was only 5.6. As pH values in Amazonian soils are mainly between 4 and 5 (e.g. Sombroek, 1966; Huguet et al., 2010) and CBT-based pH value reconstructions are as high as 6.9 (GeoB3918; Fig. 3.3d; Table 3.2) and 6.2 (Pleistocene samples of GeoB1514; Fig. 3.3i; Table 3.3), a pH bias by in-situ production of branched GDGTs in a floodplain lake seems reasonable. However, based on these indications it is suggested that the material deposited within Amazon shelf and fan sediments has previously been eroded from floodplain lakes and therefore reflects reworked OC.

Additional evidence for reworking processes on the continent comes from pollen records from the Amazon Fan. Hoorn (1997) report considerably high abundances of pre-Quaternary, reworked pollen and spores in Amazon Fan sediments. This includes pollen from *Grimsdalea magnaclavata* which are typical for Miocene sediments from Amazonia (Hoorn, 1997), i.e. the Pebas or Solimões Formations. Interestingly, as Lago Socó – even though a Quaternary feature itself – is located within the Pebas Formation, both, pollen and biomarker records, indicate the delivery of organic material from this region of the Amazon Basin to the Amazon Fan.

Reconstructed MAT for the Holocene samples from the Amazon shelf (24.5 to 25.9°C; Fig. 3.3e) are at the lower end of actually measured MAT in the Amazon Basin (26 to 27.3°C (KNMI, 1997)). Slightly lower reconstructed MAT might have been caused by in situ production of branched GDGTs in the floodplain lake (Tierney and Russell, 2009). Reconstructed MAT for the Pleistocene samples from the Amazon Fan are about 3 to 4°C lower than Holocene temperatures (22.6 to 24.1°C; Fig. 3.3j). This is consistent with a temperature difference of 2 to 6°C between the Last Glacial Maximum and the Holocene as reported by van der Hammen and Absy (1994) but slightly lower as the temperature difference of 5°C suggested e.g. by Stute et al. (1995), Colinvaux et al. (1996), Haberle (1997) and Bendle et al. (2010). The MAT-trend in GeoB1514 is very similar to the record of Bendle et al. (2010) who also investigated a sediment core (ODP942) from the Amazon Fan (Fig. 3.7). The age model of core ODP942 can thus be adopted for GeoB1514 by aligning the MAT records, suggesting that the oldest samples in this core were deposited ~37 ka BP. MAT-reconstructions are nearly identical within analytical error whether MAT are calculated using the Weijers et al. (2007a) calibration or the newly introduced regional calculation of Bendle et al.

(2010). We nevertheless use the Weijers et al. (2007a) calibration as the regional calibration gives unrealistically low MAT estimates for Amazon shelf sediments. However, in both records from the Amazon Fan Holocene samples show abnormally low MAT. Bendle et al. (2010) suggest that the low Holocene temperatures in Amazon Fan sediments are caused by an increased delivery of organic matter from the cold Andean region instead of OC produced in the eastern Amazonian lowlands. In contrast we argue that MAT of Holocene sediments from the Amazon Fan are simply biased by low concentrations of branched GDGTs. Material delivered by the Amazon River during the Holocene has been deposited on the Amazon shelf (e.g. Milliman et al., 1975), reducing sediment transport to the Amazon deep sea fan as indicated by the BIT index, TOC content and biomarker concentrations (Fig. 3.2 to 3.4). Additionally, MAT-reconstructions from GeoB3918 (Fig. 3.3e) using the Weijers et al. (2007a) calibration reflect actually measured air temperatures from the Amazon Basin, which clearly argues against the admixture of larger amounts of Andean material. A decrease in cold-adapted pollen taxa (Haberle, 1997) and an increase of the soil-derived clay minerals kaolinite and smectite – relative to the rock-derived clay minerals illite and chlorite (Debrabant et al., 1997) – towards the Holocene support this conclusion. A dominance of organic matter from the Amazon Basin rather than the Andes during the Holocene would also be consistent with observations from the Ganga-Brahmaputra system where it has been shown that at least 50 % of the organic material delivered from the Himalaya is oxidized in the floodplains and replaced by lowland organic carbon (Galy et al., 2008).

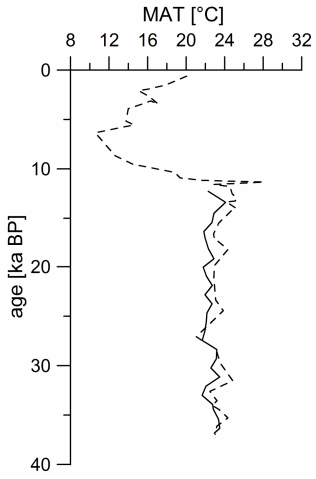

Figure 3.7. Comparison between the MAT-records of GeoB1514 (solid line) and ODP942 from Bendle et al. (2010) (dashed line). The age model is from Bendle et al. (2010).

3.4.2 Terrigenous material and transport processes

The transport of terrigenous material into marine sediments can also be evaluated using lithogenic elements (e.g. Al, Ti, K, Rb, Zr) and their ratios that can provide additional information about environmental conditions and transport processes (Schneider et al., 1997; Zabel et al., 2001). The ratio of the two lithogenic elements aluminum and titanium has been widely applied as a proxy for grain size and transport velocity, representing current or wind strength (Zabel et al., 1999 and references therein). Al/Ti-ratios as high as 20.2 have been reported from the Amazon Fan (Kronberg et al., 1986) and 16.4 in Amazon River particulate matter (Martin and Meybeck, 1979) reflecting spatial differences on gravitational effects (e.g. Spears and Kanaris-Sotiriou, 1976). Al/Ti in GeoB3918 fluctuates around ~19 reflecting a relatively long transport path of the lithogenic material. The switch in Al/Ti from 20 to 18 at 5 m in GeoB1514, however, might well reflect a more proximal river mouth during past glacial periods and therefore a more direct transport of terrigenous material to the Amazon deep sea fan consistent with previous studies (Milliman et al., 1975; Schlünz et al., 1999; Maslin et al., 2000).

The TOC content and the BIT both reflect the trends observed in Al/Ti, i.e. no large changes are observed in shelf sediments. This suggests that the source of the material and the depositional processes were close to constant over the last ~700 years covered by the shelf sediment core, within the time resolution achieved in this study. Accordingly, the most recent variations in precipitation and vegetation in the Amazon region (Eisma et al., 1991; Haug et al., 2001; Cohen et al., 2009) are not reflected by the proxy records, or they are not resolved in the sediments studied. A different picture emerges from the proxy records from the deep Amazon Fan (GeoB1514). Here, very low TOC, BHP and GDGT concentrations and a low BIT in the uppermost, Holocene interval are consistent with a higher sea level and preferential deposition of terrigenous matter on the Amazon shelf (e.g. Milliman et al., 1975). Increased BIT values, higher branched GDGT concentrations and TOC contents below ~0.7 m are in agreement with a more proximal river mouth during the LGM and the last deglaciation, reflecting colder climate conditions and a lower sea level that has led to the transport of terrigenous material to the deep fan (Milliman et al., 1975). Sediments below 5 m (reflecting a deposition before ~29 ka BP) show even higher BIT values, TOC contents and branched GDGT concentrations. Depleted $\delta^{13}C_{org}$ values as low as -27.7 ‰ in this part of the record (Schlünz et al., 1999) are consistent with an increased contribution of C_3 plant material. The increase in the abundances of terrigenous material might have been caused by the erosion of shelf sediments due to a transgressional trend of the sea level at this time (McGuire et al., 1997) and/or a higher transport energy as indicated by lowered Al/Ti-

ratios. A weak negative correlation between TOC and Al/Ti in GeoB1514 ($R^2 = 0.67$; $p < 0.01$) suggests that TOC is mainly associated with the same mineral fraction that transports Ti, which could explain the increased TOC contents below 5 m. The same might be true for the branched GDGTs which slightly co-vary with TOC ($R^2 = 0.47$; $p < 0.01$) and Ti ($R^2 = 0.52$; $p < 0.01$). In addition, marine productivity was lower during this time period as visible in the lower crenarchaeol concentrations (Fig. 3.3g). The exact identification of the processes leading to elevated abundances of terrigenous material in sediments deposited between ~29 and 37 ka BP, however, was beyond the scope of this study. Earlier estimates that terrigenous OC makes up 60 to 90 % of the Pleistocene sediments in GeoB1514 (Schlünz, 1998) are consistent with high BIT values obtained in this study, suggesting 70 – 92 % terrigenous OC.

Downcore trends of BHPs show no major similarity to the BIT, TOC and Al/Ti records. Assuming that the terrigenous material was probably mainly delivered from floodplain lakes it might be speculated that deviations in the downcore trends of BHPs and GDGTs have been caused by variations in biomarker input to the lake (e.g. deposition of soil-marker BHPs and branched GDGTs), productivity of lake-living microorganisms (BHPs specific for aerobic methane oxidation and a fraction of the branched GDGTs), and/or different efficiencies in erosion and riverine transport. Even though all processes are probably affected by climatic variations (e.g. precipitation, nutrient availability, riverine flux rates) these changes are not directly translated into the proxy records, especially as the residence time of the material in the floodplain lakes and its variability in the past is not known. While molecular and radiocarbon proxy records suggest that the OC has been pre-aged in soils and floodplain lakes before deposition on the Amazon shelf and fan, the influence of (shallow) oceanic currents on sediment dispersal or possible reworking processes also need to be considered but are beyond the scope of this study.

3.5 Conclusions

The delivery of terrigenous organic carbon to marine sediments is an important factor in constraining the global carbon cycle. In particular, the fact that OC can be extensively pre-aged in soils or other widespread environments of large tropical watersheds, e.g. floodplain lakes, can lead to elevated ^{14}C ages of sedimentary OC in marine records. This mechanism can further be biased or amplified by reworking processes. This study presents combined biomarker and ^{14}C records from Holocene shelf and Late Quaternary fan sediments from the Amazon that emphasize the important role of old OC.

Branched GDGTs and soil-marker BHPs were used to track the transport of soil organic carbon to the Amazon shelf and fan. We observe a strikingly constant composition of BHPs in both cores, which strongly argues for a common source. Strong similarities in BHP composition in the cores with those found in a floodplain lake sample from the Amazon catchment suggest preferential delivery from floodplain lakes, an environment that is widespread in all large tropical watersheds. We propose that BHPs represent an eroded and redeposited signal from current and old floodplain strata either from within the Amazon catchment or eroded from exposed older (glacial) strata on the shelf. A similar history is suggested for the branched GDGTs which seem to be produced not only in soils but also (probably to a minor extent) within floodplain lakes, in accordance with Tierney and Russell (2009) and Tierney et al. (2010).

Variations in precipitation or vegetation in the Amazon catchment are not recorded in the proxy records on the Amazon shelf consistent with the proposed erosional history of the terrigenous material. An additional influence of reworking processes by shallow ocean currents cannot be excluded but is beyond the scope of this study. This study shows evidence in support of the idea that erosional processes efficiently occur on the continent/in the watershed which lead to the delivery of not only pre-aged, but also reworked material to the ocean. We suggest that these fundamental observations have to be taken into account when interpreting sedimentary records from continental margins and reconstructing the global carbon cycle.

3.6 Acknowledgments

Helge Arz is thanked for providing two ^{14}C-ages for GeoB3918. Thanks to Janet Rethemeyer for assistance during the first BHP extractions. The technical staff from FB5 and Marum (Bremen) is thanked for support, especially Ralph Kreutz for assistance during lab work and Brit Kockisch for TOC-measurements on GeoB3918.

This study was supported by the DFG International Graduate College EUROPROX. We thank the Science Research Infrastructure Fund (SRIF) from HEFCE for funding the purchase of the ThermoFinnigan LCQ ion trap mass spectrometer (Newcastle University). Thomas Wagner acknowledges support from the Royal Society Wolfson Research Merit Award.

3.7 Appendix

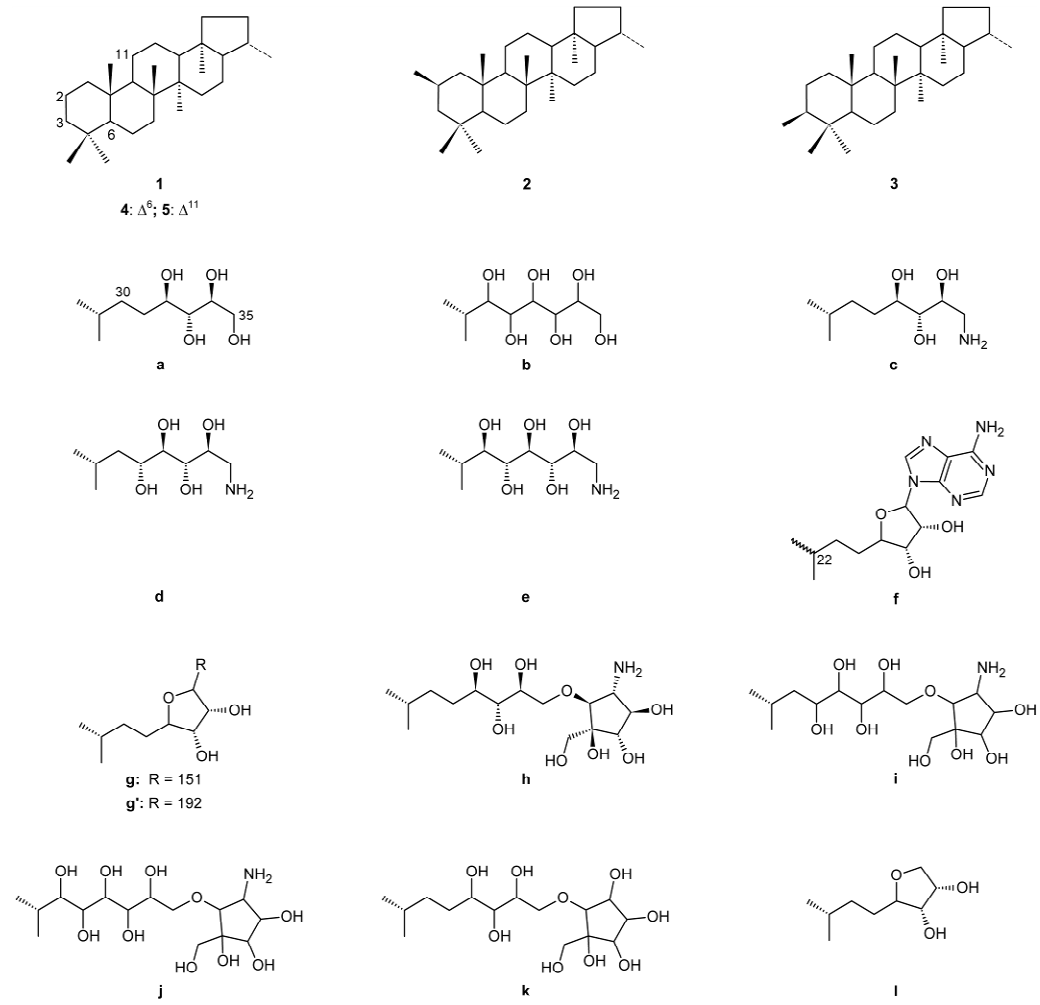

Appendix 3.1. Structures of BHPs identified in this study. Compounds were measured as their acetylated derivatives.

4. Manuscript III

Multi-proxy reconstruction of terrigenous input and sea-surface temperatures in the eastern Gulf of Guinea over the last ~35 ka

Wiebke Kallweit[a], Gesine Mollenhauer[b,c], Matthias Zabel[c]

[a] University of Bremen, Department of Geosciences, P.O. Box 330440, 28334 Bremen, Germany

[b] Alfred-Wegener Institute for Polar and Marine Research, Am Handelshafen 12, 27570 Bremerhaven, Germany

[c] University of Bremen, MARUM – Center for Marine Environmental Sciences, P.O. Box 330440, 28334 Bremen, Germany

Manuscript submitted to *Marine Geology*.

Abstract

A tight coupling between the atmospheric and oceanic circulation in the equatorial Atlantic region makes this area to an important region for paleoclimatic research. Previous studies report the occurrence of huge amounts of terrigenous material and soil organic carbon (SOC) within the marine sediments of the eastern Gulf of Guinea. We use the accumulation rates (AR) of branched glycerol dialkyl glycerol tetraethers (GDGTs) and the BIT index to identify variations in SOC delivery to the Niger Fan over the last 35 ka, and compare these records to an inorganic proxy for terrigenous input (aluminum AR) and to proxies for the marine productivity (AR of carbonate and crenarchaeol). In addition, sea surface temperatures (SSTs) are calculated based on the TEX_{86}^{H} index and environmental factors affecting the SST-reconstructions are discussed.

The BIT index clearly shows that SOC constitutes only a minor fraction of the terrigenous material deposited on the Niger Fan. Al AR are closely connected to the rate of mean sea level change after 15 ka BP, with an additional influence of the increased monsoonal precipitation and extended vegetation cover corresponding to the African Humid Period (14.8 – 5.5 ka BP). Branched GDGT AR are determined by shelf erosion in addition to the interplay of monsoonal precipitation and vegetation cover controlling soil erosion.

Paleo-SSTs show a clear shift from colder temperatures during the last glacial period (20 – 22°C) to warmer temperatures during the Holocene (24 – 26°C). However, TEX_{86}^{H}-based SSTs are cold-

biased compared to recent SSTs and Mg/Ca-based SST reconstructions, which is probably caused by a high seasonality of the Thaumarchaeota, with a maximum productivity of these organisms during the cold summer months.

4.1 Introduction

The equatorial Atlantic Ocean is a key area for paleoclimatic research as the atmospheric and oceanic circulations are tightly coupled in this region. Many studies have been conducted in this region to investigate (interacting) effects of both systems on climate change (e.g. Sarnthein et al., 1981; Pokras and Mix, 1985; McIntyre, 1989; Hughen et al., 1996; Zabel et al., 1999; Zabel et al., 2001; Schefuß et al., 2005; Mulitza et al., 2008; Tjallingii et al., 2008; Collins et al., 2010). These previous studies focused on glacial-interglacial changes of the African monsoon system, driven by precessional forcing (Pokras and Mix, 1987), as well as changes in continental vegetation and sea surface temperatures (e.g. deMenocal and Rind, 1993; Verardo and McIntyre, 1994; Dupont et al., 1998; Weldeab et al., 2007b). A very important archive in this context is terrigenous material deposited in marine sediments, which allows for simultaneous reconstructions of marine and terrestrial environmental conditions including the sources of terrigenous material, possible transport pathways and phase relationships of prevailing climate conditions.

The deposition of terrigenous material in the eastern equatorial Atlantic Ocean has been investigated via the chemical composition of the sediments and bulk organic proxies such as $\delta^{13}C_{org}$, C/N and Rock-Eval pyrolysis (Zabel et al., 2001; Adegbie et al., 2003; Holtvoeth et al., 2005). Previous studies have proposed that Niger Fan sediments mainly consist of terrigenous material. Holtvoeth et al. (2005) have further reported that a substantial amount of terrigenous organic matter is derived from the erosion of undeveloped soils with C_4-plant vegetation. To test this hypothesis we use branched glycerol dialkyl glycerol tetraethers (GDGTs) and the Branched and Isoprenoid Tetraether (BIT) index (Hopmans et al., 2004), which allow to distinguish between the soil organic carbon (SOC) fraction and the bulk terrigenous organic carbon (OC).

The reconstruction of paleo-sea surface temperatures (SSTs) is an important tool in paleoceanographic research. SSTs are a critical parameter in general circulation models of atmosphere and oceans and their reconstruction is essential for understanding past climate changes and interpreting the processes and mechanisms behind such changes (CLIMAP Project Members, 1976), and proxy parameters based on fauna, inorganic and organic geochemical properties of sediments have been developed. However, in many cases disagreement has been observed between SST reconstructions based on different proxies as each of them may record

different paleo-temperatures (Weldeab et al., 2007a; Lee et al., 2008; Castañeda et al., 2010; Leider et al., 2010).

We present data from the upper three meters of gravity core GeoB4901 obtained from the Gulf of Guinea at the Niger River deep sea fan, which represent a period of the last ~35 ka. Our aims are to investigate probable variations in the delivery of soil organic carbon to the Atlantic Ocean, as indicated by accumulation rates (AR) of branched GDGTs, and the BIT index. These data are compared with indicators for the input of inorganic particles (aluminum AR) and marine productivity (AR of carbonate and crenarchaeol). Furthermore, we reconstruct SSTs based on abundance ratios of isoprenoid GDGTs, i.e. the TEX_{86}^{H} index (Schouten et al., 2002; Kim et al., 2010) and discuss which environmental factors might have potentially affected SST-reconstructions based on this proxy.

4.2 Material and methods

4.2.1 Study area and sampling

The Niger River drains an area of ~1.21 × 10^6 km² and discharges ~192 km³/yr of water and ~40 × 10^6 t/yr of sediment into the Atlantic Ocean (Milliman and Meade, 1983). The total suspended load of the Niger River, however, is only about 26 g/m³ and therefore remarkably low (Konta, 1985 and references therein). The Niger River passes several vegetation zones, including the sub-desert zone and the Sahelian zone as well as the area of tropical rain forest near the Niger Delta (Martins and Probst, 1991). Highly weathered lateritic soils are the most common soil type in the Niger basin (Martins, 1982) which is reflected in the very high kaolinite content of the river suspended material (Konta, 1985).

Gravity core GeoB4901-8 was taken on the Niger Fan at 2184 m water depth (2.6783°N; 6.7200°E; Fig. 4.1). Since its recovery, the core was stored at +4°C. For this study only the upper three meters of the 20.2 m long core were sub-sampled. Based on radiocarbon dating, this upper section has been deposited continuously during the last ~35 ka. GDGTs were analyzed in 30 samples taken at intervals of ~10 cm while samples for element measurement were taken every centimeter. Sediment samples were freeze-dried and homogenized before analysis.

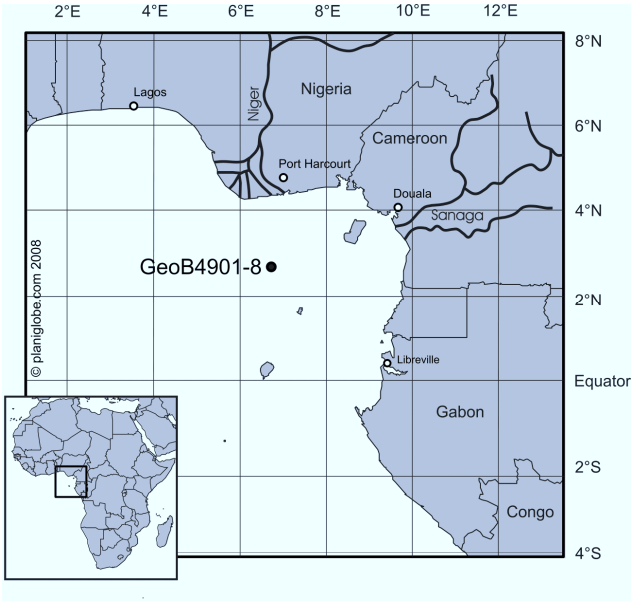

Figure 4.1. Location of core GeoB4901-8 in the Gulf of Guinea.

4.2.2 Bulk parameters

Total organic carbon (TOC) was measured with a Leco CS-300 elemental analyzer using standard procedures. For aluminum and calcium concentrations, samples were prepared by total digestion and measured with inductively coupled plasma atomic emission spectrometry (ICP-AES; Perkin Elmer, Optima 3000RL) (details in Zabel et al., 2001). Calcium concentrations were used to calculate the carbonate content and the carbonate accumulation rates.

4.2.3 Lipid extraction

About 5 g of freeze-dried, homogenized sediment were extracted with 25 ml of methanol (MeOH), dichloromethane:methanol (DCM:MeOH 1:1, v/v) and DCM, respectively. Each addition of solvents was followed by 5 minutes of sonication and 5 minutes of centrifugation. Known amounts of a C_{46}-GDGT were added as internal standard before the extraction. Total lipid extracts were combined, washed with bi-distilled water (Seralpure) to remove salts, dried over anhydrous Na_2SO_4 and concentrated under nitrogen. The total lipid extracts were re-dissolved in *n*-hexane and compounds were separated into three fractions applying column chromatography on silica gel columns. Hydrocarbons were eluted with 2 ml of *n*-hexane, ketones with 2 ml DCM:*n*-hexane (2:1, v/v), and alcohol fractions containing the GDGTs with 2 ml MeOH.

For GDGT-measurement 50 % of the MeOH-fraction were dried, weighed, re-dissolved in DCM and filtered through 0.45 μm syringe filters (Whatman) as described by Hopmans et al. (2000) and Hopmans et al. (2004). The solvents were evaporated under nitrogen and lipids were re-dissolved

in *n*-hexane:isopropanol (99:1, v/v) with a concentration of 2 mg/ml (Schouten et al., 2009) for HPLC-measurement.

4.2.4 GDGT analysis and SST estimates

Measurement of GDGTs was accomplished with a high performance liquid chromatography-atmospheric pressure chemical ionization-mass spectrometer (HPLC-APCI-MS) using an Agilent 1200 series HPLC coupled to an HP 6120 MSD equipped with automatic injector and HP Chemstation software. A detailed description of the instrumental settings for GDGT measurement is given by Leider et al. (2010). GDGT concentrations were calculated from the characteristic base peak areas of individual GDGTs relative to the base peak area of the internal standard at m/z 744. TEX_{86}^{H} and the temperature conversion were based on the equations of Kim et al. (2010). The BIT index (Hopmans et al., 2004) was calculated for the estimation of SOC input to the core location. Analytical precision was determined by repeated extraction and measurement of a lab-internal sediment standard. The analytical error for GDGT quantification was ± 10 %, deviation of BIT values was < 0.01 units. The standard deviation for TEX_{86} was 0.01, translating to an uncertainty of 0.5°C in reconstructed SSTs.

4.3 Results

4.3.1 Radiocarbon dates and age model

The age model was established by AMS ^{14}C-ages obtained on TOC of 13 samples from parallel core GeoB4901-9 (Table 4.1; Fig. 4.2). Core GeoB4901-8 could be correlated perfectly on the basis of aluminum and calcium sediment concentration profiles. AMS radiocarbon dating was conducted at the Leibniz laboratory AMS facility in Kiel (Germany). According to the reasonable assumption that a substantial portion of the organic material in these sediments was delivered by the Niger River (cf. section 4.4.1), ^{14}C-ages were converted into calendar years using the CALIB 6.0 algorithm (Stuiver et al., 2010) and a mixed marine/northern hemisphere calibration based on the Marine09 and the Intcal09 data sets (Reimer et al., 2009). The reservoir age of the South Atlantic (315 ± 18 years) was used for correction as the reservoir age of sediments from the Gulf of Guinea is not known. The relative abundances of the marine OC fraction were estimated based on the BIT index. An underestimation of the terrigenous organic fraction could result in a maximum error of 500 years based on the approximate difference between 'pure' Intcal09 and Marine09

calibrations. Consequently, given values could potentially be shifted towards younger ages. As the main purpose of this study is not to assess the exact timing of climate change but to evaluate the relative variations within single data sets, to compare different methods, and to interpret disagreements between the individual signals, this increased uncertainty is of minor importance. However, differences in the relative timing of the records are discussed if these time differences are larger than the potential error of our age model.

Table 4.1. Radiocarbon and calibrated ages (^{14}C ages and age BP, respectively) of parallel core GeoB4901-9. Calibration of ^{14}C dates is based on a mixed marine/northern hemisphere calibration. The abundance of marine OC was estimated on the basis of the BIT index.

depth [m]	^{14}C age [ka BP]	age error [ka]	age [ka BP]	fMC[a]
0.060	2.270	0.030	1.560	0.7537 ± 0.0028
0.105	3.520	0.035	3.060	0.6458 ± 0.0027
0.225	5.320	0.030	5.390	0.5159 ± 0.0020
0.345	7.420	0.040	7.630	0.3970 ± 0.0019
0.500	8.370	0.050	8.580	0.3529 ± 0.0022
0.695	9.030	0.050	9.460	0.3251 ± 0.0021
0.895	10.720	0.070	11.640	0.2632 ± 0.0024
1.095	13.040	0.080	14.390	0.1973 ± 0.0021
1.495	17.320	0.090	19.850	0.1158 ± 0.0013
1.795	20.080	0.120	23.240	0.0821 ± 0.0012
2.095	23.050	0.160	27.230	0.0567 ± 0.0011
2.495	26.340	0.180	30.580	0.0377 ± 0.0008
2.995	30.930	0.300	34.870	0.0213 ± 0.0008

[a]fMC = fraction modern carbon

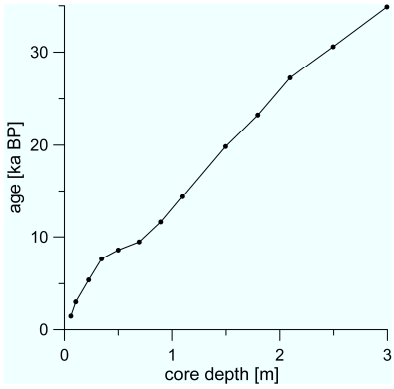

Figure 4.2. Age-depth relation for parallel core GeoB4901-9 based on 13 calibrated AMS radiocarbon ages.

4.3.2 Bulk parameters

The TOC content ranges from 1.1 to 1.8 weight (wt) % (Fig. 4.3a) and shows the lowest values around 12 ka BP. The carbonate content varies from 10.6 to 35.3 wt%, with lowest values between 10 and 6 ka BP and a maximum around 15 ka BP (Fig. 4.3b). As to be expected, the trend of the Al content is contrary to the carbonate record, with a minimum at 15 ka BP and maximum values between 10 and 7 ka BP. Al contents vary between 5.50 and 8.31 wt% (Fig. 4.3c).

TOC accumulation rates (AR) peak at 8 ka BP. During the last deglaciation (between 20 and 12 ka BP) TOC AR were four times higher than during the late Holocene (Fig. 4.3d). Carbonate AR increase at 30 ka BP and decrease after 25 ka BP (Fig. 4.3e). At 17 ka BP a sharp increase is noted. Late Holocene carbonate AR are substantially lower than carbonate AR of the last glacial period. When calculating AR, the strong contrast between Al and carbonate disappears. Al AR fluctuate around 0.08 and 0.3 g/cm² ka (Holocene and last glacial period, respectively), with generally higher values during the last glacial and a distinct, absolute maximum at about 8 ka BP (Fig. 4.3f). After ~8 ka BP Al AR decrease continuously.

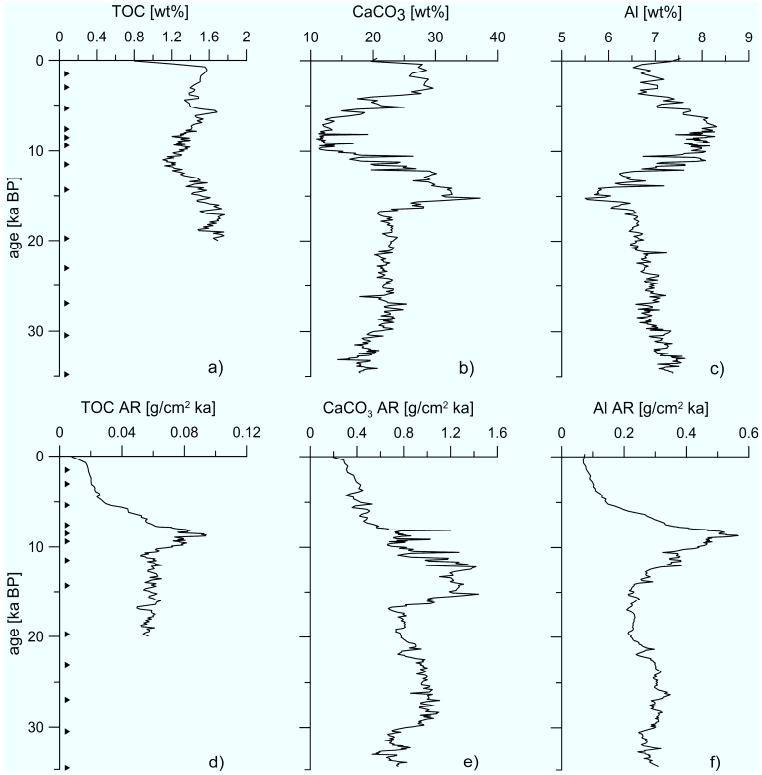

Figure 4.3. Downcore profiles of relative abundances of a) TOC, b) $CaCO_3$ and c) Al and accumulation rates of d) TOC, e) $CaCO_3$ and f) Al. Triangles in a) and d) mark depths for which ^{14}C-ages of bulk TOC exist.

4.3.3 GDGTs and BIT

The distribution of GDGTs is dominated by crenarchaeol (including its regio-isomer) and, to a lesser extent, by caldarchaeol (GDGT-0; see e.g. Hopmans et al., 2004; Weijers et al., 2007 for GDGT structures) (Table 4.2). Concentrations of archaeal GDGTs 1-3 range from 15.9 to 73.2 μg/g TOC while for the bacterial branched GDGTs (GDGTs I-III) usually lower concentrations were measured (10.3 to 32.5 μg/g TOC; Table 2). Concentrations of the branched GDGTs are nearly at the same level during the last glacial period and the late Holocene (after ca. 6.5 ka BP), but show a

sharp peak at ~10 ka BP (Fig. 4.4a). The trend in archaeal GDGTs is parallel to that of crenarchaeol concentrations which start to increase at ~17 ka BP and peak at 15 and around 10 ka BP (Fig. 4.4b). In contrast to branched GDGTs, crenarchaeol concentrations stay on a high level during the Holocene relative to the last glacial. The AR of branched GDGTs and crenarchaeol (Fig. 4.4d and 4.4e) show records similar to those of TOC and Al, including a peak at ~8 ka BP. Crenarchaeol AR, however, are not higher during the last glacial period than during the late Holocene.

The BIT index (Fig. 4.4f) shows values between 0.06 and 0.23 with a slightly decreasing trend toward the youngest sample. These values are within the range observed before for coastal to open marine settings (Hopmans et al., 2004; Kim et al., 2006).

Table 4.2. Concentrations of GDGTs [µg /g TOC], BIT, TEX $^{H}_{86}$ and reconstructed SSTs. For structures of GDGTs see e.g. Hopmans et al. (2004) or Weijers et al. (2007).

depth	age [ka BP]	TOC [wt%]	GDGT-0	crenarchaeol	crenarchaeol regio-isomer	GDGTs 1-3	branched GDGTs	BIT	TEX^{H}_{86}	SST [°C] after Kim et al. (2010)
10	2.90	1.42	96.6	173.4	10.1	56.8	10.3	0.06	-0.21	23.5
20	4.91	1.39	111.9	195.0	12.1	65.4	15.7	0.07	-0.21	24.0
30	6.80	1.50	93.6	177.8	10.6	58.4	14.7	0.08	-0.21	23.9
40	7.97	1.34	92.9	172.3	10.0	55.1	18.2	0.10	-0.21	23.5
49	8.52	1.35	118.5	217.9	13.8	73.2	23.1	0.10	-0.20	25.4
57	8.90	1.28	103.8	198.4	12.4	68.0	20.8	0.09	-0.20	24.4
69	9.44	1.31	104.9	205.5	12.5	67.7	27.5	0.12	-0.19	25.6
79	10.50	1.30	99.4	195.3	12.2	65.4	32.5	0.14	-0.20	24.7
89	11.59	1.18	73.0	144.1	9.5	51.0	18.8	0.12	-0.20	24.9
100	13.08	1.47	62.0	112.0	7.1	37.8	10.9	0.09	-0.19	26.1
109	14.32	1.53	111.1	194.5	10.9	67.1	13.0	0.06	-0.22	23.0
119	15.69	1.52	83.0	140.6	8.0	48.7	12.6	0.08	-0.20	25.2
129	17.05	1.68	52.7	77.1	3.4	25.0	13.2	0.15	-0.23	21.1
142	18.82	1.49	44.0	64.6	2.9	20.8	12.3	0.16	-0.23	21.1
149	19.78	1.66	51.2	72.2	2.9	22.9	12.1	0.14	-0.25	19.3
159	20.92	1.61	55.4	74.1	2.7	23.1	13.2	0.15	-0.27	17.6
170	22.17	1.53	65.2	87.3	3.1	27.7	13.0	0.13	-0.27	17.6
179	23.18	1.45	50.1	68.8	2.4	21.6	12.7	0.16	-0.26	17.8
190	24.64	1.45	64.5	87.7	3.4	28.2	15.8	0.15	-0.26	18.4
200	25.97	1.47	54.8	86.3	3.7	27.1	15.3	0.15	-0.24	20.1
209	27.16	1.55	39.2	52.6	1.9	15.9	15.5	0.23	-0.25	19.6
219	28.03	1.50	54.6	84.8	3.9	28.4	18.5	0.18	-0.23	21.1
231	29.03	1.63	46.0	65.0	2.6	21.3	14.2	0.18	-0.25	18.8
242	29.95	1.66	71.7	102.6	3.7	33.2	16.3	0.14	-0.26	17.8
249	30.54	1.54	64.5	91.7	3.3	30.2	19.9	0.18	-0.26	18.7
259	31.34	1.57	48.0	71.2	3.0	23.3	17.4	0.20	-0.25	19.4
270	32.22	1.64	133.2	197.6	7.8	69.6	20.8	0.10	-0.25	19.4
279	32.94	1.69	62.6	9.2	3.6	29.5	16.7	0.15	-0.25	19.0
290	33.82	1.80	32.4	49.9	2.3	16.1	14.2	0.22	-0.24	20.6
299	34.54	1.67	76.1	112.3	4.8	37.5	17.7	0.14	-0.24	19.9

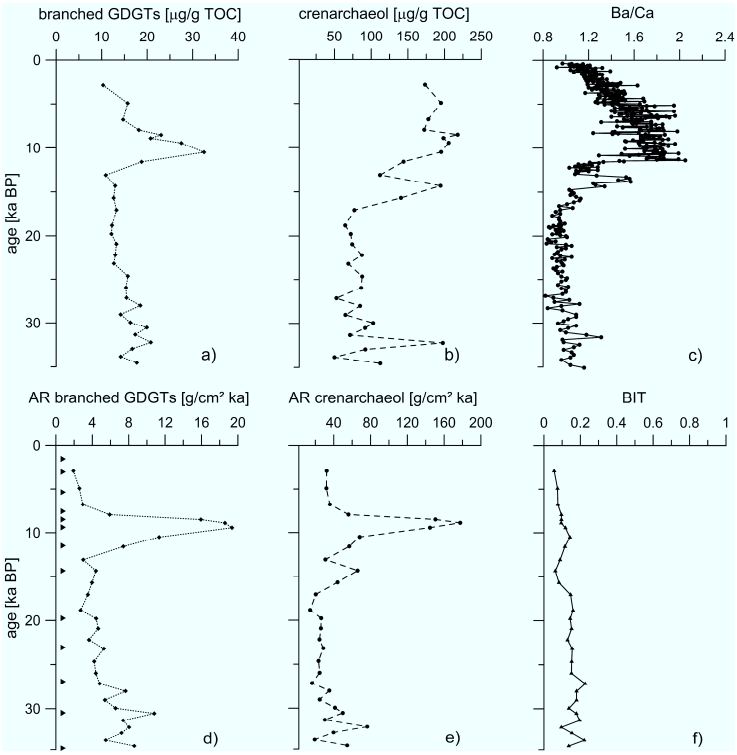

Figure 4.4. Downcore profiles of the concentrations of a) branched GDGTs and b) crenarchaeol, the accumulation rates of d) branched GDGTs, e) crenarchaeol and f) the BIT index. c) shows the Ba/Ca-record reflecting riverine discharge from Weldeab et al. (2007b). Triangles in d) mark depths for which ^{14}C-ages of bulk TOC exist.

4.3.4 SST estimates based on TEX_{86}^{H}

SST reconstructions based on the TEX_{86}^{H}-index (Kim et al., 2010) show consistently lower values during the last glacial period (20 to 22°C) than during the Holocene (24 to 26°C) with an increase towards modern values between ~20 and 16 ka BP (Fig. 4.5). This translates to a glacial to Holocene temperature difference of ~3°C in the tropical Atlantic Ocean, which is in accordance with earlier studies (e.g. Bard, 2001 and references therein). If the TEX_{86}-index with its original calibration (Schouten et al., 2002) is used, a systematic offset is observed showing lower estimates for SSTs (-1.3 to -1.8°C during the Holocene, -2.5 to -3°C before ~17 ka BP). The mean annual SST in this region is given with 27°C, and cold summer SSTs are reported to range between 25 and 26°C (Locarnini, 2010). Reconstructions based on the TEX_{86}^{H} index result in core-top SST estimates only about 1°C colder than measured summer SST.

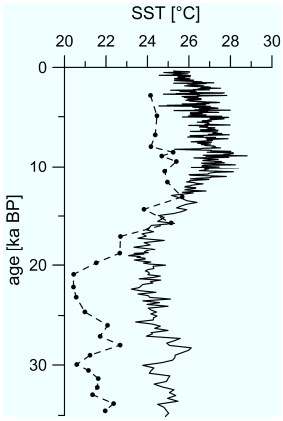

Figure 4.5. Comparison between TEX $^{H}_{86}$ -SST estimates (dashed line) and the Mg/Ca-SST record (solid line) of Weldeab et al. (2007b) for the last 35 ka BP.

4.4 Discussion

4.4.1 Terrigenous input

Terrigenous input, riverine discharge and shelf erosion

In comparison to the late Holocene, inorganic and organic terrigenous components show higher accumulation rates on the Niger Fan during the last glacial period. The parallel increase of Al AR and branched GDGT AR at ~13 ka BP is associated with increases in humidity (Gasse et al., 2008 and references therein) and riverine discharge (e.g. Pastouret, 1978; Pokras, 1987; Lézine & Cazet, 2005) reported for the Pleistocene-Holocene transition. This increased humidity starting between ~13 and 12 ka BP (Lézine and Casanova, 1989; Maley and Brenac, 1998) marks the beginning of the African Humid Period (14.8 to 5.5 ka BP; deMenocal et al., 2000; Gasse, 2000) and is the consequence of an intensification of the African monsoon (Cole et al., 2009). During the African Humid Period the Sahara was covered by a denser vegetation including a higher biodiversity and a northward expansion of tropical humid plants (Salzmann and Waller, 1998; Gasse, 2000; Salzmann et al., 2002; Watrin et al., 2009).

A maximum of riverine discharge into the eastern Gulf of Guinea at the Pleistocene-Holocene transition in connection with the onset of the African Humid Period has also been noted by Weldeab et al. (2007b) who used the Ba/Ca-ratio within the shells of planktonic foraminifera (Hall and Chan, 2004) to monitor the paleo-discharge of the Sanaga River (Cameroon) during the past 155 ka BP. The trends observed in the Ba/Ca-record of Weldeab et al. (2007b) (Fig. 4.4c) during the last glacial to Holocene time interval are similar to the trends of the Al content and branched

GDGT concentrations of core GeoB4901 (Fig. 4.3c and 4.4a). This includes in particular the sharp increase after ~13 ka BP as a consequence of the increased monsoonal precipitation (Gasse, 2000; Weldeab et al., 2005; Weldeab et al., 2007b), but also the decrease of the concentrations of terrigenous components and discharge during the late Holocene. The latter has probably been caused by a southward retreat of the monsoonal rainfall front (Weldeab et al., 2007b and references therein) and is contemporary with the end of the African Humid Period at about 5.5 ka BP (deMenocal et al., 2000). However, some discrepancies can be observed between the records, including a missing retroflection of the Younger Dryas (YD; 12.9 to 11.6 ka BP; NGRIP members, 2004) in the Al and branched GDGT records. The Younger Dryas is known to be a cooling event and a short return of dry conditions on the African continent due to a decrease in monsoonal precipitation, causing a sharp decrease in riverine discharge, reflecting surface runoff from poorly vegetated areas, and an increase in sea surface salinities (Hughen et al., 1996 and references therein; Lézine et al., 2005; Weldeab et al., 2007b). Most terrestrial records from equatorial Africa usually reflect the YD period (Gasse et al., 2008), while it is not resolved in our Al and branched GDGT data. For the branched GDGT record this may be due to a low temporal resolution of our samples.

Another possible interpretation of our records of core GeoB4901 is that the deposition of terrigenous components on the Niger Fan is dominantly affected by the erosion and re-deposition of shelf sediments during the post-glacial sea level rise. Shelf erosion might then have concealed the signal of the YD even if it might have been exported by the Niger River. Figure 4.6 shows the rate of mean sea level change compared to the AR of aluminum and branched GDGTs. The record of the Al AR shows – within the limitations of the age model – a high similarity to the rate of mean sea level change after 15 ka BP. It seems therefore likely that the Al AR – in addition to being influenced by riverine runoff – has also been affected by shelf erosion during deglacial sea level rise as highest Al AR are noted during periods of high rates of sea level rise. Before 15 ka BP sea level change only influenced the deposition of terrigenous material on the Niger Fan if the mean sea level was less than 80 meters below the present level. However, during most of the last glacial period after 35 ka BP the mean sea level was mainly more than 80 meters below the present level (Tastet et al., 1993; McGuire et al., 1997).

After ~7 ka BP the Al content decreases which is concurrent with a decreased discharge reported for the Niger River after 7.1 ka BP (Lézine et al., 2005) and a shift towards more arid conditions in the catchment area of the Niger River (Lézine and Casanova, 1989; Salzmann et al., 2002), but also with a decrease in the rate of mean sea level change. For the Sanaga River a major decrease in

discharge has only been observed at 5.1 ka BP (Weldeab et al., 2007b),. This time offset between the two river systems might have been caused by local changes in precipitation as they have been described for the middle to late Holocene before (Lézine and Casanova, 1989; Salzmann et al., 2002). The decrease in the Al content, however, might only partly be caused by a decrease in monsoonal precipitation and erosion, but might be due to a decrease in the rate of mean sea level change and associated shelf erosion.

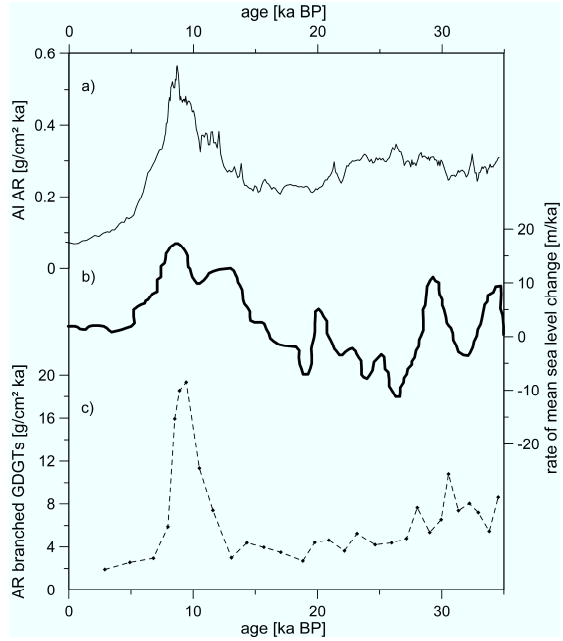

Figure 4.6. Comparison between a) the Al AR with b) the rate of mean sea level change (modified after McGuire et al., 1997) and c) the branched GDGT AR.

In contrast to the Al AR, branched GDGT AR exhibit a less pronounced connection to the rate of sea level change. However, the major peak in branched GDGT AR occurs about contemporaneously with the maximum rate of sea level change illustrating the effect of shelf erosion on the accumulation of terrigenous material at our deep-sea site. It is nevertheless suggested that branched GDGT AR are furthermore affected by the continental conditions, i.e. the soil erosion as a consequence of the interplay between high precipitation and extending vegetation cover. This might imply that – regardless of still high discharge – the increased precipitation led to a higher vegetation cover in the Niger basin, which hindered erosion and therefore lowered the amount of branched GDGTs delivered to the open ocean. This is consistent with Dupont et al. (2000) who noted an increase in rain forest pollen taxa after 14 ka BP, with a maximum extension in the early Holocene (10 to 5 ka BP), while during the LGM savannah and open forest vegetation were more abundant.

Soil organic carbon and higher plant material

BIT values are highest during the last glacial period and slowly decrease towards the late Holocene, implying that the relative amount of SOC deposited on the Niger Fan slightly decreased towards present day conditions. This small shift in SOC abundance can either be attributed to a more distal river mouth due to deglacial sea level rise (Burke, 1972) or to a reduction in precipitation as a result of a southward displacement and weakening of the West African monsoon (Weldeab et al., 2007b), or a combination of both factors. During the time period from ~16 to 12 ka BP, increasing marine productivity and rising sea level causing a landward shift of the river mouth lead to reduced BIT index values. At the Pleistocene-Holocene transition between 12 and 10 ka BP, the BIT index is slightly higher either due to an increased soil erosion and delivery of branched GDGTs to the Atlantic Ocean as a consequence of intensified monsoonal precipitation, or as a result of shelf erosion during sea level rise. After ~10 ka BP the BIT as well as concentrations of branched GDGTs decrease even though the West African monsoon is intensified, indicating that during this time period the landward shift of the river mouth is the controlling factor. A decrease in the monsoon activity is only noted after ~5 ka BP (Weldeab et al., 2007b), which however is not recorded as a further reduction of the BIT index in our core. It is therefore suggested that the dominating factor controlling the BIT index is the position of the river mouth as a consequence of deglacial sea level rise, while the West African monsoon has an additional influence especially at the beginning of the Holocene.

A relatively low supply of SOC, as indicated by the generally low values of the BIT index, seems to be contradictory to Holtvoeth et al. (2005) who reported high abundances of SOC in Niger Fan sediments. Based on the C_{org}/N_{tot} ratio and stable carbon isotopic signatures, these authors argue that a major portion of the organic fraction consists of poorly developed soil (Entisol) and C_4-plant material. If the terrigenous material was derived from poorly developed soils it would be possible that Niger Fan sediments only contained low amounts of branched GDGTs as the duration of soil formation determines the abundance of branched GDGTs (Peterse et al., 2009b). However, if pedogenesis did not proceed over a longer time period, the incorporation of plant material into these undeveloped soils should also be limited.

The determination of the exact proportions of C_3- and C_4-plant material within sediments from the Niger Fan was beyond the scope of this study. Nevertheless, published stable carbon isotopes of

long chain *n*-alkanes as constituents of epicuticular plant waxes in sediments from the eastern Gulf of Guinea in close proximity to the core location of GeoB4901 reveal that only 20 to 30 % of the OC is derived from C_4-plants (Huang et al., 2000), which is consistent with pollen records (Dupont and Agwu, 1991). However, pollen and long chain *n*-alkanes (e.g. Simoneit et al., 1977; Gagosian et al., 1981) are predominantly delivered to the ocean by eolian transport. Branched GDGTs, on the contrary, are not delivered by eolian, but by riverine transport (Hopmans et al., 2004). According to Huang et al. (2000) riverine transport to the equatorial Atlantic Ocean favors the delivery of C_3-plant material from the tropical forest, leading to more negative $\delta^{13}C$ values near the African continent. In addition, OC delivered by eolian transport mainly from the Sahara and Sahel zone (Chester et al., 1972; Simoneit et al., 1977; Cox et al., 1982; Huang et al., 2000) and deposited in the eastern Gulf of Guinea reflects only a maximum of 30 % C_4-plant material (Huang et al., 2000). The Sahara and Sahel zone represent those regions in NW Africa where undeveloped soils and C_4-vegetation predominate (Eswaran et al., 1997; Collatz et al., 1998). Low abundances of C_4-plant material within OC delivered from these regions therefore argue against a large impact of C_4-plant material on stable carbon isotopes as proposed by Holtvoeth et al. (2005). The $\delta^{13}C$ values of the samples from the Niger Fan consequently suggest that these sediments consist of a mixture of marine OC and C_3-/C_4-plant material with a predominance of C_3-plant material. In accordance with the low BIT values we therefore suggest that the delivery of major amounts of SOC with enhanced C_4-plant contributions as proposed by Holtvoeth et al. (2005) to the Niger Fan is unlikely. This is furthermore consistent with high abundances of kaolinite within the river suspended material (Konta, 1985) and in the marine sediments off the Niger River mouth (Pastouret, 1978) which indicate that at least a fraction of the terrigenous material was delivered from developed soils, as kaolinite is a typical clay mineral of lateritic soils (Fütterer, 2006).

Considering, however, that sediments from the Niger Fan have independently been reported to contain large amounts of terrigenous material using several organic and inorganic proxies (Zabel et al., 2001; Adegbie et al., 2003; Holtvoeth et al., 2005) we conclude that the BIT as a proxy for SOC underestimates the presence of terrigenous material within these sediments. Discrepancies between the amounts of terrigenous input estimated by different organic proxies ($\delta^{13}C_{org}$, C/N and lignin phenols vs. BIT) have been reported before (Walsh et al., 2008; Weijers et al., 2009b). Our results indicate that SOC reflects only a relatively small proportion of the terrigenous material deposited on the Niger Fan, while inorganic terrigenous material and possibly fresh higher plant material constitute the dominant part of the terrigenous material in these sediments. These differences might be explained by a predominance of surface runoff feeding the Niger River as it

has been reported by Martins (1982). Surface runoff might deliver high abundances of inorganic terrigenous material and fresh higher plant material into the Niger River. Soil erosion, on the contrary, presumably takes place only during the wet season, as the organic carbon pool is located in that part of the floodplain which is above the water stage during low water (Martins, 1982). In addition, a large fraction of the suspended material is delivered to the river by eolian transport (Martins, 1982), which might also increase the relative abundance of inorganic terrigenous material in comparison to SOC within the suspended load and, consequently, in the marine sediments.

4.4.2 Marine productivity

Carbonate AR are substantially higher during the last glacial period than during the late Holocene, indicating a higher marine productivity during the last glacial period. The higher marine productivity during glacials has probably been caused by an increased sediment and nutrient supply to the core site via the Niger River (Zabel et al., 2001). During the early deglaciation, at ~17 ka BP, carbonate AR and crenarchaeol AR sharply increase. The increase in carbonate and crenarchaeol AR probably indicates an increase in marine productivity which might have been stimulated by a first slight increase in riverine runoff (Weldeab et al., 2007b) supplying nutrients.
Major differences between the records of carbonate AR and crenarchaeol AR are the reflection of the Younger Dryas by the crenarchaeol AR (low values around 13 ka BP) and the different timing of maximum carbonate (between 15 and 12 ka BP) and crenarchaeol (at ~8 ka BP) AR. The peak in crenarchaeol AR at 8 ka BP is coupled with a contemporaneous peak in the AR of branched GDGTs. The concurrence of highest AR of marine (crenarchaeol) and terrigenous (branched GDGTs) compounds may indicate that marine archaeal productivity was influenced by discharge or rather by the nutrients which have been delivered by riverine runoff. In fact, as the trend in crenarchaeol AR is very similar to that of branched GDGT AR, while the discharge record shows some deviations from this trend, it might be suggested that crenarchaeol AR is determined by soil erosion rather than by riverine discharge itself. Thaumarchaeota have been shown to be nitrifiers (Könneke et al., 2005; Wuchter et al., 2006a; Herfort et al., 2007) and it is suggested that nutrients (ammonia) stored in soils were delivered to the ocean during maximum riverine, allowing for a higher productivity of the Thaumarchaeota. Lower carbonate AR at 8 ka BP may indicate that coccolithophorid productivity was lowered which might be supported by the concentrations of alkenones – lipids produced exclusively by several coccolithophorid species (Volkman et al., 1980;

Volkman et al., 1995) – measured by Weldeab et al. (2007a). As coccolithophorids are good competitors for inorganic phosphate, but are outcompeted for nitrogen by other phytoplankton groups, e.g. diatoms (Riegman et al., 2000; Baumann et al., 2005), it might be suggested that the river probably exported excess nitrogen, but not enough inorganic phosphate to trigger the productivity of coccolithophorids.

After 8 ka BP, carbonate and crenarchaeol AR decrease simultaneously with Al and branched GDGT AR. This concurrence has probably been caused by the decrease in riverine discharge and soil erosion, which not only leads to a decrease in the delivery of terrigenous material (Al and branched GDGTs), but also of nutrients. Reduced riverine nutrient supply might hence have induced a decrease of the marine productivity.

4.4.3 SST reconstructions

Mean annual SSTs measured today in the eastern Gulf of Guinea are 27°C, lowest temperatures of 25 to 26°C are observed during boreal summer (Locarnini, 2010). TEX_{86}^{H}-based SST reconstructions are about 2 to 3°C lower than measured mean annual SSTs. Several factors may account for this 'cold-bias' of TEX_{86}^{H}-based SST estimates.

One potential reason for biased SST-reconstructions is the input of terrigenous material containing also archaeal GDGTs. However, as this bias has only been observed at BIT values above 0.4 (Weijers et al., 2006a) its influence on SST reconstructions of our samples should be negligible as BIT values of our samples are low (0.06 – 0.23). Degradation under oxic conditions results in TEX_{86}^{H}-based SST estimates to be biased towards warmer values (Huguet et al., 2009; Kim et al., 2009). As we observe a bias towards colder temperatures we conclude that degradation did not play a major role for our samples. Lateral advection of (older) material has often been discussed to be a major factor influencing alkenone paleothermometry (Ohkouchi et al., 2002; Mollenhauer et al., 2003; Mollenhauer et al., 2005). In contrast to alkenones, GDGTs – and therefore the TEX_{86}-paleothermometry – seem to reflect a more local signal and are hardly influenced by lateral advection (Mollenhauer et al., 2007; Mollenhauer et al., 2008; Shah et al., 2008). This is possibly due to a higher degradation of GDGTs during transport (Mollenhauer et al., 2008), implying that also for our core site lateral advection of GDGTs did not play an important role.

Growth season and the depth habitat of Thaumarchaeota likely have a stronger impact on TEX_{86}^{H}-based SST reconstructions (Herfort et al., 2006; Huguet et al., 2006; Lee et al., 2008; Rommerskirchen et al., 2011). Thaumarchaeota have been described to be abundant throughout

the water column (Karner et al., 2001) and a subsurface production was noticed in different environments (e.g. Huguet et al., 2007; Lee et al., 2008; Rommerskirchen et al., 2011). Huguet et al. (2007) report a production mainly at 100 to 300 m water depth for the Santa Barbara Basin. For our study region we exclude GDGT production in such great water depth. In the Gulf of Guinea subsurface annual mean temperatures are between 16°C (100 m water depth) and below 12°C (300 m depth) (Locarnini, 2010). Instead, cold season SSTs during boreal summer are between 25 and 26°C (Locarnini, 2010) suggesting seasonal thaumarchaeotal near-surface production. Highest productivity of Thaumarchaeota during summer seems reasonable as this is the season of highest precipitation and therefore riverine runoff (Martins, 1982; Gasse, 2000), bringing additional amounts of ammonia into the ocean which are used by the Thaumarchaeota for their metabolism (Wuchter et al., 2006a; Herfort et al., 2007). Moreover, maximum productivity of Thaumarchaeota during the cold season (boreal summer) would be consistent with reports of highest coccolithophorid (Sikes and Keigwin, 1994; Leduc et al., 2010) and phytoplankton (Gregg and Conkright, 2001) productivity during the warm season (boreal winter/early spring) as Thaumarchaeota have been observed to bloom during times when phytoplankton productivity is low (Wuchter et al., 2005; Leider et al., 2010). However, given the importance of thaumarchaeotal subsurface production reported in other studies (Huguet et al., 2007; Lee et al., 2008; Rommerskirchen et al., 2011) subsurface production might potentially have affected TEX_{86}^{H}-based SST estimates also in this study. Hence the observed cold-bias in SST reconstructions could also be explained by the production of archaeal lipids within the thermocline (30 – 70 m water depth) during the warm season (winter).

The temperature difference between Holocene and LGM observed for TEX_{86}^{H}-based SST estimates is about 3°C, which is within the range of values found in other studies (e.g. Mix et al., 1999; Bard, 2001; Mulitza et al., 2007). This cooling during the LGM has been suggested to result from stronger circulation within the cooler thermocline and advection of subpolar waters into the tropics, in combination with equatorial and eastern boundary upwelling (Mix et al., 1999 and references therein; Niebler et al., 2003; Mulitza et al., 2007). Our results corroborate the finding of a gradual increase of SSTs from the LGM to ~10 ka BP without evidence for cooling during Heinrich Event 1 and the Younger Dryas as has been reported for other marine records from the eastern Gulf of Guinea (Gasse et al., 2008; note the contrast to terrestrial records of the region).

SST reconstructions from this study were compared to paleo-SST estimates based on foraminiferal Mg/Ca-ratios that were calculated for two cores off the Sanaga River mouth (Cameroon) ~300 km

east of our core site (Weldeab et al., 2005; Weldeab et al., 2007b). It is obvious that Mg/Ca-SST estimates are up to 2°C higher than GDGT-based SST estimates during the mid-Holocene and this temperature difference is even bigger (up to 4°C) in the Late Pleistocene (Fig. 4.5). As discussed above, these differences could be the result of different seasonal productivity of Thaumarchaeota and planktonic foraminifera, respectively. Furthermore, TEX_{86}^{H}-based SST estimates suggest stronger glacial to Holocene warming (3 to 4°C) than Mg/Ca-based SSTs (2°C), which were shown to reflect annual mean SSTs. The large temperature offset between Mg/Ca- and TEX_{86}^{H}-SST reconstructions in the Pleistocene might be explained by a greater seasonality during the LGM (4°C instead of 3°C during the Holocene) as reported by Niebler et al. (2003).

4.5 Conclusions

The relative abundance of soil organic carbon within marine sediments from the eastern Gulf of Guinea decreases from the last glacial period until the latest Holocene as reflected by the BIT index. This was probably caused by a landward shift of the Niger River mouth as a consequence of the rising sea level during the last deglaciation. An additional influence of the West African monsoon on the BIT index seems likely for the early and possibly also the late Holocene. Highest accumulation rates (AR) of terrigenous material (Al and branched GDGTs) are observed between 10 and 8 ka BP, which is the time of highest riverine discharge. The increase in riverine discharge after 12 ka BP has been caused by an increased precipitation as a consequence of an intensified West African monsoon (Cole et al., 2009) and reflects the African Humid Period (deMenocal et al., 2000). However, the rate of mean sea level change exerted the dominant influence on Al AR after 15 ka BP. During periods of high rates of sea level rise Al AR are highest, indicating that shelf erosion relocated Al formerly deposited on the shelf towards the Niger Fan. On the contrary, shelf erosion seems to be less important for the branched GDGTs, even though the peak in branched GDGT AR occurs during the time period of maximum sea level rise. It is nevertheless suggested that the peak in branched GDGT AR was amplified by soil erosion due to a high precipitation. Interestingly, crenarchaeol AR are highest during times of maximum branched GDGT AR, suggesting that Thaumarchaeota are more productive when additional nutrients (ammonia) are delivered by the rivers as a consequence of soil erosion.

SST estimates based on TEX_{86}^{H} are cold-biased in relation to modern SSTs (Locarnini, 2010) and Mg/Ca-based SST reconstructions from the eastern Gulf of Guinea (Weldeab et al., 2005; Weldeab et al., 2007b). A possible explanation for this cold-bias is the influence of a pronounced seasonality

of biomarker production. We suggest that highest thaumarchaeotal productivity occurs during the cold boreal summer months when phytoplankton is less active. In addition, highest discharge of the Niger River (Martins, 1982; Gasse, 2000) and therefore nutrient delivery occurs during boreal summer, enhancing thaumarchaeotal productivity by nutrient delivery. During the last glacial period SSTs were about 3 to 4°C lower than during the Holocene with an increase towards modern values between 20 and 16 ka BP. The amplitude between glacial and interglacial SSTs is higher for TEX_{86}^{H}-SST estimates than for Mg/Ca-based SSTs, which is probably caused by a higher temperature difference between the seasons during the LGM.

4.6 Acknowledgements

We thank Ralph Kreutz for laboratory assistance. Friedrich Schröder and Anja Bräunig are thanked for help with sample preparation. This work was funded by the DFG International Graduate College EUROPROX.

5. Conclusions and Outlook

5.1 Conclusions

This thesis comprises three case studies focused on the transport and deposition of terrigenous material in the Atlantic Ocean. Eolian transport is the second most important pathway for the transport of terrigenous material into the ocean. One case study therefore deals with the chemical signature of eolian dust collected off the NW African coast. However, the majority of terrigenous material is transported to the oceans by rivers, which is why two river systems were chosen for evaluating the deposition of terrigenous material in the adjacent continental margin systems. These studies used a multi-proxy approach combining inorganic (elements and element ratios) and organic (biomarker) proxies. Three sediment cores were chosen for this approach, including one core each from the Amazon shelf and Amazon deep sea fan and another core from the deep Niger Fan. Besides tracing terrigenous input into these environments the Amazon case study also reconstructed paleo-conditions on the continent based on specific biomarkers (GDGTs). For the Gulf of Guinea sea surface temperatures (SSTs) were reconstructed in addition to research on the deposition of terrigenous material.

5.1.1 Eolian dust off the NW African coast

Eolian dust samples taken off the NW African coast between the equator and 35°N were investigated for their chemical composition to identify the 'primary signal' of eolian dust from this region (Manuscript I). A high variability of the chemical composition of these dust samples was observed, with a clearly higher variability for samples taken between the equator and 10°N as well as north of 20°N. On the contrary, near-crustal values of element ratios are noted for samples taken between 10 and 20°N. Besides this connection between chemical composition and latitudinal sampling position the chemical composition also depends on the atmospheric dust concentration. The largest scatter in chemical composition occurs during periods of low dust concentrations while under high dust conditions element ratios similar to crustal values were observed. A possible explanation for these features is the admixture of aerosols from different sources – sea spray as well as aerosols from biomass burning or anthropogenic activities – under low dust conditions which might bias the signal of the eolian dust particles emitted from Saharan and Sahelian sources. Biomass burning is especially abundant between the equator and 10°N which is clearly reflected by the elevated K/Al-ratios of dust samples from this region. On the

contrary, between 10 and 20°N samples were mainly taken under high dust concentrations which might explain the relatively constant chemical composition of samples from this region.

The results from this study clearly show that it is not possible to define one 'primary signal' for eolian dust delivered to the Atlantic Ocean off NW Africa. A clear source assignment based on the chemical composition of eolian dust has proven very difficult (this study; Arimoto, 2001; Trapp et al., 2010) especially as mineral aerosols from different sources are already mixed during uplifting (Schütz and Sebert, 1987; Trapp et al., 2010). Additional modifications occur during transport by wind direction and strength and transport path. The large variability in the chemical composition of eolian dust might also be expressed in the marine sediment record. Without a clear 'primary signal' it is difficult to identify alterations of the dust particles occurring during transport through the water column. However, largest amounts of eolian dust are presumably deposited under high dust conditions when the variability in the chemical composition of the dust is relatively small. Moreover, sediments integrate over a long time period and a large number of dust events which might also reduce the variability in the chemical composition reflected in marine sediments. Further research is nevertheless needed to investigate the coupling between the 'primary signal' in eolian dust and the signal reflected by marine sediments.

5.1.2 Deposition of terrigenous material in continental margin systems

5.1.2.1 The Amazon continental margin

The delivery of soil organic carbon (SOC) into sediments from the Amazon shelf and deep sea fan has been successfully proven in this study by measurement of branched GDGTs and (soil-marker) BHPs (Manuscript II). The BIT index has been calculated for assessment of the relative abundance of SOC in the marine sediments. The results show that the relative abundance of SOC is even higher in Amazon Fan sediments than on the Amazon shelf. This is consistent with a more direct delivery of terrigenous material due to an offshore shift of the river mouth caused by glacial sea level fall. Unexpectedly invariant BHP and branched GDGT compositions within each of the two gravity cores led to the conclusion that the material was delivered from one single source region. Based on unexpectedly high relative abundances of BHPs specific for aerobic methane oxidation a floodplain lake source was suggested as larger amounts of these specific BHPs are not known from marine environments or soils. This hypothesis is supported by the high similarity between the BHP composition of the marine sediments and a sediment sample from a recent floodplain lake in the western Amazon Basin (Lago Socó). These results indicate that the OC deposited on the Amazon

shelf and fan has already experienced reworking on the continent as compounds were presumably produced and/or temporarily stored in a floodplain lake environment. High ^{14}C ages of TOC in Amazon shelf sediments and the presence of pre-Quaternary pollen in Amazon Fan sediments (Hoorn, 1997) support this conclusion of sediment storage and pre-aging on the continent. However, ^{14}C ages of TOC in Amazon Fan sediments do not indicate a high importance of old OC. The influence of reworking by currents on the marine sediments and the biomarker signals could not be assessed, but it can definitely not be excluded as reworking is an important and common process in continental margin systems. Reworked OC in continental margin systems off large rivers seems to be more important than commonly considered, which has implications for the interpretation of proxy records from such sediments and for constraining the global carbon cycle.

Branched GDGTs were also used for reconstruction of mean annual air temperatures (MAT) and soil pH. Reconstructed soil pH values are considerably higher than actually measured pH values in soils from the Amazon Basin. Based on this observation it is suggested that branched GDGTs were also produced in situ within the floodplain lake as has been reported before (e.g. Tierney and Russell, 2009; Tierney et al., 2010). A slight cold-bias of reconstructed MAT might also be due to in situ production of branched GDGTs within floodplain lakes. However, MAT-reconstructions for Amazon shelf sediments are at the lower end of recently measured air temperatures in the Amazon Basin. MAT reconstructed for the glacial sediments from the Amazon Fan are about 3 to 4°C lower than recent temperatures. Glacial MAT estimates show a trend nearly identical with that observed by Bendle et al. (2010) on an ODP core from the Amazon Fan. Very low MAT are also observed for Holocene samples from the Amazon Fan, but in contrast to Bendle et al. (2010) we assume that this is due to the very low amounts of terrigenous material being delivered to the Amazon Fan during the Holocene as the major deposition area is now located on the Amazon shelf. Based on the MAT estimates from the Amazon shelf which reflect recent measured air temperatures it is argued against an increased delivery of Andean material in the Holocene as proposed by Bendle et al. (2010). This might be supported by reports from the Ganga-Brahmaputra system – which is similar to the Amazon concerning the dispersal system (Walsh and Nittrouer, 2009) – where recent studies have shown that at least 50 % of material delivered from the Himalaya are oxidized in the floodplain and replaced by lowland organic carbon (Galy et al., 2011). The climatic signal delivered from the mountains is therefore to a large extent overprinted by lowland signatures, which is suggested to be the case also in the Amazon Basin.

5.1.2.2 The Niger Fan

The delivery of terrigenous material to the Niger Fan during the last ~35 ka BP has been investigated based on the accumulation rates of aluminum (as a lithogenic element) and branched GDGTs. Low BIT values in contrast to reports of a predominance of terrigenous material in these sediments (Zabel et al., 2001; Adegbie et al., 2003; Holtvoeth et al., 2005) indicate that only a minor portion of the terrigenous material represents SOC. The relative abundance of SOC relative to marine OC decreases towards the Holocene, probably caused by a landward shift of the river mouth due to a rising sea level during the last deglaciation, with additional influence of monsoonal precipitation during the early and late Holocene. The trend in the Al AR after 15 ka BP shows a high similarity to the rate of mean sea level change, indicating that Al AR are predominantly determined by shelf erosion as a consequence of deglacial sea level rise. Al AR are additionally modified by the increased intensity and resulting precipitation of the West African monsoon during the African Humid Period (14.8 - 5.5 ka BP; deMenocal et al., 2000). Branched GDGT AR, on the contrary, seems to be less affected by shelf erosion but appears to be mainly controlled by soil erosion as a result of the interplay between increased monsoonal precipitation and corresponding vegetation cover. A high similarity between the branched GDGT and crenarchaeol AR indicates that thaumarchaeotal productivity might have been enhanced by the delivery of nutrients from soils. Carbonate AR reflect a higher marine productivity during the last glacial period, probably due to increased nutrient concentrations in the surface ocean. In accordance with Zabel et al. (2001) it is suggested that the increase in marine productivity was induced by nutrients delivered to the ocean by the Niger River.

Paleo-SSTs for the Gulf of Guinea were reconstructed based on GDGTs and TEX_{86}^{H}. Comparison with actually measured SSTs in the Gulf of Guinea (Locarnini, 2010) and SST estimates by Weldeab et al. (2005; 2007b) (based on Mg/Ca-ratios of planktonic foraminifera) reveals that TEX_{86}^{H}-SST reconstructions show a cold-bias of ~2°C in the Holocene and up to 4°C in the Late Pleistocene. This is explained by a high seasonality of biomarker production, with Thaumarchaeota being especially active during cold boreal summer when phytoplankton is less active. However, an additional influence of thaumarchaeotal subsurface production can not be excluded. The temperature difference between the Holocene and the LGM is higher for TEX_{86}^{H}-SST estimates compared to Mg/Ca-based SSTs (3 and 2°C, respectively). The larger difference between Mg/Ca-based SST-estimates (Weldeab et al., 2005; Weldeab et al., 2007b) and TEX_{86}^{H}-SSTs during the last

glacial period might have been caused by a larger temperature difference between the different seasons during the LGM (Niebler et al., 2003).

5.1.2.3 Organic carbon in Niger and Amazon continental margin systems

The two continental margin systems investigated in this study were both affected by sea level changes in association with changes between glacial and interglacial conditions. Lowered sea level during the last glacial period led to a more direct delivery of terrigenous material to the Amazon and Niger deep sea fans. However, several differences can be noted between the two settings. The most apparent difference is the clearly lower abundance of soil organic carbon in the sediments of the Niger Fan compared to the Amazon shelf and fan sediments. While BIT values of 0.62 and even up to 0.92 are reported from the Amazon shelf and fan, BIT in Niger Fan sediments only reaches a maximum value of 0.23. Soil-marker BHPs were identified in all but the uppermost Holocene sample from the Amazon Fan (and shelf) but a test study based on six samples showed that soil-marker BHPs are only present in the deeper part of the Niger Fan core (Table 5.1), representing sediments from the last glacial period. During recent times soil-marker BHP concentrations are probably below detection limit. However, TOC contents are clearly higher in sediments from the Niger Fan (1.2 to 1.8 wt%) compared to the Amazon shelf (0.6 to 0.7 wt%) and fan (Holocene: 0.3 wt%; Pleistocene: 0.5 to 1 wt%). This might indicate a higher marine productivity in the Gulf of Guinea, but former studies have shown that sediments from this region mainly consist of terrigenous material (Zabel et al., 2001; Adegbie et al., 2003; Holtvoeth et al., 2005). It is consequently suggested that the organic terrigenous fraction on the Niger Fan mainly consists of fresh plant material in addition to inorganic terrigenous matter, but only a small fraction of SOC. Accordingly, in this region the BIT significantly underestimates the terrigenous input, as reported before from the Vancouver Fjord (Walsh et al., 2008). On the contrary, Amazon shelf and fan sediments contain a higher abundance of SOC compared to fresh plant material (Aller et al., 1986; Hedges et al., 1986b). Given the often high ^{14}C-ages of SOC (e.g. Martinelli et al., 1996; Pessenda et al., 2010 and references therein) organic carbon in marine sediments containing large SOC amounts can be significantly older than its depositional age as it has been shown for Amazon shelf sediments (e.g. Sommerfield et al., 1995; this study). However, similar observations have not been made for the Niger Fan sediments, indicating that ^{14}C-ages of TOC are not biased by the deposition of old SOC.

Table 5.1: BHP concentrations for six samples of GeoB4901. Compound structures as in Appendix 3.1 (section 3.7).

Sample no.	Depth [m]	TOC [wt%]	m/z 613[a] **1l**	m/z 655[b] **1a**	m/z 714[a] **1c**	m/z 746[a] **1f**	m/z 830[a] **1e**	m/z 1002[a] **1h**	Total
3	0.30	1.500	7.3	18.2	2.1	0.0	1.2	0.0	28.8
8	0.79	1.300	6.4	14.2	2.4	0.0	1.0	0.0	24.0
13	1.29	1.680	9.8	17.0	3.0	0.0	1.6	0.0	31.4
18	1.79	1.450	0.0	19.2	6.7	3.8	1.5	6.8	38.0
23	2.31	1.630	0.0	16.7	3.8	4.2	1.1	4.2	29.9
28	2.90	1.800	6.6	15.6	3.5	6.0	1.8	3.3	36.7

[a] $[M + H]^+$
[b] $[M + H - CH_3COOH]^+$

5.2 Outlook

Eolian dust

Earlier studies suggest that the chemical composition and grain size distribution of eolian dust samples taken off the West-African coast show a clear latitudinal trend and allow a distinction of different source areas (Stuut et al., 2005; M. Zabel, unpublished data). However, the chemical composition of eolian dust samples taken between the equator and 35°N shows a large variability and does not reflect a clear trend (Manuscript I). It is therefore difficult to define a clear 'primary signal' of eolian dust input into the Atlantic Ocean. However, further research should not simply concentrate on the primary signal (eolian dust) or the interpretation of the sedimentary signal, but it should rather investigate the coupling between these two signals. Considering that sedimentary signals are used to reconstruct paleoclimatic conditions it is important to know what happens to the eolian dust during its transport through the water column. It has been shown that microbial activity, aggregation, adsorption, mineralization and dissolution can severely alter particulate matter in the water column (e.g. Fowler and Knauer, 1986). The effect of these alteration processes need to be assessed and, if possible, quantified to improve the accuracy of paleoclimatic reconstructions. First results already show that large changes in element concentrations and element ratios are observed with increasing water depth (M. Zabel, unpublished data; W. Kallweit, unpublished data). It is nevertheless essential to collect more samples of particulate matter from a large range of water depths (in continuous profiles) and locations, ideally in different seasons. This might help to reveal if the changes in the chemical composition we observe in the water column reflect a rather constant situation or if the variations with depth are directly related to the delivery of eolian dust particles during the last days or weeks before sampling. The latter would imply that the eolian dust signal is directly exported to the deep sea.

Biomarkers

Further research is clearly needed concerning the BHPs and their distribution in specific microorganisms and environments. Even though many bacterial taxa have already been screened for their BHP content there are still compounds that have not been identified in cultured bacteria yet (e.g. Talbot and Farrimond, 2007 and references therein). A more comprehensive screening of bacteria for their BHP content might therefore enhance the interpretation of BHP signals from environmental samples. However, it should be considered that it will never be possible to screen the full range of hopanoid producing bacteria, e.g. due to the fact that some microorganisms might not be cultivable. A more promising approach might therefore be the microbiological investigation of specific genes encoding for enzymes involved in hopanoid biosynthesis (Bradley et al., 2010). This approach might also lead to new hypotheses concerning the interpretation of BHP abundances. For example, Bradley et al. (2010) propose that the high concentrations of adenosylhopane in soils might simply be due to the lower activity of a specific gene (hpnG) encoding the enzyme for cleaving adenine from adenosylhopane. This would indicate that adenosylhopane rather reflects certain physiological or environmental conditions but that its potential for use as a phylogenetic marker is limited.

An assessment of the possible role or source organisms of adenosylhopane and related compounds would also be helpful in comparison of soil-marker BHPs with branched GDGTs. Both compound groups are presumably produced by soil-living bacteria, but the actual producers have not been identified yet. It is nevertheless assumed that soil-marker BHPs are produced by aerobic, probably nitrogen-fixing, bacteria (Kim et al., 2011), while branched GDGTs are synthesized by heterotrophic, anaerobic Acidobacteria (Weijers et al., 2009a; Weijers et al., 2010). Consequently, soil-marker BHPs and branched GDGTs seem to be produced in different ecological niches of the soils which might explain missing correlations between the two biomarker groups (Kim et al., 2011). While detailed studies of branched GDGTs in soils and their relationship to soil pH and mean air temperature exist (e.g. Weijers et al., 2007a; Peterse et al., 2010; Weijers et al., 2011), similar studies should be conducted on BHPs. Environmental conditions might be an important factor affecting BHP diversity (Pearson et al., 2009). Further research should address the response of the BHP distribution to changes in environmental conditions such as temperature or precipitation, varying vegetation cover, soil type and soil pH. First indications exist linking BHP diversity with soil pH (Kim et al., 2011). Deciphering their linkage with environmental conditions, BHP distribution might potentially give additional information about the environmental conditions

during BHP production, beyond the simple identification of soil organic carbon transport into aquatic sediments.

Compound-specific radiocarbon dating

A promising approach in identifying organic carbon sources and depositional processes is compound-specific radiocarbon dating (e.g. Mollenhauer and Rethemeyer, 2009 and references therein). This technique might provide insight into the depositional processes occurring for example in the Amazon shelf and fan region. Our hypothesis of resuspension and redeposition of floodplain lake sediments containing BHPs might be tested by compound-specific radiocarbon dating. It would also be possible to identify age offsets between the radiocarbon ages of different biomarker compounds, e.g. branched GDGTs and various BHPs. Such an approach might provide the basis for quantifying the extent of old carbon deposition and sediment reworking, not only in Amazon shelf and fan sediments but also in other continental margin systems. For this approach additional samples from different floodplains and floodplain lakes, Amazon soils and also the Amazon River (suspended material as well as riverine sediments) would be needed to compare the biomarker signatures and radiocarbon ages of recent materials for a better source assignment of the biomarkers identified in the marine sediments. However, it should be taken into account that the riverine particulate matter is not representative for the organic matter accumulating on the Amazon shelf (Sommerfield et al., 1996). Processes affecting the organic matter at the river mouth or the influence of oceanic currents should therefore also be considered.

Different fractions of terrigenous material in marine sediments

The case study from the Niger Fan (Manuscript III) has shown that it is important to differentiate between the sources of terrigenous material deposited in marine sediments. It has previously been reported that the amount of terrigenous material in marine sediments can vary significantly if different organic proxies (e.g. $\delta^{13}C$, C/N, lignin phenols and the BIT index) are applied for these assessments (Walsh et al., 2008; Weijers et al., 2009b). The largest difference is noted if the BIT index is compared to other proxies for terrigenous input (including lithogenic elements as inorganic proxy), as the BIT only reflects the relative abundance of soil organic carbon, which can be significantly lower than the overall terrigenous input. A differentiation between the fractions of terrigenous material (e.g. SOC, inorganic material or fresh higher plant material) is not only important with regard to estimations of the terrigenous input, but also in terms of reconstructing the dominant sedimentation processes. The Niger Fan case study shows that the controlling

factors on the deposition of different terrigenous compounds can vary even for samples from one location, underlining the importance to discriminate between the fractions of terrigenous material if the deposition history of these materials shall be reconstructed.

6. References

Adegbie A. T., Schneider R. R., Röhl U., Wefer G. (2003) Glacial millennial-scale fluctuations in central African precipitation recorded in terrigenous sediment supply and freshwater signals offshore Cameroon. *Palaeogeography, Palaeoclimatology, Palaeoecology* **197**, 323-333.

Aller R. C., Mackin J. E., Cox R. T., Jr. (1986) Diagenesis of Fe and S in Amazon inner shelf muds: apparent dominance of Fe reduction and implications for the genesis of ironstones. *Continental Shelf Research* **6**, 263-289.

Aller R. C. (1998) Mobile deltaic and continental shelf muds as suboxic, fluidized bed reactors. *Marine Chemistry* **61**, 143-155.

Andreae M. O. (1983) Soot carbon and excess fine potassium: Long-range transport of combustion-derived aerosols. *Science* **220**, 1148-1151.

Arimoto R., Duce R. A., Ray B. J., Ellis W. G., Jr., Cullen J. D., Merrill J. T. (1995) Trace elements in the atmosphere over the North Atlantic. *Journal of Geophysical Research* **100**, 1199-1213.

Arimoto R. (2001) Eolian dust and climate: relationships to sources, tropospheric chemistry, transport and deposition. *Earth-Science Reviews* **54**, 29-42.

Auguet J.-C., Casamayor E. O. (2008) A hotspot for cold crenarchaeota in the neuston of high mountain lakes. *Environmental Microbiology* **10**, 1080-1086.

Avila A., Queralt-Mitjans I., Alarcón M. (1997) Mineralogical composition of African dust delivered by red rains over northeastern Spain. *Journal of Geophysical Research* **102**, 21977-21996.

Baker A. R., Kelly S. D., Biswas K. F., Witt M., Jickells T. D. (2003) Atmospheric deposition of nutrients to the Atlantic Ocean. *Geophysical Research Letters* **30**, 2296, doi:10.1029/2003GL018518.

Bard E. (2001) Comparison of alkenone estimates with other paleotemperature proxies. *Geochemistry Geophysics Geosystems* **2**, 1002, doi:10.1029/2000GC000050.

Barnes R. O., Goldberg E. D. (1976) Methane production and consumption in anoxic marine sediments. *Geology* **4**, 297-300.

Baumann K.-H., Andruleit H., Böckel B., Geisen M., Kinkel H. (2005) The significance of extant coccolithophores as indicators of ocean water masses, surface water temperature, and palaeoproductivity: a review. *Paläontologische Zeitschrift* **79**, 93-112.

Bechtel A., Smittenberg R. H., Bernasconi S. M., Schubert C. J. (2010) Distribution of branched and isoprenoid tetraether lipids in an oligotrophic and a eutrophic Swiss lake: insights into sources and GDGT-based proxies. *Organic Geochemistry* **41**, 822-832.

Bendle J. A., Weijers J. W. H., Maslin M. A., Sinninghe Damsté J. S., Schouten S., Hopmans E. C., Boot C. S., Pancost R. D. (2010) Major changes in glacial and Holocene terrestrial temperatures and sources of organic carbon recorded in the Amazon fan by tetraether lipids. *Geochemistry Geophysics Geosystems* **11**, Q12007, doi: 10.1029/2010gc003308.

Bergametti G., Gomes L., Coude-Gaussen G., Rognon P., Le Coustumer M.-N. (1989) African dust observed over Canary Islands: Source-regions identification and transport pattern for some summer situations. *Journal of Geophysical Research* **94**, 14855-14864.

Berner R. A. (1989) Biogeochemical cycles of carbon and sulfur and their effect on atmospheric oxygen over phanerozoic time. *Palaeogeography, Palaeoclimatology, Palaeoecology* **75**, 97-122.

Bird M. I., Summons R. E., Gagan M. K., Roksandic Z., Dowling L., Head J., Keith Fifield L., Cresswell R. G., Johnson D. P. (1995) Terrestrial vegetation change inferred from *n*-alkane $\delta^{13}C$ analysis in the marine environment. *Geochimica et Cosmochimica Acta* **59**, 2853-2857.

Blaga C. I., Reichart G.-J., Heiri O., Sinninghe Damsté J. S. (2009) Tetraether membrane lipid distributions in water-column particulate matter and sediments: a study of 47 European lakes along a north-south transect. *Journal of Paleolimnology* **41**, 523-540.

Blair N. E., Aller R. C. (1995) Anaerobic methane oxidation on the Amazon shelf. *Geochimica et Cosmochimica Acta* **59**, 3707-3715.

Blair N. E., Leithold E. L., Ford S. T., Peeler K. A., Holmes J. C., Perkey D. W. (2003) The persistence of memory: the fate of ancient sedimentary organic carbon in a modern sedimentary system. *Geochimica et Cosmochimica Acta* **67**, 63-73.

Blair N. E., Leithold E. L., Aller R. C. (2004) From bedrock to burial: the evolution of particulate organic carbon across coupled watershed-continental margin systems. *Marine Chemistry* **92**, 141-156.

Bligh E. G., Dyer W. J. (1959) A rapid method of total lipid extraction and purification. *Canadian Journal of Biochemistry and Physiology* **37**, 911-917.

Boot C. S., Ettwein V. J., Maslin M. A., Weyhenmeyer C. E., Pancost R. D. (2006) A 35,000 year record of terrigenous and marine lipids in Amazon Fan sediments. *Organic Geochemistry* **37**, 208-219.

Borbély-Kiss I., Kiss Á. Z., Koltay E., Szabó G., Bozó L. (2004) Saharan dust episodes in Hungarian aerosol: elemental signatures and transport trajectories. *Journal of Aerosol Science* **35**, 1205-1224.

Boyle E. A. (1983) Chemical accumulation variations under the Peru Current during the past 130,000 years. *Journal of Geophysical Research* **88**, 7667-7680.

Bradley A. S., Pearson A., Sáenz J. P., Marx C. J. (2010) Adenosylhopane: The first intermediate in hopanoid side chain biosynthesis. *Organic Geochemistry* **41**, 1075-1081.

Bristow C. S., Drake N., Armitage S. (2009) Deflation in the dustiest place on Earth: The Bodélé Depression, Chad. *Geomorphology* **105**, 50-58.

Bristow C. S., Hudson-Edwards K. A., Chappell A. (2010) Fertilizing the Amazon and equatorial Atlantic with West African dust. *Geophysical Research Letters* **37**, L14807, doi:10.1029/2010GL043486.

Brochier-Armanet C., Boussau B., Gribaldo S., Forterre P. (2008) Mesophilic crenarchaeota: proposal for a third archaeal phylum, the Thaumarchaeota. *Nature Reviews Microbiology* **6**, 245-252.

Brocks J. J., Summons R. E. (2004) Sedimentary hydrocarbons, biomarkers for early life. In: *Treatise on Geochemistry* 8 (Schlesinger W. H. (Ed.)). Pergamon Press, Oxford, 63-115.

Brocks J. J., Pearson A. (2005) Building the biomarker tree of life. *Reviews in Mineralogy and Geochemistry* **59**, 233-258.

Burdige D. J. (2005) Burial of terrestrial organic matter in marine sediments: A re-assessment. *Global Biogeochemical Cycles* **19**, GB4011, doi: 10.1029/2004gb002368.

Burdige D. J. (2007) Preservation of organic matter in marine sediments: Controls, mechanisms, and an imbalance in sediment organic carbon budgets? *Chemical Reviews* **107**, 467-485.

Burke K. (1972) Longshore drift, submarine canyons, and submarine fans in development of Niger Delta. *The American Association of Petroleum Geologists Bulletin* **56**, 1975-1983.

Calvert S. E. (1976) The mineralogy and geochemistry of nearshore sediments. In: *Treatise on chemical oceanography* 6 (Riley J. P., Chester R. (Eds.)). Academic Press, San Diego, 187-280.

Caquineau S., Gaudichet A., Gomes L., Magonthier M.-C., Chatenet B. (1998) Saharan dust: Clay ratio as a relevant tracer to assess the origin of soil-derived aerosols. *Geophysical Research Letters* **25**, 983-986.

Caquineau S., Gaudichet A., Gomes L., Legrand M. (2002) Mineralogy of Saharan dust transported over northwestern tropical Atlantic Ocean in relation to source regions. *Journal of Geophysical Research* **107**, D15, doi:10.1029/2000JD000247.

Castañeda I. S., Schefuß E., Pätzold J., Sinninghe Damsté J. S., Weldeab S., Schouten S. (2010) Millennial-scale sea surface temperature changes in the eastern Mediterranean (Nile River Delta region) over the last 27,000 years. *Paleoceanography* **25**, PA1208, doi: 10.1029/2009PA001740.

Castillo S., Moreno T., Querol X., Alastuey A., Cuevas E., Herrmann L., Mounkaila M., Gibbons W. (2008) Trace element variation in size-fractionated African desert dusts. *Journal of Arid Environments* **72**, 1034-1045.

Cerling T. E., Harris J. M., MacFadden B. J., Leakey M. G., Quade J., Eisenmann V., Ehleringer J. R. (1997) Global vegetation change through the Miocene/Pliocene boundary. *Nature* **389**, 153-158.

Chen Y., Siefert R. L. (2004) Seasonal and spatial distributions and dry deposition fluxes of atmospheric total and labile iron over the tropical and subtropical North Atlantic Ocean. *Journal of Geophysical Research* **109**, D09305, doi:10.1029/2003JD003958.

Chester R., Elderfield H., Griffin J. J. (1971) Dust transported in the north-east and south-east trade winds in the Atlantic Ocean. *Nature* **233**, 474-476.

Chester R., Elderfield H., Griffin J. J., Johnson L. R., Padgham R. C. (1972) Eolian dust along the eastern margins of the Atlantic Ocean. *Marine Geology* **13**, 91-105.

Chester R., Griffiths A. G., Hirst J. M. (1979) The influence of soil-sized atmospheric particulates on the elemental chemistry of the deep-sea sediments of the northeastern Atlantic. *Marine Geology* **32**, 141-154.

Chiapello I., Bergametti G., Chatenet B., Bousquet P., Dulac F., Santos Soares E. (1997) Origins of African dust transported over the northeastern tropical Atlantic. *Journal of Geophysical Research* **102**, 13701-13709.

CLIMAP Project Members (1976) The surface of the ice-age earth. *Science* **191**, 1131-1137.

Cohen M., Behling H., Lara R., Smith C., Matos H., Vedel V. (2009) Impact of sea-level and climatic changes on the Amazon coastal wetlands during the late Holocene. *Vegetation History and Archaeobotany* **18**, 425-439.

Cole J. M., Goldstein S. L., deMenocal P. B., Hemming S. R., Grousset F. E. (2009) Contrasting compositions of Saharan dust in the eastern Atlantic Ocean during the last deglaciation and African Humid Period. *Earth and Planetary Science Letters* **278**, 257-266.

Colinvaux P. A., De Oliveira P. E., Moreno J. E., Miller M. C., Bush M. B. (1996) A long pollen record from lowland Amazonia: forest and cooling in glacial times. *Science* **274**, 85-88.

Collatz G. J., Berry J. A., Clark J. S. (1998) Effects of climate and atmospheric CO_2 partial pressure on the global distribution of C_4 grasses: present, past, and future. *Oecologia* **114**, 441-454.

Collins J. A., Schefuß E., Heslop D., Mulitza S., Prange M., Zabel M., Tjallingii R., Dokken T. M., Huang E., Mackensen A., Schulz M., Tian J., Zarriess M., Wefer G. (2010) Interhemispheric symmetry of the tropical African rainbelt over the past 23,000 years. *Nature Geoscience* **4**, 42-45.

Cooke M. P., Talbot H. M., Farrimond P. (2008a) Bacterial populations recorded in bacteriohopanepolyol distributions in soils from Northern England. *Organic Geochemistry* **39**, 1347-1358.

Cooke M. P., Talbot H. M., Wagner T. (2008b) Tracking soil organic carbon transport to continental margin sediments using soil-specific hopanoid biomarkers: A case study from the Congo fan (ODP site 1075). *Organic Geochemistry* **39**, 965-971.

Cooke M. P., van Dongen B. E., Talbot H. M., Semiletov I., Shakhova N., Guo L., Gustafsson Ö. (2009) Bacteriohopanepolyol biomarker composition of organic matter exported to the Arctic Ocean by seven of the major Arctic rivers. *Organic Geochemistry* **40**, 1151-1159.

Cooke M. P. (2010) The role of bacteriohopanepolyols as biomarkers for soil bacterial communities and soil derived organic matter. PhD Thesis, Newcastle University.

Coolen M. J. L., Talbot H. M., Abbas B. A., Ward C., Schouten S., Volkman J. K., Sinninghe Damsté J. S. (2008) Sources for sedimentary bacteriohopanepolyols as revealed by 16S rDNA stratigraphy. *Environmental Microbiology* **10**, 1783-1803.

Cox R. E., Mazurek M. A., Simoneit B. R. T. (1982) Lipids in Harmattan aerosols of Nigeria. *Nature* **296**, 848-849.

Cvejic J. H., Bodrossy L., Kovács K. L., Rohmer M. (2000) Bacterial triterpenoids of the hopane series from the methanotrophic bacteria *Methylocaldum* spp.: phylogenetic implications and first evidence for an unsaturated aminobacteriohopanepolyol. *FEMS Microbiology Letters* **182**, 361-365.

da Silveira I. C. A., de Miranda L. B., Brown W. S. (1994) On the origins of the North Brazil Current. *Journal of Geophysical Research* **99**, 22501-22512.

Damuth J. E., Flood R. D. (1984) Morphology, sedimentation processes, and growth pattern of the Amazon deep-sea fan. *Geo-Marine Letters* **3**, 109-117.

Debrabant T., Lopez M., Chamley H. (1997) Clay mineral distribution and significance in quaternary sediments of the Amazon fan. In: *Proceedings of the Ocean Drilling Program, Scientific Results* 155 (Flood R. D., Piper D. J. W., Klaus A., Peterson L. C. (Eds.)), College Station, TX (Ocean Drilling Program), 177-192.

Deines P. (1980) The isotopic composition of reduced organic carbon. In: *Handbook of environmental isotope geochemistry, Vol. 1* (Fritz P., Fontes C. (Eds.)). Elsevier, New York, 239-406.

deMenocal P. B., Rind D. (1993) Sensitivity of Asian and African climate to variations in seasonal insolation, glacial ice cover, sea surface temperature, and Asian orography. *Journal of Geophysical Research* **98**, 7265-7287.

deMenocal P. B., Ortiz J., Guilderson T., Adkins J., Sarnthein M., Baker L., Yarusinsky M. (2000) Abrupt onset and termination of the African Humid Period: rapid climate responses to gradual insolation forcing. *Quaternary Science Reviews* **19**, 347-361.

Dickens A. F., Gelinas Y., Masiello C. A., Wakeham S., Hedges J. I. (2004) Reburial of fossil organic carbon in marine sediments. *Nature* **427**, 336-339.

Duce R. A., Liss P. S., Merrill J. T., Atlas E. L., Buat-Ménard P., Hicks B. B., Miller J. M., Prospero J. M., Arimoto R., Church T. M., Ellis W., Galloway J. N., Hansen L., Jickells T. D., Knap A. H., Reinhardt K. H., Schneider B., Soudine A., Tokos J. J., Tsunogai S., Wollast R., Zhou M. (1991) The atmospheric input of trace species to the world ocean. *Global Biogeochemical Cycles* **5**, 193-259.

Dunne T., Mertes L. A. K., Meade R. H., Richey J. E., Forsberg B. R. (1998) Exchanges of sediment between the flood plain and channel of the Amazon River in Brazil. *Geological Society of America Bulletin* **110**, 450-467.

Dupont L., Agwu C. (1991) Environmental control of pollen grain distribution patterns in the Gulf of Guinea and offshore NW-Africa. *Geologische Rundschau* **80**, 567-589.

Dupont L. M., Weinelt M. (1996) Vegetation history of the savanna corridor between the Guinean and the Congolian rain forest during the last 150,000 years. *Vegetation History and Archaeobotany* **5**, 273-292.

Dupont L. M., Marret F., Winn K. (1998) Land-sea correlation by means of terrestrial and marine palynomorphs from the equatorial East Atlantic: phasing of SE trade winds and the oceanic productivity. *Palaeogeography, Palaeoclimatology, Palaeoecology* **142**, 51-84.

Dupont L. M., Jahns S., Marret F., Ning S. (2000) Vegetation change in equatorial West Africa: time-slices for the last 150 ka. *Palaeogeography, Palaeoclimatology, Palaeoecology* **155**, 95-122.

Eglinton T. I., Eglinton G. (2008) Molecular proxies for paleoclimatology. *Earth and Planetary Science Letters* **275**, 1-16.

Eisma D., Augustinus P. G. E. F., Alexander C. (1991) Recent and subrecent changes in the dispersal of Amazon mud. *Netherlands Journal of Sea Research* **28**, 181-192.

Engelstaedter S., Tegen I., Washington R. (2006) North African dust emissions and transport. *Earth-Science Reviews* **79**, 73-100.

Eswaran H., Almaraz R., van den Berg E., Reich P. (1997) An assessment of the soil resources of Africa in relation to productivity. *Geoderma* **77**, 1-18.

Farquhar G. D., Ehleringer J. R., Hubick K. T. (1989) Carbon isotope discrimination and photosynthesis. *Annual Review of Plant Physiology and Plant Molecular Biology* **40**, 503-537.

Farrimond P., Fox P. A., Innes H. E., Miskin I. P., Head I. M. (1998) Bacterial sources of hopanoids in recent sediments: Improving our understanding of ancient hopane biomarkers. *Ancient Biomolecules* **2**, 147-166.

Farrimond P., Head I. M., Innes H. E. (2000) Environmental influence on the biohopanoid composition of recent sediments. *Geochimica et Cosmochimica Acta* **64**, 2985-2992.

Figueiredo A. G., Jr., Nittrouer C. A., Costa E. d. A. (1996) Gas-charged sediments in the Amazon submarine delta. *Geo-Marine Letters* **16**, 31-35.

Flood R. D., Piper D. J. W., Shipboard Scientific Party (1995) Introduction. In: *Proceedings of the Ocean Drilling Program, Initial Reports* 155 (Flood R. D., Piper D. J. W., Klaus A., et al. (Eds.)), College Station, TX (Ocean Drilling Program), 5-16.

Formenti P., Rajot J. L., Desboeufs K. V., Caquineau S., Chevaillier S., Nava S., Gaudichet A., Journet E., Triquet S., Alfaro S. C., Chiari M., Haywood J., Coe H., Highwood E. (2008) Regional variability of the composition of mineral dust from western Africa: Results from the AMMA SOP0/DABEX and DODO field campaigns. *Journal of Geophysical Research* **113**, D00C13, doi:10.1029/2008JD009903.

Fowler S. W., Knauer G. A. (1986) Role of large particles in the transport of elements and organic compounds through the oceanic water column. *Progress In Oceanography* **16**, 147-194.

Franzén L. (1989) A dustfall episode on the Swedish West Coast, October 1987. *Geografiska Annaler. Series A, Physical Geography* **71**, 263-267.

Franzén L. G., Hjelmroos M., Kållberg P., Brorström-Lunden E., Juntto S., Savolainen A.-L. (1994) The 'yellow snowepisode' of northern Fennoscandia, march 1991--A case study of long-distance transport of soil, pollen and stable organic compounds. *Atmospheric Environment* **28**, 3587-3604.

Fütterer D. K. (2006) The solid phase of marine sediments. In: *Marine Geochemistry* (Schulz H. D., Zabel M. (Eds.)). Springer-Verlag, Berlin Heidelberg, 1-25.

Gagosian R. B., Peltzer E. T., Zafiriou O. C. (1981) Atmospheric transport of continentally derived lipids to the tropical North Pacific. *Nature* **291**, 312-314.

Galy V., France-Lanord C., Lartiges B. (2008) Loading and fate of particulate organic carbon from the Himalaya to the Ganga-Brahmaputra delta. *Geochimica et Cosmochimica Acta* **72**, 1767-1787.

Galy V., Eglinton T., France-Lanord C., Sylva S. (2011) The provenance of vegetation and environmental signatures encoded in vascular plant biomarkers carried by the Ganges-Brahmaputra rivers. *Earth and Planetary Science Letters* **304**, 1-12.

Ganor E. (1994) The frequency of Saharan dust episodes over Tel Aviv, Israel. *Atmospheric Environment* **28**, 2867-2871.

Gasse F. (2000) Hydrological changes in the African tropics since the Last Glacial Maximum. *Quaternary Science Reviews* **19**, 189-211.

Gasse F., Chalié F., Vincens A., Williams M. A. J., Williamson D. (2008) Climatic patterns in equatorial and southern Africa from 30,000 to 10,000 years ago reconstructed from terrestrial and near-shore proxy data. *Quaternary Science Reviews* **27**, 2316-2340.

Gaudichet A., Echalar F., Chatenet B., Quisefit J. P., Malingre G., Cachier H., Buat-Menard P., Artaxo P., Maenhaut J. (1995) Trace elements in tropical African savanna biomass burning aerosols. *Journal of Atmospheric Chemistry* **22**, 19-39.

Ginoux P., Chin M., Tegen I., Prospero J. M., Holben B., Dubovik O., Lin S.-J. (2001) Sources and distributions of dust aerosols simulated with the GOCART model. *Journal of Geophysical Research* **106**, 20255-20273.

Glaccum R. A., Prospero J. M. (1980) Saharan aerosols over the tropical North Atlantic — Mineralogy. *Marine Geology* **37**, 295-321.

Goñi M. A. (1997) Record of terrestrial organic matter composition in Amazon fan sediments. In: *Proceedings of the Ocean Drilling Program, Scientific Results* 155 (Flood R. D., Piper D. J. W., Klaus A., Peterson L. C. (Eds.)), College Station, TX (Ocean Drilling Program), 519-530.

Goñi M. A., Yunker M. B., Macdonald R. W., Eglinton T. I. (2005) The supply and preservation of ancient and modern components of organic carbon in the Canadian Beaufort Shelf of the Arctic Ocean. *Marine Chemistry* **93**, 53-73.

Gordon E. S., Goñi M. A. (2003) Sources and distribution of terrigenous organic matter delivered by the Atchafalaya River to sediments in the northern Gulf of Mexico. *Geochimica et Cosmochimica Acta* **67**, 2359-2375.

Goudie A. S., Middleton N. J. (2001) Saharan dust storms: nature and consequences. *Earth-Science Reviews* **56**, 179-204.

Gregg W. W., Conkright M. E. (2001) Global seasonal climatologies of ocean chlorophyll: Blending in situ and satellite data for the Coastal Zone Color Scanner era. *Journal of Geophysical Research* **106**, 2499-2515.

Guo L., Semiletov I., Gustafsson Ö., Ingri J., Andersson P., Dudarev O., White D. (2004) Characterization of Siberian Arctic coastal sediments: Implications for terrestrial organic carbon export. *Global Biogeochemical Cycles* **18**, GB1036, doi: 10.1029/2003gb002087.

Haberle S. G. (1997) Upper Quaternary vegetation and climate history of the Amazon Basin: Correlating marine and terrestrial pollen records. In: *Proceedings of the Ocean Drilling Program, Scientific Results* 155 (Flood R. D., Piper D. J. W., Klaus A., Peterson L. C. (Eds.)), College Station, TX (Ocean Drilling Program), 381-396.

Haberle S. G., Maslin M. A. (1999) Late Quaternary vegetation and climate change in the Amazon Basin based on a 50,000 year pollen record from the Amazon Fan, ODP Site 932. *Quaternary Research* **51**, 27-38.

Hall J. M., Chan L.-H. (2004) Ba/Ca in *Neogloboquadrina pachyderma* as an indicator of deglacial meltwater discharge into the western Arctic Ocean. *Paleoceanography* **19**, PA1017, doi: 10.1029/2003PA000910.

Hand J. L., Mahowald N., Chen Y., Siefert R. L., Luo C., Subramaniam A., Fung I. (2004) Estimates of soluble iron from observations and a global mineral aerosol model: biogeochemical implications. *Journal of Geophysical Research* **109**, D17205, doi:10.1029/2004JD004574.

Haug G. H., Hughen K. A., Sigman D. M., Peterson L. C., Röhl U. (2001) Southward migration of the Intertropical Convergence Zone through the Holocene. *Science* **293**, 1304-1308.

Hedges J. I., Clark W. A., Quay P. D., Richey J. E., Devol A. H., de M. Santos U. (1986a) Compositions and fluxes of particulate organic material in the Amazon River. *Limnology and Oceanography* **31**, 717-738.

Hedges J. I., Ertel J. R., Quay P. D., Grootes P. M., Richey J. E., Devol A. H., Farwell G. W., Schmidt F. W., Salati E. (1986b) Organic Carbon-14 in the Amazon River System. *Science* **231**, 1129-1131.

Hedges J. I., Keil R. G. (1995) Sedimentary organic matter preservation: an assessment and speculative synthesis. *Marine Chemistry* **49**, 81-115.

Henrich R., Baumann K.-H., Gerhardt S., Gröger M., Volbers A. (2003) Carbonate preservation in deep and intermediate water masses in the South Atlantic: Evaluation and geological record (a review). In: *The South Atlantic in the Late Quaternary: Reconstruction of material budgets and current systems* (Wefer G., Mulitza S., Ratmeyer V. (Eds.)). Springer-Verlag, Berlin Heidelberg, 645-670.

Herfort L., Schouten S., Boon J. P., Sinninghe Damsté J. S. (2006) Application of the TEX_{86} temperature proxy to the southern North Sea. *Organic Geochemistry* **37**, 1715-1726.

Herfort L., Schouten S., Abbas B., Veldhuis M. J. W., Coolen M. J. L., Wuchter C., Boon J. P., Herndl G. J., Sinninghe Damsté J. S. (2007) Variations in spatial and temporal distribution of Archaea in the North Sea in relation to environmental variables. *FEMS Microbiology Ecology* **62**, 242-257.

Herrmann L., Jahn R., Stahr K. (1996) Identification and quantification of dust additions in peri-Saharan soils. In: *The impact of desert dust across the Mediterranean* (Guerzoni S., Chester R. (Eds.)), Environmental science and technology library 11. Kluwer Academic Publisher, Dordrecht Boston London, 173-182.

Hessler I., Dupont L., Bonnefille R., Behling H., González C., Helmens K. F., Hooghiemstra H., Lebamba J., Ledru M.-P., Lézine A.-M., Maley J., Marret F., Vincens A. (2010) Millennial-scale changes in vegetation records from tropical Africa and South America during the last glacial. *Quaternary Science Reviews* **29**, 2882-2899.

Hinrichs K.-U., Rullkötter J. (1997) Terrigenous and marine lipids in Amazon Fan sediments: Implications for sedimentological reconstructions. In: *Proceedings of the Ocean Drilling Program, Scientific Results* 155 (Flood R. D., Piper D. J. W., Klaus A., Peterson L. C. (Eds.)), College Station, TX (Ocean Drilling Program), 539-553.

Holtvoeth J., Wagner T., Schubert C. J. (2003) Organic matter in river-influenced continental margin sediments: The land-ocean and climate linkage at the Late Quaternary Congo fan (ODP Site 1975). *Geochemistry Geophysics Geosystems* **4**, 1109-1135.

Holtvoeth J., Kolonic S., Wagner T. (2005) Soil organic matter as an important contributor to Late Quaternary sediments of the tropical West African continental margin. *Geochimica et Cosmochimica Acta* **69**, 2031-2041.

Holz C., Stuut J.-B. W., Henrich R. (2004) Terrigenous sedimentation processes along the continental margin off NW Africa: implications from grain-size analysis of seabed sediments. *Sedimentology* **51**, 1145-1154.

Hoorn C. (1997) Palynology of the Pleistocene glacial/interglacial cycles of the Amazon Fan (Holes 940A, 944A, and 946A). In: *Proceedings of the Ocean Drilling Program, Scientific Results* 155 (Flood R. D., Piper D. J. W., Klaus A., Peterson L. C. (Eds.)), College Station, TX (Ocean Drilling Program), 397-409.

Hopmans E. C., Schouten S., Pancost R. D., van der Meer M. T. J., Sinninghe Damsté J. S. (2000) Analysis of intact tetraether lipids in archaeal cell material and sediments by high performance liquid chromatography/atmospheric pressure chemical ionization mass spectrometry. *Rapid Communications in Mass Spectrometry* **14**, 585-589.

Hopmans E. C., Weijers J. W. H., Schefuß E., Herfort L., Sinninghe Damsté J. S., Schouten S. (2004) A novel proxy for terrestrial organic matter in sediments based on branched and isoprenoid tetraether lipids. *Earth and Planetary Science Letters* **224**, 107-116.

Huang Y., Dupont L., Sarnthein M., Hayes J. M., Eglinton G. (2000) Mapping of C_4 plant input from North West Africa into North East Atlantic sediments. *Geochimica et Cosmochimica Acta* **64**, 3505-3513.

Hughen K. A., Overpeck J. T., Peterson L. C., Trumbore S. (1996) Rapid climate changes in the tropical Atlantic region during the last deglaciation. *Nature* **380**, 51-54.

Huguet A., Fosse C., Metzger P., Fritsch E., Derenne S. (2010) Occurrence and distribution of extractable glycerol dialkyl glycerol tetraethers in podzols. *Organic Geochemistry* **41**, 291-301.

Huguet C., Kim J.-H., Sinninghe Damsté J. S., Schouten S. (2006) Reconstruction of sea surface temperature variations in the Arabian Sea over the last 23 kyr using organic proxies (TEX_{86} and $U^{K'}_{37}$). *Paleoceanography* **21**, PA3003, doi: 10.1029/2005pa001215.

Huguet C., Schimmelmann A., Thunell R., Lourens L. J., Sinninghe Damsté J. S., Schouten S. (2007) A study of the TEX_{86} paleothermometer in the water column and sediments of the Santa Barbara Basin, California. *Paleoceanography* **22**, PA3203, doi: 10.1029/2006PA001310.

Huguet C., Kim J.-H., de Lange G. J., Sinninghe Damsté J. S., Schouten S. (2009) Effects of long term oxic degradation on the $U^{K'}_{37}$, TEX_{86} and BIT organic proxies. *Organic Geochemistry* **40**, 1188-1194.

Husar R. B., Prospero J. M., Stowe L. L. (1997) Characterization of tropospheric aerosols over the oceans with the NOAA advanced very high resolution radiometer optical thickness operational product. *Journal of Geophysical Research* **102**, 16889-16909.

Hwang J., Druffel E. R. M., Komada T. (2005) Transport of organic carbon from the California coast to the slope region: A study of $\Delta^{14}C$ and $\delta^{13}C$ signatures of organic compound classes. *Global Biogeochemical Cycles* **19**, GB2018, doi: 10.1029/2004gb002422.

Inthorn M., Wagner T., Scheeder G., Zabel M. (2006) Lateral transport controls distribution, quality, and burial of organic matter along continental slopes in high-productivity areas. *Geology* **34**, 205-208.

Ittekkot V., Safiullah S., Arain R. (1986) Nature of organic matter in rivers with deep sea connections: The Ganges-Brahmaputra and Indus. *The Science of the Total Environment* **58**, 93-107.

Jickells T. D., An Z. S., Andersen K. K., Baker A. R., Bergametti G., Brooks N., Cao J. J., Boyd P. W., Duce R. A., Hunter K. A., Kawahata H., Kubilay N., LaRoche J., Liss P. S., Mahowald N., Prospero J. M., Ridgwell A. J., Tegen I., Torres R. (2005) Global iron connections between desert dust, ocean biogeochemistry, and climate. *Science* **308**, 67-71.

Jiménez-Vélez B., Detrés Y., Armstrong R. A., Gioda A. (2009) Characterization of African Dust ($PM_{2.5}$) across the Atlantic Ocean during AEROSE 2004. *Atmospheric Environment* **43**, 2659-2664.

Johansen A. M., Siefert R. L., Hoffmann M. R. (2000) Chemical composition of aerosols collected over the tropical North Atlantic Ocean. *Journal of Geophysical Research* **105**, 15277-15312.

Karner M. B., DeLong E. F., Karl D. M. (2001) Archaeal dominance in the mesopelagic zone of the Pacific Ocean. *Nature* **409**, 507-510.

Kates M. (1975) Techniques of lipodology. In: *Laboratory techniques in biochemistry and molecular biology* (Work T. S., Work E. (Eds.)), 269-610.

Keil R. G., Tsamakis E., Wolf N., Hedges J. I., Goni M. A. (1997) Relationships between organic carbon preservation and mineral surface area in Amazon Fan sediments (Holes 932A and 942A). In: *Proceedings of the Ocean Drilling Program, Scientific Results* 155 (Flood R. D., Piper D. J. W., Klaus A., Peterson L. C. (Eds.)), College Station, TX (Ocean Drilling Program), 531-538.

Keough B. P., Schmidt T. M., Hicks R. E. (2003) Archaeal nucleic acids in picoplankton from great lakes on three continents. *Microbial Ecology* **46**, 238-248.

Kim J.-H., Schouten S., Buscail R., Ludwig W., Bonnin J., Sinninghe Damsté J. S., Bourrin F. (2006) Origin and distribution of terrestrial organic matter in the NW Mediterranean (Gulf of Lions): Exploring the newly developed BIT index. *Geochemistry Geophysics Geosystems* **7**, Q11017, doi: 10.1029/2006GC001306.

Kim J.-H., Schouten S., Hopmans E. C., Donner B., Sinninghe Damsté J. S. (2008) Global sediment core-top calibration of the TEX_{86} paleothermometer in the ocean. *Geochimica et Cosmochimica Acta* **72**, 1154-1173.

Kim J.-H., Huguet C., Zonneveld K. A. F., Versteegh G. J. M., Roeder W., Sinninghe Damsté J. S., Schouten S. (2009) An experimental field study to test the stability of lipids used for the TEX_{86} and $U^{K'}_{37}$ palaeothermometers. *Geochimica et Cosmochimica Acta* **73**, 2888-2898.

Kim J.-H., van der Meer J., Schouten S., Helmke P., Willmott V., Sangiorgi F., Koç N., Hopmans E. C., Sinninghe Damsté J. S. (2010) New indices and calibrations derived from the distribution of crenarchaeal isoprenoid tetraether lipids: Implications for past sea surface temperature reconstructions. *Geochimica et Cosmochimica Acta* **74**, 4639-4654.

Kim J.-H., Talbot H. M., Zarzycka B., Bauersachs T., Wagner T. (2011) Occurrence and abundance of soil-specific bacterial membrane lipid markers in the Têt watershed (Southern France): soil-specific BHPs and branched GDGTs. *Geochemistry Geophysics Geosystems* **12**, Q02008, doi:10.1029/2010GC003364.

Kim J.-H., Zarzycka, B., Buscail, R., Peterse, F., Bonnin, J., Ludwig, W., Schouten, S., Sinninghe-Damsté, J.S. (2010) Contribution of river-borne soil organic carbon to the Gulf of Lions (NW Mediterranean). *Limnology and Oceanography* **55**, 507-518.

Knippertz P., Christoph M., Speth P. (2003) Long-term precipitation variability in Morocco and the link to the large-scale circulation in recent and future climates. *Meteorology and Atmospheric Physics* **83**, 67-88.

KNMI (1997) World Climate Information (WKI) 2.0, Online version at http://www.knmi.nl/klimatologie/normalen1971-2000/wki.html, Koninklijk Nederlands Meteorologisch Instituut (KNMI), De Bilt, The Netherlands.

Könneke M., Bernhard A. E., de la Torre J. R., Walker C. B., Waterbury J. B., Stahl D. A. (2005) Isolation of an autotrophic ammonia-oxidizing marine archaeon. *Nature* **437**, 543-546.

Konta J. (1985) Mineralogy and chemical maturity of suspended matter in major rivers sampled under the SCOPE/UNEP project. In: *Transport of carbon and minerals in major world rivers, part 3* (Degens E. T., Kempe S., Herrera R. (Eds.))), Mitteilungen aus dem Geologisch-Paläontologischen Institut der Universität Hamburg S58, 569-592.

Kronberg B. I., Nesbitt H. W., Lam W. W. (1986) Upper Pleistocene Amazon deep-sea fan muds reflect intense chemical weathering of their mountainous source lands. *Chemical Geology* **54**, 283-294.

Kuehl S. A., DeMaster D. J., Nittrouer C. A. (1986) Nature of sediment accumulation on the Amazon continental shelf. *Continental Shelf Research* **6**, 209-225.

Leduc G., Schneider R., Kim J.-H., Lohmann G. (2010) Holocene and Eemian sea surface temperature trends as revealed by alkenone and Mg/Ca paleothermometry. *Quaternary Science Reviews* **29**, 989-1004.

Lee K. E., Kim J.-H., Wilke I., Helmke P., Schouten S. (2008) A study of the alkenone, TEX_{86}, and planktonic foraminifera in the Benguela Upwelling System: Implications for past sea surface temperature estimates. *Geochemistry Geophysics Geosystems* **9**, Q10019, doi: 10.1029/2008GC002056.

Leider A., Hinrichs K.-U., Mollenhauer G., Versteegh G. J. M. (2010) Core-top calibration of the lipid-based $U^{K'}_{37}$ and TEX_{86} temperature proxies on the southern Italian shelf (SW Adriatic Sea, Gulf of Taranto). *Earth and Planetary Science Letters* **300**, 112-124.

Leininger S., Urich T., Schloter M., Schwark L., Qi J., Nicol G. W., Prosser J. I., Schuster S. C., Schleper C. (2006) Archaea predominate among ammonia-oxidizing prokaryotes in soils. *Nature* **442**, 806-809.

Lézine A.-M., Casanova J. (1989) Pollen and hydrological evidence for the interpretation of past climates in tropical west Africa during the holocene. *Quaternary Science Reviews* **8**, 45-55.

Lézine A.-M., Cazet J.-P. (2005) High-resolution pollen record from core KW31, Gulf of Guinea, documents the history of the lowland forests of West Equatorial Africa since 40,000 yr ago. *Quaternary Research* **64**, 432-443.

Lézine A.-M., Duplessy J.-C., Cazet J.-P. (2005) West African monsoon variability during the last deglaciation and the Holocene: Evidence from fresh water algae, pollen and isotope data from core KW31, Gulf of Guinea. *Palaeogeography, Palaeoclimatology, Palaeoecology* **219**, 225-237.

Lipp J. S., Morono Y., Inagaki F., Hinrichs K.-U. (2008) Significant contribution of Archaea to extant biomass in marine subsurface sediments. *Nature* **454**, 991-994.

Lisitzin A. P. (1996) *Oceanic sedimentation. Lithology and geochemistry*. AGU, Washington D.C., 400 pp.

Locarnini R. A., Mishonov, A.V., Antonov, J.I., Boyer, T.P., Garcia, H.E., Baranova, O.K, Zweng, M.M., Johnson, D.R. (2010) *World Ocean Atlas 2009, Volume 1: Temperature*. U.S. Government Printing Office, Washington D.C., 184 pp.

Loomis S. E., Russell J. M., Sinninghe Damsté J. S. (2011) Distributions of branched GDGTs in soils and lake sediments from western Uganda: Implications for a lacustrine paleothermometer. *Organic Geochemistry* **42**, 739-751.

Loye-Pilot M. D., Martin J. M., Morelli J. (1986) Influence of Saharan dust on the rain acidity and atmospheric input to the Mediterranean. *Nature* **321**, 427-428.

Maher B. A., Prospero J. M., Mackie D., Gaiero D., Hesse P. P., Balkanski Y. (2010) Global connections between aeolian dust, climate and ocean biogeochemistry at the present day and at the last glacial maximum. *Earth-Science Reviews* **99**, 61-97.

Mahowald N. M., Baker A. R., Bergametti G., Brooks N., Duce R. A., Jickells T. D., Kubilay N., Prospero J. M., Tegen I. (2005) Atmospheric global dust cycle and iron inputs to the ocean. *Global Biogeochemical Cycles* **19**, GB4025, doi: 10.1029/2004gb002402.

Maley J., Brenac P. (1998) Vegetation dynamics, palaeoenvironments and climatic changes in the forests of western Cameroon during the last 28,000 years B.P. *Review of Palaeobotany and Palynology* **99**, 157-187.

Mariotti A. (1991) Le carbone 13 en abondance naturelle, traceur de la dynamique de la matière organique des sols et de l'évolution des paléoenvironnements continentaux. *Cahiers ORSTOM, Série Pédologie* **26**, 299-313.

Martin J.-M., Meybeck M. (1979) Elemental mass-balance of material carried by major world rivers. *Marine Chemistry* **7**, 173-206.

Martin J. H., Gordon R. M., Fitzwater S. E. (1991) The case for iron. *Limnology and Oceanography* **36**, 1793-1802.

Martinelli I. A., Pessenda L. C. R., Espinoza E., Camargo P. B., Telles F. C., Cerri C. C., Victoria R. L., Aravena R., Richey J., Trumbore S. (1996) Carbon-13 variation with depth in soils of Brazil and climate change during the Quaternary. *Oecologia* **106**, 376-381.

Martinez P., Bertrand P., Shimmield G. B., Karen C., Jorissen F. J., Foster J., Dignan M. (1999) Upwelling intensity and ocean productivity changes off Cape Blanc (northwest Africa) during the last 70,000 years: geochemical and micropalaeontological evidence. *Marine Geology* **158**, 57-74.

Martins O. (1982) Geochemistry of the Niger River. In: *Transport of carbon and minerals in major world rivers, part 1* (Degens E. T. (Ed.))), Mitteilungen aus dem Geologisch-

Paläontologischen Institut der Universität Hamburg, SCOPE/UNEP Sonderband 52, 397-418.

Martins O., Probst J.-L. (1991) Biogeochemistry of major African rivers: Carbon and mineral transport. In: *Biogeochemistry of major world rivers* (Degens E. T., Kempe S., Richey J. E. (Eds.)), SCOPE 42. John Wiley & Sons, Chichester, 127-155.

Masiello C. A., Druffel E. R. M. (2001) Estimating global land use change over the past 300 years: The HYDE Database. *Global Biogeochemical Cycles* **15**, 407-416.

Maslin M. (1998) Equatorial western Atlantic Ocean circulation changes linked to the Heinrich events: deep-sea sediment evidence from the Amazon Fan. In: *Geological evolution of ocean basins: Results from the Ocean Drilling Program* (Cramp A., MacLeod C. J., Lee S. V., Jones E. J. W. (Eds.)). Geological Society, London, Special Publications, 131, 1-127.

Maslin M. A., Durham E., Burns S. J., Platzman E., Grootes P., Greig S. E. J., Nadeau M.-J., Schleicher M., Pflaumann U., Lomax B., Rimington N. (2000) Palaeoreconstruction of the Amazon River freshwater and sediment discharge using sediments recovered at Site 942 on the Amazon Fan. *Journal of Quaternary Science* **15**, 419-434.

Matthewson A. P., Shimmield G. B., Kroon D., Fallick A. E. (1995) A 300 kyr high-resolution aridity record of the North African continent. *Paleoceanography* **10**, 677-692.

McGuire W. J., Howarth R. J., Firth C. R., Solow A. R., Pullen A. D., Saunders S. J., Stewart I. S., Vita-Finzi C. (1997) Correlation between rate of sea-level change and frequency of explosive volcanism in the Mediterranean. *Nature* **389**, 473-476.

McIntyre A., Ruddiman, William F., Karlin, Karen, Mix, Alan C. (1989) Surface water response of the equatorial Atlantic Ocean to orbital forcing. *Paleoceanography* **4**, 19-55.

McKee B. A., Aller R. C., Allison M. A., Bianchi T. S., Kineke G. C. (2004) Transport and transformation of dissolved and particulate materials on continental margins influenced by major rivers: benthic boundary layer and seabed processes. *Continental Shelf Research* **24**, 899-926.

Metcalf W. G., Stalcup M. C. (1967) Origin of the Atlantic Equatorial Undercurrent. *Journal of Geophysical Research* **72**, 4959-4975.

Meybeck M., Ragu, A. (1996) *River discharges to the Oceans: An assessement of suspended solids, major ions and nutrients. Environment Information and Assessment Rpt. UNEP*. Nairobi, 250 pp.

Meyer I. (2011) Holocene climate trends in NW Africa: Inferences from grain-size distributions of terrigenous sediments and isotopic provenance studies. PhD Thesis, University of Bremen.

Meyers P. A. (1994) Preservation of elemental and isotopic source identification of sedimentary organic matter. *Chemical Geology* **114**, 289-302.

Middleton N. J., Goudie A. S. (2001) Saharan dust: sources and trajectories. *Transactions of the Institute of British Geographers* **26**, 165-181.

Milliman J. D., Summerhayes C. P., Barretto H. T. (1975) Quaternary sedimentation on the Amazon continental margin: A model. *Geological Society of America Bulletin* **86**, 610-614.

Milliman J. D., Meade R. H. (1983) World-wide delivery of river sediment to the oceans. *The Journal of Geology* **91**, 1-21.

Mittelstaedt E. (1991) The ocean boundary along the northwest African coast: Circulation and oceanographic properties at the sea surface. *Progress In Oceanography* **26**, 307-355.

Mix A. C., Morey A. E., Pisias N. G., Hostetler S. W. (1999) Foraminiferal faunal estimates of paleotemperature: circumventing the no-analog problem yields cool ice age tropics. *Paleoceanography* **14**, 350-359.

Mollenhauer G., Schneider R. R., Müller P. J., Spieß V., Wefer G. (2002) Glacial/interglacial variablity in the Benguela upwelling system: Spatial distribution and budgets of organic carbon accumulation. *Global Biogeochemical Cycles* **16**, 1134, doi: 10.1029/2001gb001488.

Mollenhauer G., Eglinton T. I., Ohkouchi N., Schneider R. R., Müller P. J., Grootes P. M., Rullkötter J. (2003) Asynchronous alkenone and foraminifera records from the Benguela Upwelling System. *Geochimica et Cosmochimica Acta* **67**, 2157-2171.

Mollenhauer G., Kienast M., Lamy F., Meggers H., Schneider R. R., Hayes J. M., Eglinton T. I. (2005) An evaluation of ^{14}C age relationships between co-occurring foraminifera, alkenones, and total organic carbon in continental margin sediments. *Paleoceanography* **20**, PA1016, doi:10.1029/2004PA001103.

Mollenhauer G., Inthorn M., Vogt T., Zabel M., Sinninghe Damsté J. S., Eglinton T. I. (2007) Aging of marine organic matter during cross-shelf lateral transport in the Benguela upwelling system revealed by compound-specific radiocarbon dating. *Geochemistry Geophysics Geosystems* **8**, Q09004, doi:10.1029/2007GC001603.

Mollenhauer G., Eglinton T. I., Hopmans E. C., Sinninghe Damsté J. S. (2008) A radiocarbon-based assessment of the preservation characteristics of crenarchaeol and alkenones from continental margin sediments. *Organic Geochemistry* **39**, 1039-1045.

Mollenhauer G., Rethemeyer J. (2009) Compound-specific radiocarbon analysis – analytical challenges and applications. *IOP Conference Series: Earth and Environmental Science* **5, 012006**, doi: 10.1088/1755-1307/5/1/012006.

Moreno T., Querol X., Castillo S., Alastuey A., Cuevas E., Herrmann L., Mounkaila M., Elvira J., Gibbons W. (2006) Geochemical variations in aeolian mineral particles from the Sahara–Sahel Dust Corridor. *Chemosphere* **65**, 261-270.

Moulin C., Lambert C. E., Dayan U., Masson V., Ramonet M., Bousquet P., Legrand M., Balkanski Y. J., Guelle W., Marticorena B., Bergametti G., Dulac F. (1998) Satellite climatology of African dust transport in the Mediterranean atmosphere. *Journal of Geophysical Research* **103**, 13137-13144.

Mulitza S., Paul A., Wefer G. (2007) Late Pleistocene South Atlantic. In: *Encyclopedia of Quaternary Science 3* (Elias S. A. (Ed.)). Elsevier, Amsterdam, 1816-1831.

Mulitza S., Prange M., Stuut J.-B. W., Zabel M., von Dobeneck T., Itambi A. C., Nizou J., Schulz M., Wefer G. (2008) Sahel megadroughts triggered by glacial slowdowns of Atlantic meridional overturning. *Paleoceanography* **23**, PA4206, doi:10.1029/2008PA001637.

Neunlist S., Rohmer M. (1985) Novel hopanoids from the methylotrophic bacteria *Methylococcus capsulatus* and *Methylomonas methanica*. *Biochemical Journal* **231**, 635-639.

NGRIP members (2004) High-resolution record of Northern Hemisphere climate extending into the last interglacial period. *Nature* **431**, 147-151.

Nicholson S. E. (2000) The nature of rainfall variability over Africa on time scales of decades to millennia. *Global and Planetary Change* **26**, 137-158.

Niebler H.-S., Arz H. W., Donner B., Mulitza S., Pätzold J., Wefer G. (2003) Sea surface temperatures in the equatorial and South Atlantic Ocean during the Last Glacial Maximum (23-19 ka). *Paleoceanography* **18**, 1069, doi: 10.1029/2003PA000902.

O'Leary M. H. (1988) Carbon isotopes in photosynthesis. *BioScience* **38**, 328-336.

Ohkouchi N., Eglinton T. I., Keigwin L. D., Hayes J. M. (2002) Spatial and temporal offsets between proxy records in a sediment drift. *Science* **298**, 1224-1227.

Ourisson G., Rohmer M., Poralla K. (1987) Prokaryotic hopanoids and other polyterpenoid sterol surrogates. *Annual Review of Microbiology* **41**, 301-333.

Ourisson G., Albrecht P. (1992) Hopanoids. 1. Geohopanoids: the most abundant natural products on Earth? *Accounts of Chemical Research* **25**, 398-402.

Pastouret L. (1978) Late Quaternary deep sea sedimentation off the Niger delta. *Oceanologica Acta* **1**, 217-232.

Pearson A., Flood Page S. R., Jorgenson T. L., Fischer W. W., Higgins M. B. (2007) Novel hopanoid cyclases from the environment. *Environmental Microbiology* **9**, 2175-2188.

Pearson A., Leavitt W. D., Sáenz J. P., Summons R. E., Tam M. C. M., Close H. G. (2009) Diversity of hopanoids and squalene-hopene cyclases across a tropical land-sea gradient. *Environmental Microbiology* **11**, 1208-1223.

Pearson E. J., Juggins S., Talbot H. M., Weckström J., Rosén P., Ryves D. B., Roberts S. J., Schmidt R. (2011) A lacustrine GDGT-temperature calibration from the Scandinavian Arctic to Antarctic: renewed potential for the application of GDGT-paleothermometry in lakes. *Geochimica et Cosmochimica Acta* **75**, 6225-6238.

Pessenda L. C. R., Gouveia S. E. M., Aravena R., Gomes B. M., Boulet R., Ribeiros A. S. (1998) ^{14}C dating and stable carbon isotopes of soil organic matter in forest-savanna boundary areas in the southern Brazilian Amazon region. *Radiocarbon* **40**, 1013-1022.

Pessenda L. C. R., Gouveia S. E. M., Aravena R. (2001) Radiocarbon dating of total soil organic matter and humin fraction and its comparison with ^{14}C ages of fossil charcoal. *Radiocarbon* **43**, 595-601.

Pessenda L. C. R., Gouveia S. E. M., Ribeiro A. d. S., De Oliveira P. E., Aravena R. (2010) Late Pleistocene and Holocene vegetation changes in northeastern Brazil determined from carbon isotopes and charcoal records in soils. *Palaeogeography, Palaeoclimatology, Palaeoecology* **297**, 597-608.

Peters K. E., Walter C. C., Moldowan J. M. (2004) *The Biomarker Guide: Volume I: Biomarkers and isotopes in the environments and human history*. Cambridge University Press, Cambridge, 490 pp.

Peterse F., Schouten S., van der Meer J., van der Meer M. T. J., Sinninghe Damsté J. S. (2009a) Distribution of branched tetraether lipids in geothermally heated soils: Implications for the MBT/CBT temperature proxy. *Organic Geochemistry* **40**, 201-205.

Peterse F., Kim J.-H., Schouten S., Kristensen D. K., Koç N., Sinninghe Damsté J. S. (2009b) Constraints on the application of the MBT/CBT palaeothermometer at high latitude environments (Svalbard, Norway). *Organic Geochemistry* **40**, 692-699.

Peterse F., Nicol G. W., Schouten S., Damsté J. S. S. (2010) Influence of soil pH on the abundance and distribution of core and intact polar lipid-derived branched GDGTs in soil. *Organic Geochemistry* **41**, 1171-1175.

Peterson R. G., Stramma L. (1991) Upper-level circulation in the South Atlantic Ocean. *Progress In Oceanography* **26**, 1-73.

Philander S. G. H., Pacanowski R. C. (1986) A model of the seasonal cycle in the tropical Atlantic Ocean. *Journal of Geophysical Research* **91**, 14192-14206.

Pitcher A., Hopmans E. C., Mosier A. C., Park S.-J., Rhee S.-K., Francis C. A., Schouten S., Sinninghe Damste J. S. (2011) Core and intact polar glycerol dibiphytanyl glycerol tetraether lipids of ammonia-oxidizing Archaea enriched from marine and estuarine sediments. *Applied and Environmental Microbiology* **77**, 3468-3477.

Pokras E. M., Mix A. C. (1985) Eolian evidence for spatial variability of Late Quaternary climates in tropical Africa. *Quaternary Research* **24**, 137-149.

Pokras E. M. (1987) Diatom record of late Quaternary climatic change in the eastern equatorial Atlantic and tropical Africa. *Paleoceanography* **2**, 273-286.

Pokras E. M., Mix A. C. (1987) Earth's precession cycle and Quaternary climatic change in tropical Africa. *Nature* **326**, 486-487.

Powers L. A., Werne J. P., Johnson T. C., Hopmans E. C., Sinninghe Damsté J. S., Schouten S. (2004) Crenarchaeotal membrane lipids in lake sediments: A new paleotemperature proxy for continental paleoclimate reconstruction? *Geology* **32**, 613-616.

Powers L. A., Werne J. P., Vanderwoude A. J., Sinninghe Damsté J. S., Hopmans E. C., Schouten S. (2010) Applicability and calibration of the TEX_{86} paleothermometer in lakes. *Organic Geochemistry* **41**, 404-413.

Prospero J. M., Carlson T. N. (1972) Vertical and areal distribution of Saharan dust over the Western Equatorial North Atlantic Ocean. *Journal of Geophysical Research* **77**, 5255-5265.

Prospero J. M., Ginoux P., Torres O., Nicholson S. E., Gill T. E. (2002) Environmental characterization of global sources of atmospheric soil dust identified with the Nimbus 7 total ozone mapping spectrometer (TOMS) absorbing aerosol product. *Reviews of Geophysics* **40**, 1-31.

Prospero J. M., Lamb P. J. (2003) African droughts and dust transport to the Caribbean: climate change implications. *Science* **302**, 1024-1027.

Pye K. (1987) *Aeolian dust and dust deposits*. Elsevier, New York, 334 pp.

Räsänen M. E., Salo J. S., Jungner H. (1991) Holocene floodplain lake sediments in the Amazon: ^{14}C dating and palaeoecological use. *Quaternary Science Reviews* **10**, 363-372.

Raymond P. A., Bauer J. E. (2001) Riverine export of aged terrestrial organic matter to the North Atlantic Ocean. *Nature* **409**, 497-500.

Rea D. K. (1994) The paleoclimatic record provided by eolian deposition in the deep sea: The geologic history of wind. *Reviews of Geophysics* **32**, 159-195.

Reed R. J., Norquist D. C., Recker E. E. (1977) The structure and properties of African wave disturbances as observed during phase III of GATE. *Monthly Weather Review* **105**, 317-333.

Reimer P., Baillie M., Bard E., Bayliss A., Beck J., Blackwell P., Bronk Ramsey C., Buck C., Burr G., Edwards R., Friedrich M., Grootes P., Guilderson T., Hajdas I., Heaton T., Hogg A., Hughen K., Kaiser K., Kromer B., McCormac F., Manning S., Reimer R., Richards D., Southon J., Talamo S., Turney C. S. M., van der Plicht J., Weyhenmeyer C. E. (2009) IntCal09 and Marine09 Radiocarbon age calibration curves, 0–50,000 years cal BP. *Radiocarbon* **51**, 1111-1150.

Rethemeyer J., Schubotz F., Talbot H. M., Cooke M. P., Hinrichs K.-U., Mollenhauer G. (2010) Distribution of polar membrane lipids in permafrost soils and sediments of a small high Arctic catchment. *Organic Geochemistry* **41**, 1130-1145.

Richardson P. L., Walsh D. (1986) Mapping climatological seasonal variations of surface currents in the tropical Atlantic using ship drifts. *Journal of Geophysical Research* **91**, 10537-10550.

Riegman R., Stolte W., Noordeloos A. A. M., Slezak D. (2000) Nutrient uptake and alkaline phosphatase (EC 3:1:3:1) activity of *Emiliania huxleyi* (Prymnesiophyceae) during growth under N and P limitation in continuous cultures. *Journal of Phycology* **36**, 87-96.

Rohmer M., Bouvier-Nave P., Ourisson G. (1984) Distribution of hopanoid triterpenes in prokaryotes. *Journal of General Microbiology* **130**, 1137-1150.

Rohmer M. (1993) The biosynthesis of triterpenoids of the hopane series in the Eubacteria: A mine of new enzyme reactions. *Pure and Applied Chemistry* **65**, 1293-1298.

Rommerskirchen F., Condon T., Mollenhauer G., Dupont L., Schefuss E. (2011) Miocene to Pliocene development of surface and sub-surface temperatures in the Benguela Current System. *Paleoceanography* **26**, PA3216, doi:10.1029/2010PA002074.

Rueda G., Rosell-Melé A., Escala M., Gyllencreutz R., Backman J. (2009) Comparison of instrumental and GDGT-based estimates of sea surface and air temperatures from the Skagerrak. *Organic Geochemistry* **40**, 287-291.

Sáenz J. P. (2010) Hopanoid enrichment in a detergent resistant membrane fraction of *Crocosphaera watsonii*: Implications for bacterial lipid raft formation. *Organic Geochemistry* **41**, 853-856.

Salzmann U., Waller M. (1998) The Holocene vegetational history of the Nigerian Sahel based on multiple pollen profiles. *Review of palaeobotany and palynology* **100**, 39-72.

Salzmann U., Hoelzmann P., Morczinek I. (2002) Late Quaternary climate and vegetation of the Sudanian Zone of Northeast Nigeria. *Quaternary Research* **58**, 73-83.

Sarnthein M., Tetzlaff G., Koopmann B., Wolter K., Pflaumann U. (1981) Glacial and interglacial wind regimes over the eastern subtropical Atlantic and North-West Africa. *Nature* **293**, 193-196.

Sarnthein M., Thiede J., Pflaumann U., Erlenkeuser H., Fütterer D., Koopmann B., Lange H., Seibold E. (1982) Atmospheric and oceanic circulation patterns off Northwest Africa during the past 15 million years. In: *Geology of the Northwest African continental margin* (von Rad U., Hinz K., Sarnthein M., Seibold E. (Eds.)). Springer-Verlag, Berlin Heidelberg, 545-604.

Schefuß E., Schouten S., Jansen J. H. F., Sinninghe Damsté J. S. (2003) African vegetation controlled by tropical sea surface temperatures in the mid-Pleistocene period. *Nature* **422**, 418-421.

Schefuß E., Versteegh G. J. M., Jansen J. H. F., Sinninghe Damsté J. S. (2004) Lipid biomarkers as major source and preservation indicators in SE Atlantic surface sediments. *Deep Sea Research Part I: Oceanographic Research Papers* **51**, 1199-1228.

Schefuß E., Schouten S., Schneider R. R. (2005) Climatic controls on central African hydrology during the past 20,000 years. *Nature* **437**, 1003-1006.

Schlünz B. (1998) Riverine organic carbon input to the ocean in relation to Late Quaternary climate change. PhD Thesis, University of Bremen.

Schlünz B., Schneider R. R., Müller P. J., Showers W. J., Wefer G. (1999) Terrestrial organic carbon accumulation on the Amazon deep sea fan during the last glacial sea level low stand. *Chemical Geology* **159**, 263-281.

Schmidt M. W. I., Noack A. G. (2000) Black carbon in soils and sediments: Analysis, distribution, implications, and current challenges. *Global Biogeochemical Cycles* **14**, 777-793.

Schneider R. R., Price B., Müller P. J., Kroon D., Alexander I. (1997) Monsoon related variations in Zaire (Congo) sediment load and influence of fluvial silicate supply on marine producitivity in the east equatorial Atlantic during the last 200,000 years. *Paleoceanography* **12**, 463-481.

Schott F. A., Stramma L., Fischer J. (1995) The warm water inflow into the western tropical Atlantic boundary regime, spring 1994. *Journal of Geophysical Research* **100**, 24745-24760.

Schouten S., Hopmans E. C., Pancost R. D., Sinninghe Damsté J. S. (2000) Widespread occurrence of structurally diverse tetraether membrane lipids: Evidence for the ubiquitous presence of low-temperature relatives of hyperthermophiles. *Proceedings of the National Academy of Sciences of the USA* **97**, 14421-14426.

Schouten S., Hopmans E. C., Schefuß E., Sinninghe Damsté J. S. (2002) Distributional variations in marine crenarchaeotal membrane lipids: a new tool for reconstructing ancient sea water temperatures? *Earth and Planetary Science Letters* **204**, 265-274.

Schouten S., Hopmans E. C., Forster A., van Breugel Y., Kuypers M. M. M., Damsté J. S. S. (2003) Extremely high sea-surface temperatures at low latitudes during the middle Cretaceous as revealed by archaeal membrane lipids. *Geology* **31**, 1069-1072.

Schouten S., Forster A., Panoto F. E., Sinninghe Damsté J. S. (2007) Towards calibration of the TEX_{86} palaeothermometer for tropical sea surface temperatures in ancient greenhouse worlds. *Organic Geochemistry* **38**, 1537-1546.

Schouten S., Eldrett J., Greenwood D. R., Harding I., Baas M., Damsté J. S. S. (2008) Onset of long-term cooling of Greenland near the Eocene-Oligocene boundary as revealed by branched tetraether lipids. *Geology* **36**, 147-150.

Schouten S., Hopmans E. C., van der Meer J., Mets A., Bard E., Bianchi T. S., Diefendorf A., Escala M., Freeman K. H., Furukawa Y., Huguet C., Ingalls A., Ménot-Combes G., Nederbragt A. J., Oba M., Pearson A., Pearson E. J., Rosell-Melé A., Schaeffer P., Shah S. R., Shanahan T. M., Smith R. W., Smittenberg R., Talbot H. M., Uchida M., Van Mooy B. A. S., Yamamoto M., Zhang Z., Sinninghe Damsté J. S. (2009) An interlaboratory study of TEX_{86} and BIT analysis

using high-performance liquid chromatography-mass spectrometry. *Geochemistry Geophysics Geosystems* **10**, Q03012, doi: 10.1029/2008GC002221.

Schroth A. W., Crusius J., Sholkovitz E. R., Bostick B. C. (2009) Iron solubility driven by speciation in dust sources to the ocean. *Nature Geoscience* **2**, 337-340.

Schulz H. D., Andersen N., Breitzke M., Burda D., Dehning K., Diekamp V., Felis T., Gerlach H., Gumprecht R., Hinrichs S., Petermann H., Pimenta C. C., Pototzki F., Probst U., Rode H., Sagemann J., SchinzeI U., Schmidt H., Schneider R., Segl M., Showers W. J., Tegeler M. D., Thiessen W., Treppke U., Zabel M. (1991) *Bericht und erste Ergebnisse über die Meteor-Fahrt M 16/2. Recife - Belem, 28.4. - 21.5.1991. Berichte, Fachbereich Geowissenschaften, Universität Bremen*, Bremen, 149 pp.

Schulz H. D., Dahmke A., Schinzel U., Wallmann K., Zabel M. (1994) Early diagenetic processes, fluxes, and reaction rates in sediments of the South Atlantic. *Geochimica et Cosmochimica Acta* **58**, 2041-2060.

Schütz L., Rahn K. A. (1982) Trace-element concentrations in erodible soils. *Atmospheric Environment* **16**, 171-176.

Schütz L., Sebert M. (1987) Mineral aerosols and source identification. *Journal of Aerosol Science* **18**, 1-10.

Shah S. R., Mollenhauer G., Ohkouchi N., Eglinton T. I., Pearson A. (2008) Origins of archaeal tetraether lipids in sediments: Insights from radiocarbon analysis. *Geochimica et Cosmochimica Acta* **72**, 4577-4594.

Shipboard Scientific Party (1995) Site 931. In: *Proceedings of the Ocean Drilling Program, Initial Reports* 155 (Flood R. D., Piper D. J. W., Klaus A., et al. (Eds.)), College Station, TX (Ocean Drilling Program), 123-174.

Showers W. J., Angle D. G. (1986) Stable isotopic characterization of organic carbon accumulation on the Amazon continental shelf. *Continental Shelf Research* **6**, 227-244.

Sikes E. L., Keigwin L. D. (1994) Equatorial Atlantic sea surface temperature for the last 30 kyr: A comparison of $U^{K'}_{37}$, $\delta^{18}O$ and foraminiferal assemblage temperature estimates. *Paleoceanography* **9**, 31-45.

Simoneit B. R. T., Chester R., Eglinton G. (1977) Biogenic lipids in particulates from the lower atmosphere over the eastern Atlantic. *Nature* **267**, 682-685.

Sinninghe Damsté J. S., Hopmans E. C., Pancost R. D., Schouten S., Geenevasen J. A. J. (2000) Newly discovered non-isoprenoid glycerol dialkyl glycerol tetraether lipids in sediments. *Chemical Communications* **17**, 1683-1684.

Sinninghe Damsté J. S., Rijpstra W. I. C., Hopmans E. C., Prahl F. G., Wakeham S. G., Schouten S. (2002) Distribution of membrane lipids of planktonic Crenarchaeota in the Arabian Sea. *Applied and Environmental Microbiology* **68**, 2997-3002.

Sinninghe Damsté J. S., Ossebaar J., Schouten S., Verschuren D. (2008) Altitudinal shifts in the branched tetraether lipid distribution in soil from Mt. Kilimanjaro (Tanzania): Implications for the MBT/CBT continental palaeothermometer. *Organic Geochemistry* **39**, 1072-1076.

Sluijs A., Schouten S., Pagani M., Woltering M., Brinkhuis H., Sinninghe Damsté J. S., Dickens G. R., Huber M., Reichart G.-J., Stein R., Matthiessen J., Lourens L. J., Pedentchouk N., Backman J., Moran K., the Expedition 302 Scientists (2006) Subtropical Arctic Ocean temperatures during the Palaeocene/Eocene thermal maximum. *Nature* **441**, 610-613.

Sombroek W. G. (1966) *Amazon Soils. A reconnaissance of the soils of the Brazilian Amazon region*. Pudoc, Wageningen, 292 pp.

Sommerfield C. K., Nittrouer C. A., Figueiredo A. G. (1995) Stratigraphic evidence of changes in Amazon shelf sedimentation during the late Holocene. *Marine Geology* **125**, 351-371.

Sommerfield C. K., Nittrouer C. A., DeMaster D. J. (1996) Sedimentary carbon-isotope systematics on the Amazon shelf. *Geo-Marine Letters* **16**, 17-23.

Spang A., Hatzenpichler R., Brochier-Armanet C., Rattei T., Tischler P., Spieck E., Streit W., Stahl D. A., Wagner M., Schleper C. (2010) Distinct gene set in two different lineages of ammonia-oxidizing archaea supports the phylum Thaumarchaeota. *Trends in Microbiology* **18**, 331-340.

Spears D. A., Kanaris-Sotiriou R. (1976) Titanium in some Carboniferous sediments from Great Britain. *Geochimica et Cosmochimica Acta* **40**, 345-351.

Stramma L., Fischer J., Reppin J. (1995) The North Brazil Undercurrent. *Deep Sea Research Part I: Oceanographic Research Papers* **42**, 773-795.

Stramma L., Schott F. (1999) The mean flow field of the tropical Atlantic Ocean. *Deep Sea Research Part II: Topical Studies in Oceanography* **46**, 279-303.

Stuiver M., Reimer P. J., Reimer R. (2010) CALIB - Radiocarbon Calibration, Version 6.0. Available from: http://calib.qub.ac.uk/calib/.

Stute M., Forster M., Frischkorn H., Serejo A., Clark J. F., Schlosser P., Broecker W. S., Bonani G. (1995) Cooling of tropical Brazil (5°C) during the Last Glacial Maximum. *Science* **269**, 379-383.

Stuut J.-B., Zabel M., Ratmeyer V., Helmke P., Schefuß E. (2005) Provenance of present-day eolian dust collected off NW Africa. *Journal of Geophysical Research* **110**, D04202, doi:10.1029/2004JD005161.

Stuut J.-B., Smalley I., O'Hara-Dhand K. (2009) Aeolian dust in Europe: African sources and European deposits. *Quaternary International* **198**, 234-245.

Stuut J.-B. W., Prins M. A., Schneider R. R., Weltje G. J., Jansen J. H. F., Postma G. (2002) A 300-kyr record of aridity and wind strength in southwestern Africa: inferences from grain-size distributions of sediments on Walvis Ridge, SE Atlantic. *Marine Geology* **180**, 221-233.

Sunnu A., Afeti G. M., Resch F. (2008) A long-term experimental study of the Saharan dust presence in West Africa. *Atmospheric Research* **87**, 13-26.

Talbot H. M., Watson D. F., Murrell J. C., Carter J. F., Farrimond P. (2001) Analysis of intact bacteriohopanepolyols from methanotrophic bacteria by reversed-phase high-performance liquid chromatography–atmospheric pressure chemical ionisation mass spectrometry. *Journal of Chromatography A* **921**, 175-185.

Talbot H. M., Squier A. H., Keely B. J., Farrimond P. (2003a) Atmospheric pressure chemical ionisation reversed-phase liquid chromatography/ion trap mass spectrometry of intact bacteriohopanepolyols. *Rapid Communications in Mass Spectrometry* **17**, 728-737.

Talbot H. M., Summons R. E., Jahnke L. L., Farrimond P. (2003b) Characteristic fragmentation of bacteriohopanepolyols during atmospheric pressure chemical ionisation liquid chromatography/ion trap mass spectrometry. *Rapid Communications in Mass Spectrometry* **17**, 2788-2796.

Talbot H. M., Watson D. F., Pearson E. J., Farrimond P. (2003c) Diverse biohopanoid compositions of non-marine sediments. *Organic Geochemistry* **34**, 1353-1371.

Talbot H. M., Rohmer M., Farrimond P. (2007a) Structural characterisation of unsaturated bacterial hopanoids by atmospheric pressure chemical ionisation liquid chromatography/ion trap mass spectrometry. *Rapid Communications in Mass Spectrometry* **21**, 1613-1622.

Talbot H. M., Rohmer M., Farrimond P. (2007b) Rapid structural elucidation of composite bacterial hopanoids by atmospheric pressure chemical ionisation liquid chromatography/ion trap mass spectrometry. *Rapid Communications in Mass Spectrometry* **21**, 880-892.

Talbot H. M., Farrimond P. (2007) Bacterial populations recorded in diverse sedimentary biohopanoid distributions. *Organic Geochemistry* **38**, 1212-1225.

Talbot H. M., Summons R. E., Jahnke L. L., Cockell C. S., Rohmer M., Farrimond P. (2008) Cyanobacterial bacteriohopanepolyol signatures from cultures and natural environmental settings. *Organic Geochemistry* **39**, 232-263.

Tanaka T. Y., Kurosaki Y., Chiba M., Matsumura T., Nagai T., Yamazaki A., Uchiyama A., Tsunematsu N., Kai K. (2005) Possible transcontinental dust transport from North Africa and the Middle East to East Asia. *Atmospheric Environment* **39**, 3901-3909.

Tastet J. P., Martin L., Aka K. (1993) Géologie et environnements sédimentaires de la marge continentale de Côte d'Ivoire. In: *Environnement et ressources aquatiques de Côte d'Ivoire. I - Le milieu marin* (Le Loeuff P., Marchal E., Amon Kotias J. P. (Eds.)). Service didactique, ORSTOM, 23-61.

Tegen I., Lacis A. A., Fung I. (1996) The influence on climate forcing of mineral aerosols from disturbed soils. *Nature* **380**, 419-422.

Tierney J. E., Russell J. M. (2009) Distributions of branched GDGTs in a tropical lake system: Implications for lacustrine application of the MBT/CBT paleoproxy. *Organic Geochemistry* **40**, 1032-1036.

Tierney J. E., Russell J. M., Eggermont H., Hopmans E. C., Verschuren D., Sinninghe Damsté J. S. (2010) Environmental controls on branched tetraether lipid distributions in tropical East African lake sediments. *Geochimica et Cosmochimica Acta* **74**, 4901-4918.

Tjallingii R., Claussen M., Stuut J.-B. W., Fohlmeister J., Jahn A., Bickert T., Lamy F., Rohl U. (2008) Coherent high- and low-latitude control of the northwest African hydrological balance. *Nature Geoscience* **1**, 670-675.

Torres O., Bhartia P. K., Herman J. R., Ahmad Z., Gleason J. (1998) Derivation of aerosol properties from satellite measurements of backscattered ultraviolet radiation: Theoretical basis. *Journal of Geophysical Research* **103**, 17099-17110.

Torres O., Bhartia P. K., Herman J. R., Sinyuk A., Ginoux P., Holben B. (2002) A long-term record of Aerosol Optical Depth from TOMS observations and comparison to AERONET measurements. *Journal of the Atmospheric Sciences* **59**, 398-413.

Trapp J. M., Millero F. J., Prospero J. M. (2010) Temporal variability of the elemental composition of African dust measured in trade wind aerosols at Barbados and Miami. *Marine Chemistry* **120**, 71-82.

Trumbore S. E. (1993) Comparison of carbon dynamics in tropical and temperate soils using radiocarbon measurements. *Global Biogeochemical Cycles* **7**, 275-290.

Trumbore S. E., Davidson E. A., Barbosa de Camargo P., Nepstad D. C., Martinelli L. A. (1995) Belowground cycling of carbon in forests and pastures of eastern Amazonia. *Global Biogeochemical Cycles* **9**, 515-528.

Tyler J. J., Nederbragt A. J., Jones V. J., Thurow J. W. (2010) Assessing past temperature and soil pH estimates from bacterial tetraether membrane lipids: Evidence from the recent lake sediments of Lochnagar, Scotland. *Journal of Geophysical Research* **115**, G01015, doi: 10.1029/2009jg001109.

van der Hammen T., Absy M. L. (1994) Amazonia during the last glacial. *Palaeogeography, Palaeoclimatology, Palaeoecology* **109**, 247-261.

Verardo D. J., McIntyre A. (1994) Production and destruction: Control of biogenous sedimentation in the tropical Atlantic 0-300,000 years B.P. *Paleoceanography* **9**, 63-86.

Volkman J. K., Eglinton G., Corner E. D. S., Forsberg T. E. V. (1980) Long-chain alkenes and alkenones in the marine coccolithophorid *Emiliania huxleyi*. *Phytochemistry* **19**, 2619-2622.

Volkman J. K., Barrett S. M., Blackburn S. I., Sikes E. L. (1995) Alkenones in *Gephyrocapsa oceanica*: Implications for studies of paleoclimate. *Geochimica et Cosmochimica Acta* **59**, 513-520.

Walsh E. M., Ingalls A. E., Keil R. G. (2008) Sources and transport of terrestrial organic matter in Vancouver Island fjords and the Vancouver-Washington Margin: A multiproxy approach

using $\delta^{13}C_{org}$, lignin phenols, and the ether lipid BIT index. *Limnology and Oceanography* **53**, 1054-1063.

Walsh J. P., Nittrouer C. A. (2009) Understanding fine-grained river-sediment dispersal on continental margins. *Marine Geology* **263**, 34-45.

Washington R., Todd M. C. (2005) Atmospheric controls on mineral dust emission from the Bodélé Depression, Chad: The role of the low level jet. *Geophyiscal Research Letters* **32**, L11701, doi:10.1029/2005GL023597.

Washington R., Bouet C., Cautenet G., Mackenzie E., Ashpole I., Engelstaedter S., Lizcano G., Henderson G. M., Schepanski K., Tegen I. (2009) Dust as a tipping element: The Bodélé Depression, Chad. *Proceedings of the National Academy of Sciences of the USA* **106**, 20564-20571.

Watrin J., Lézine A.-M., Hély C. (2009) Plant migration and plant communities at the time of the "green Sahara". *Comptes Rendus Geoscience* **341**, 656-670.

Wefer G., Bleil U., Schulz H. D., Fischer G. (1997) *Geo Bremen South Atlantic 1996, Cruise No. 34, 21 February - 15 April 1996, Volume II. METEOR Berichte*. Universität Hamburg, Hamburg, 268 pp.

Weijers J. W. H., Schouten S., Spaargaren O. C., Sinninghe Damsté J. S. (2006a) Occurrence and distribution of tetraether membrane lipids in soils: Implications for the use of the TEX_{86} proxy and the BIT index. *Organic Geochemistry* **37**, 1680-1693.

Weijers J. W. H., Schouten S., Hopmans E. C., Geenevasen J. A. J., David O. R. P., Coleman J. M., Pancost R. D., Sinninghe Damsté J. S. (2006b) Membrane lipids of mesophilic anaerobic bacteria thriving in peats have typical archaeal traits. *Environmental Microbiology* **8**, 648-657.

Weijers J. W. H., Schouten S., van den Donker J. C., Hopmans E. C., Sinninghe Damsté J. S. (2007a) Environmental controls on bacterial tetraether membrane lipid distribution in soils. *Geochimica et Cosmochimica Acta* **71**, 703-713.

Weijers J. W. H., Schefuß E., Schouten S., Sinninghe Damsté J. S. (2007b) Coupled thermal and hydrological evolution of tropical Africa over last deglaciation. *Science* **315**, 1701-1704.

Weijers J. W. H., Panoto E., van Bleijswijk J., Schouten S., Rijpstra W. I. C., Balk M., Stams A. J. M., Sinninghe Damsté J. S. (2009a) Constraints on the biological source(s) of the orphan branched tetraether membrane lipids. *Geomicrobiology Journal* **26**, 402 - 414.

Weijers J. W. H., Schouten S., Schefuß E., Schneider R. R., Sinninghe Damsté J. S. (2009b) Disentangling marine, soil and plant organic carbon contributions to continental margin sediments: A multi-proxy approach in a 20,000 year sediment record from the Congo deep-sea fan. *Geochimica et Cosmochimica Acta* **73**, 119-132.

Weijers J. W. H., Wiesenberg G. L. B., Bol R., Hopmans E. C., Pancost R. D. (2010) Carbon isotopic composition of branched tetraether membrane lipids in soils suggest a rapid turnover and a heterotrophic life style of their source organism(s). *Biogeosciences* **7**, 2959-2973.

Weijers J. W. H., Bernhardt B., Peterse F., Werne J. P., Dungait J. A. J., Schouten S., Sinninghe Damsté J. S. (2011) Absence of seasonal patterns in MBT-CBT indices in mid-latitude soils. *Geochimica et Cosmochimica Acta* **75**, 3179-3190.

Weldeab S., Schneider R. R., Kölling M., Wefer G. (2005) Holocene African droughts relate to eastern equatorial Atlantic cooling. *Geology* **33**, 981-984.

Weldeab S., Schneider R. R., Müller P. (2007a) Comparison of Mg/Ca- and alkenone-based sea surface temperature estimates in the fresh water - influenced Gulf of Guinea, eastern equatorial Atlantic. *Geochemistry Geophysics Geosystems* **8**, Q05P22, doi: 10.1029/2006GC001360.

Weldeab S., Lea D. W., Schneider R. R., Andersen N. (2007b) 155,000 years of West African monsoon and ocean thermal evolution. *Science* **316**, 1303-1307.

Westerhausen L., Poynter J., Eglinton G., Erlenkeuser H., Sarnthein M. (1993) Marine and terrigenous origin of organic matter in modern sediments of the equatorial East Atlantic: the $\delta^{13}C$ and molecular record. *Deep Sea Research Part I: Oceanographic Research Papers* **40**, 1087-1121.

Wilson K. E., Maslin M. A., Burns S. J. (2011) Evidence for a prolonged retroflection of the North Brazil Current during glacial stages. *Palaeogeography, Palaeoclimatology, Palaeoecology* **301**, 86-96.

Wollast R. (1991) The coastal organic carbon cycle: fluxes, sources and sinks. In: *Ocean margin processes in global change* (Mantoura R. F. C., Martin J.-M., Wollast R. (Eds.)). Wiley, New York, 365-381.

Wuchter C., Schouten S., Wakeham S. G., Sinninghe Damsté J. S. (2005) Temporal and spatial variation in tetraether membrane lipids of marine Crenarchaeota in particulate organic matter: Implications for TEX_{86} paleothermometry. *Paleoceanography* **20**, PA3013, doi: 10.1029/2004PA001110.

Wuchter C., Abbas B., Coolen M. J. L., Herfort L., van Bleijswijk J., Timmers P., Strous M., Teira E., Herndl G. J., Middelburg J. J., Schouten S., Sinninghe Damsté J. S. (2006a) Archaeal nitrification in the ocean. *Proceedings of the National Academy of Sciences of the USA* **103**, 12317-12322.

Wuchter C., Schouten S., Wakeham S. G., Sinninghe Damsté J. S. (2006b) Archaeal tetraether membrane lipid fluxes in the northeastern Pacific and the Arabian Sea: Implications for TEX_{86} paleothermometry. *Paleoceanography* **21**, PA4208, doi:10.1029/2006PA001279.

Wurzler S., Reisin T. G., Levin Z. (2000) Modification of mineral dust particles by cloud processing and subsequent effects on drop size distributions. *Journal of Geophysical Research* **105**, 4501-4512.

Xu Y., Cooke M. P., Talbot H. M., Simpson M. J. (2009) Bacteriohopanepolyol signatures of bacterial populations in Western Canadian soils. *Organic Geochemistry* **40**, 79-86.

Yarincik K. M., Murray R. W., Peterson L. C. (2000) Climatically sensitive eolian and hemipelagic deposition in the Cariaco Basin, Venezuela, over the past 578,000 years: Results from Al/Ti and K/Al. *Paleoceanography* **15**, 210-228.

Zabel M., Bickert T., Dittert L., Haese R. R. (1999) Significance of the sedimentary Al:Ti ratio as an indicator for variations in the circulation patterns of the equatorial North Atlantic. *Paleoceanography* **14**, 789-799.

Zabel M., Schneider R. R., Wagner T., Adegbie A. T., de Vries U., Kolonic S. (2001) Late Quaternary climate changes in Central Africa as inferred from terrigenous input to the Niger Fan. *Quaternary Research* **56**, 207-217.

Zhu C., Talbot H. M., Wagner T., Pan J. M., Pancost R. D. (2010) Intense aerobic methane oxidation in the Yangtze Estuary: A record from 35-aminobacteriohopanepolyols in surface sediments. *Organic Geochemistry* **41**, 1056-1059.

Zhu C., Weijers J. W. H., Wagner T., Pan J.-M., Chen J.-F., Pancost R. D. (2011) Sources and distributions of tetraetherlipids in surface sediments across a large river-dominated continental margin. *Organic Geochemistry* **42**, 376-386.

Zink K.-G., Vandergoes M. J., Mangelsdorf K., Dieffenbacher-Krall A. C., Schwark L. (2010) Application of bacterial glycerol dialkyl glycerol tetraethers (GDGTs) to develop modern and past temperature estimates from New Zealand lakes. *Organic Geochemistry* **41**, 1060-1066.

Acknowledgments

First of all, I would like to thank my supervisor PD Dr. Matthias Zabel for giving me the opportunity to work on this very interesting topic, for constant support, motivation and encouragement during the past three years. Thank you also for many fruitful discussions and for letting me go my own way – in scientific as well as in private aspects.

My co-supervisor Prof. Dr. Thomas Wagner at Newcastle University is thanked for his support during my visits to Newcastle, for the co-referat and for many helpful discussions especially during manuscript preparation.

A big thank you goes to Dr. Helen M. Talbot at Newcastle University who invited and introduced me into the world of BHPs. Thank you, Helen, for showing me how to measure and identify BHPs and for your constant support over the last years, not only during my visits but also during further data evaluation and manuscript preparation.

I am indebted to Prof. Dr. Gesine Mollenhauer for the possibility to use her laboratory facilities for BHP extraction. I am grateful for the opportunity to expand my biomarker knowledge and investigate further biomarkers. Thank you for many helpful discussions and for your support during labwork, data evaluation and manuscript preparation.

I am grateful to JProf Dr. Janet Rethemeyer for her assistance in the laboratory during my very first BHP extractions. Ralph Kreutz is thanked for laboratory help concerning all kinds of biomarker extraction, measurement and data evaluation.

For any kind of support during inorganic geochemistry lab work I want to thank Karsten Enneking and Silvana Pape as well as Susanne Siemer. I would like to thank the student assistants Anja Bräunig and Friedrich Schröder for their help during sample preparation.

Thank you to Paul Donohoe (Newcastle University) for measuring my samples at the GC-MS. I would also like to thank all colleagues at Newcastle University who met me with a kind reception and made my visits in Newcastle to pleasant ones.

My colleagues and friends at the FB5 “Geochemistry and Hydrology” and the new Marum “Inorganic Aquatic Geochemistry” working groups are thanked for a friendly atmosphere, many nice coffee breaks and support. Thank you Victoria, Jan, Jörn, Jens, Luzie, Tobias, Christian, Kay, Martin, Maria, Kathrin, Jenni, Jürgen, Roy, Thomas and Frau Haack. Special thanks to Jan for help with any kind of computer problems.

The DFG-graduate college Europrox is thanked for funding. Thank you to all Europrox PhD students, to the postdocs, secretaries and speakers.

I want to thank my friends and family for their support but also for sometimes distracting me from my work. A big thank you to my parents for their permanent support and encouragement all over the years.

A very special thank you to Alexander Gehler for his support, for proof reading, endurance, encouragement and for bearing with me over the last months.